Oil & Natural Gas Technology

DOE Award No.: DE-FC26-06NT41248

Final Report

Project Title

Submitted by:
Richard Wies, Ph.D.
University of Alaska Fairbanks
PO Box 755910
Fairbanks, AK 99775-5910

Prepared for:
United States Department of Energy
National Energy Technology Laboratory

December 17, 2008

Office of Fossil Energy

Effects of Village Power Quality on Fuel Consumption and Operating Expenses

Final Report

Report Period Start: 8/2002
Report Period End: 9/2008

Principal Author(s): Richard Wies and Ron Johnson

Issued: September 2008

DOE Award Number: DE-FC26-01NT41248
Task: 1.03.1

Submitting Organization and Subrecipient:

University of Alaska Fairbanks
Institute of Northern Engineering
Arctic Energy Technology and Development Laboratory
PO Box 755910
Fairbanks, AK 99775-5910

Alaska Energy Authority
813 West Northern Lights Blvd.
Anchorage, AK 99503

DISCLAIMER --

Abstract

Alaska's rural village electric utilities are isolated from the Alaska railbelt electrical grid intertie and from each other. Different strategies have been developed for providing power to meet demand in each of these rural communities. Many of these communities rely on diesel electric generators (DEGs) for power. Some villages have also installed renewable power sources and automated generation systems for controlling the DEGs and other sources of power. For example, Lime Village has installed a diesel battery photovoltaic hybrid system, Kotzebue and Wales have wind-diesel hybrid systems, and McGrath has installed a highly automated system for controlling diesel generators. Poor power quality and diesel engine efficiency in village power systems increases the cost of meeting the load. Power quality problems may consist of poor power factor (PF) or waveform disturbances, while diesel engine efficiency depends primarily on loading, the fuel type, the engine temperature, and the use of waste heat for nearby buildings. These costs take the form of increased fuel use, increased generator maintenance, and decreased reliability. With the cost of bulk fuel in some villages approaching $1.32/liter ($5.00/gallon) a modest 5% decrease in fuel use can result in substantial savings with short payback periods depending on the village's load profile and the cost of corrective measures. This project over its five year history has investigated approaches to improving power quality and implementing fuel savings measures through the use of performance assessment software tools developed in MATLAB® Simulink® and the implementation of remote monitoring, automated generation control, and the addition of renewable energy sources in select villages. The results have shown how many of these communities would benefit from the use of automated generation control by implementing a simple economic dispatch scheme and the integration of renewable energy sources such as wind generation.

Table of Contents

List of Figures

List of Tables

1. Introduction

Alaska's rural village electric utilities are standalone systems without connections to the main Alaska “Railbelt” electrical grid intertie. Of the approximately 5,646,290 MWh of electric power generated commercially in Alaska by power utilities in 2001, 24% of the generated power is distributed over unconnected grids [1]. Many of these rural communities rely solely on diesel electric generators (DEGs) for electric power and heat with electrical energy costs subsidized through the state’s power cost equalization (PCE) program. A 2003 report by the Alaska Energy Authority (AEA) shows that 92% of the electrical production in Alaska communities not connected to the “Railbelt” electrical grid was produced by DEGs [2]. Based on a survey referenced in the *Screening Report for Alaska Rural Villages* (2001) most village utilities have a minimum of three DEGs within their systems [3]. For those communities that have installed hybrid power systems, such as wind turbine generators and solar photovoltaic arrays, DEGs are still required to make up the base load (see Figure 1.1). DEGs have the advantage of being able to generate the required electrical power when necessary. However, the use of DEGs comes with the high cost of supplying diesel fuel and the high cost of maintenance over their operational lifetime.

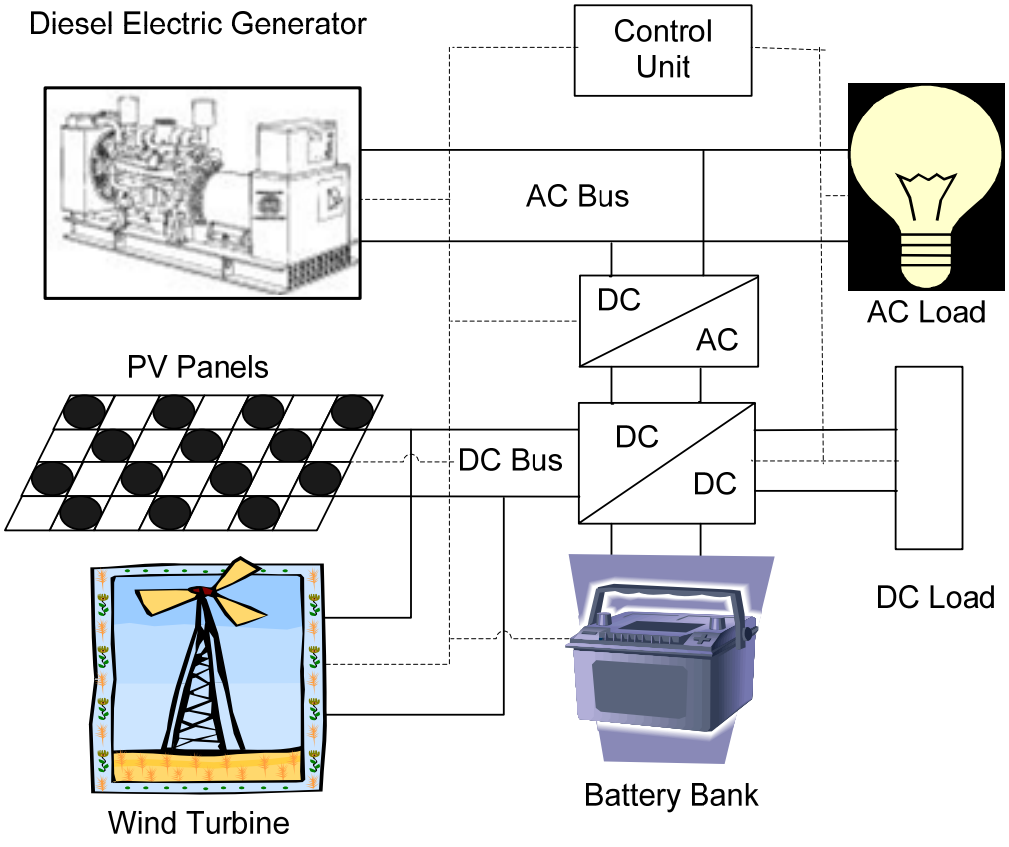

Figure 1.1: Alaska village hybrid power system.

The installation of renewable sources and automated generation control in some communities has helped to reduce fuel consumption. These fuel displacement and savings schemes are becoming more economically viable with shorter payback periods as the bulk fuel costs in some

communities approaches $1.32/liter ($5.00/gallon). On average rural communities spend significantly more for electrical energy than those communities connected to a large electrical infrastructure. For example, based on a 2001 study, villages that are a part of the Alaska Village Electric Cooperative (AVEC) on average pay $0.42/kWh compared to $0.11/kWh for those connected to the Railbelt electrical grid [1]. The rise in fuel prices has seen these average costs rise to $0.52/kWh for AVEC villages and $0.24/kWh for railbelt communities. As of June 1, 2008, residences tied to the interior railbelt system managed by Golden Valley Electric Association were paying about $0.24/kWh because of the increase in the fuel surcharge. There is currently a proposal which would increase the minimum price for electric power in all Alaska villages to $1.12/kWh for the power cost equalization (PCE) program which would likely put the average costs up around $1.50/kWh. This indicates a need for the application of technologies to reduce the cost by improving the efficiency of the DEGs and utilizing renewable energy technologies which are dependent upon the available local resources. Methods of improving the efficiency of the DEGs such as economic dispatch of generation using control systems can be used in conjunction with renewable energy technologies.

The intent of this project was to assess the current operational state of standalone power systems in select rural communities in Alaska within Alaska Energy Authority's service territory by installing remote monitoring systems, developing a performance assessment method and providing recommendations for improvement of the efficiency of these DEG systems through analysis of data collected from existing and newly installed remote monitoring systems. The purpose of this research is to develop simulation models of the diesel-electric generation systems in rural communities using MATLAB® Simulink® for predicting the impact of using renewable energy sources and economic dispatch on the system efficiency and to determine if such system upgrades would be economically viable for these villages in terms of payback from displacement of fuel costs. The model also includes a simplified thermodynamic model of the DEGs to study the effects of ambient temperature on the generation efficiency. This power system simulation model is intended to help rural utility managers to investigate methods for: 1) increasing the diesel-electric generation efficiency, 2) decreasing the DEGs fuel consumption, 3) decreasing the maintenance costs, and 4) determining if the installation of renewable sources and automated generation control systems would be economical.

2. Executive Summary

Alaska's rural village electric utilities are isolated from the Alaska railbelt electrical grid intertie and from each other. Different strategies have been developed for providing power to meet demand in each of these rural communities. However, many of the communities in rural Alaska rely solely on diesel electric generators (DEGs) for power. The project was conducted in cooperation with the Alaska Energy Authority (AEA). The main goal of this project was to create a partnership with rural utilities and state energy organizations to coordinate the collection of energy system data in a representative set of rural Alaska communities in order to establish general performance assessments, and identify strengths and weaknesses of plant operations. These results will be used to improve system design and operation.

The project technical approach involved monitoring and analyzing the performance of a representative number of systems which reflect general operating conditions in Alaska village power systems served by the Alaska Energy Authority. The studies conducted in this project centered around five main tasks: 1) the development of a consortium of Alaska rural utilities, 2) the in-house (at UAF) testing of RTUs, flow meters and sensors for DEGs like those found in Alaska village communities, 3) survey of village power systems and data collection, 4) the deployment of remote monitoring systems in 25 villages in AEAs service territory, and 5) the development of system models in MATLAB® Simulink® to determine the optimal mix of DEGs and renewable sources of power as well as the feasibility of employing economic dispatch of power from these sources to serve the village loads.

A consortium of Alaska rural utilities and state energy organizations was developed as the project progressed for the collection and sharing of ideas for monitoring remote power systems. UAF PIs Richard Wies and Ron Johnson have been promoting the standardization of instrumentation and data collection systems in the villages since 2002. After setting up remote monitoring systems for large amounts of data in various formats with different sampling rates, AEA and the AVEC partnered to develop a standard instrumentation system for collecting and downloading the data.

A number of villages in AEAs service territory were surveyed and available data was collected from a number of villages in the AEA service territory. However, a lot of this data was found to have significant portions missing or consisted of only one or two days of recordings of the electric load at 15 minute intervals when maintenance personnel were on site. AEA was able to upgrade the switchgear in 25 villages which included remote monitoring as part of the package. A $60k subcontract with AEA on this project helped in the purchase and install of some basic remote monitoring equipment in a couple of villages and a central server for collecting the large amounts of data from village monitoring systems. There is currently online access to real-time monitoring provided for about 25 villages in AEAs service territory http://www.aidea.org/aea/aearemotemon.html with limited data collection capabilities.

The UAF portion of the project consisted of three phases which resulted in one book, three peer-review journal publications, fifteen conference publications, one Ph. D. dissertation and three M. S. theses with work supervised by the PI Richard Wies and the co-PI Ron Johnson as outlined in the Project Publications section following the References section. Phase 1 (Aug 2003 - Dec 2004) consisted of testing and evaluation of a remote terminal unit, coolant flowmeters, fuel flow meters, and temperature and pressure sensors on the UAF Energy Center Diesel. Specific types of flow meters that were tested included the turbulent flow, ultrasonic, and

magnetic types. A magnetic flow meter was also tested independently in a small coolant flow loop in a UAF lab. Phase 2 (Aug 2003 - Aug 2006) overlapped phase 1 and consisted of the development of a hybrid power system model to investigate the economic feasibility of integrating renewable energy sources into existing rural village power plants. Phase 3 (Aug 2006 - Aug 2008) consisted of the development of an economic dispatch model for investigating the feasibility of integrating automated generation control to dispatch the most efficient generators to serve the load at the given operating point.

Results of testing a remote terminal unit, various types of fuel and coolant flow meters, and temperature and pressure sensors on the125 kWe Detroit DEG at UAF showed the importance of the proper selection of flow meters and sensors and remote metering. The energy balance calculated using the data collected in the RTU showed an overall error of about 2.5% using the manufacturer's specifications as a basis for comparison. A significant result occurred when fire ash in the summer of 2004 clogged the cooling system radiator and the operating temperature increased by 20 °C. In a village system without remote monitoring this situation might have led to a costly generator failure if left unchecked.

The hybrid power system model was used to evaluate the performance of power systems in Kongiganak, Lime Village, Stevens Village, and Wales Village and compared with results from the well known HOMER software developed at the National Renewable Energy Laboratory (NREL) with similar results. Our efforts were the first to include economic impacts of emissions from DEGs in Alaska rural villages in a simulation model. Results show economic feasibility through fuel savings of installing wind turbine generators in some villages. Puvarnaq Power which serves Kongiganak, AK received a Denali Commission grant for a new 3 wind-2 diesel system. A feasibility analysis using our model for the proposed system estimates the village will displace about 37,800 liters (10,000 gallons) of diesel fuel per wind turbine per year with a payback of about 3.5 years, while the contractor estimates about 45,360 liters (12,000 gallons) of diesel fuel per wind turbine per year with a payback of about 2.5 years.

A thermodynamic model of the DEG was also developed to investigate economic load dispatch incorporating ambient temperature variations. This was tested on load and ambient temperature data from Buckland, AK and Kongiganak, AK. Results of economic dispatch analysis show that Buckland, AK needs to turn off the less efficient 175 kW DEG and just operate the 455 kW DEG, so there is no real need for economic dispatch at this time. Results of an economic dispatch feasibility analysis show that Kongiganak, AK would reduce fuel consumption by about 9% by employing an economic dispatch system. Given their current cost of bulk fuel at $0.93/liter ($3.50/gallon) and the installed cost of a basic economic dispatch system at $115k results in a payback of just under a year. With respect to our analysis regarding the impact of ambient temperature on performance, a 3 °C rise in temperature over the next 50 years would result in less than 0.2% change in DEG efficiency.

The results of this project have the following benefits: 1) The development of a centralized remote monitoring system for Alaska village power systems leading to efficiency and power quality improvements that have a direct impact on the reduction of fuel consumption and operating expenses, and 2) The development of energy, economic and environmental assessment tools for evaluating long term performance of remote village power systems in Alaska incorporating diesel electric generators as their main source of electric power and heat.

3. Experimental

The following sections provide a brief discussion of the project tasks and the procedures and equipment used to complete them. A more detailed discussion of the specific procedures used to obtain the results for the items in the two lists below are presented in the Ph. D. dissertation and three M. S. theses listed in the Project Publications section.

There were five main tasks which were completed on this project with procedures as discussed in sections 3.1-3.5.

3.1 Consortium of Alaska Rural Utilities

A partnership of village electric utilities and state energy organizations was created in order to coordinate the collection of energy system data in select rural communities in order to establish general performance assessments, and identify strengths and weaknesses of plant operations. An initial meeting was held in February 2002 at AEA to discuss the needs for remote monitoring of village power systems in Alaska. After that initial meeting the PI Richard Wies met with personnel from the village electric utilities and state energy organizations at the Alaska Rural Energy conferences in September 2002, April 2004, September 2005, and April 2007, and September 2008.

3.2 RTU, Flow Meter, and Temperature Sensor Testing at UAF

Remote monitoring systems, specifically remote terminal units (RTUs), temperature sensors and flow meters were tested and evaluated on the 125 kWe Detroit diesel electric generator at the University of Alaska Fairbanks (UAF) Energy Center as shown in Figure 3.1. The detailed procedures of these tests are presented by Tyler Chubb in a master's thesis, *Performance Analysis for Remote Power Systems in Rural Alaska*, under the direction of the project PIs (see MS Thesis 2 under Project Publications). Tests were conducted using an ElectroIndustries Nexus 1252 RTU, various temperature sensors, and three types of flow meters: 1) inline turbulent flow, 2) inline electromagnetic, and 3) ultrasonic. Data was collected and accessed through the Nexus 1252 RTU which was available online with password protection. The actual testing of the flow meters and temperature sensors on the 125 kWe Detroit diesel was conducted using all or parts of the load profile shown in Figure 3.2 below.

Figure 3.1: Diesel Electric Generator (125 kWe Detroit Diesel) at UAF Energy Center.

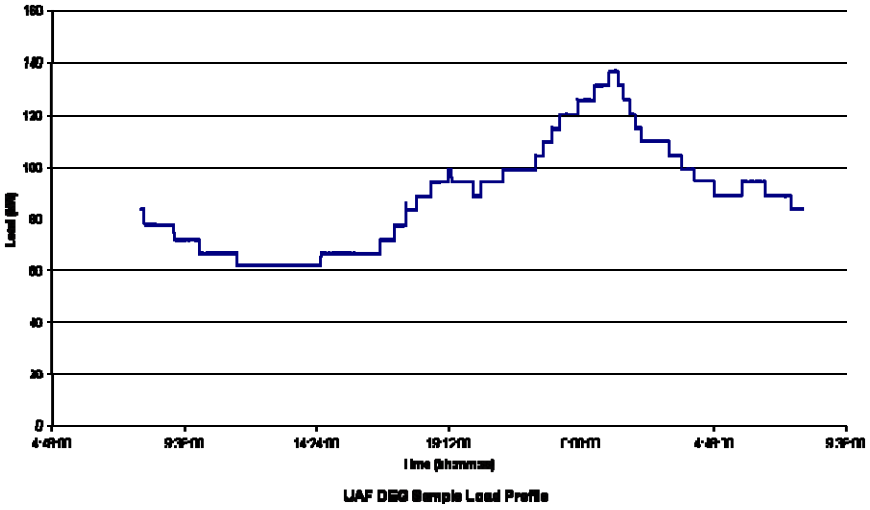

Figure 3.2: Sample load profile for the UAF Energy Center DEG.

3.2.1 RTU

Four different brands of RTU were considered for testing on the 125 kWe DEG. The first RTU that was evaluated was a National Instruments Fieldpoint 2015 [4]. The second RTU was an ION 7350 manufactured by Power Measurement Inc [5]. Much of the summer of 2003 was spent performing experiments with and programming settings into this RTU. PowerCorp, an Australian company attempting to expand into Alaska manufactures the Commander, the third brand of RTU that was considered [6]. The project did not have a chance to examine this device in as much detail as would have been sufficient to come to any conclusions about its usefulness to the project. A NEXUS 1252 series RTU manufactured by ElectroIndustries was the final device that was examined [7]. ElectroIndustries was very helpful and even loaned the project an RTU on a trial basis. Consequently, the Nexus RTU was chosen for this project.

3.2.2 Temperature Sensors

The monitoring system uses type K thermocouples to measure the temperature of different entities involved with the diesel generator. Thermocouples consist of wires made from two dissimilar metals touching at one end and left open at the other end. When the connected end is subjected to a different temperature than the open end, a voltage signal will be induced from the electron transfer caused by two different types of heated metals being in close proximity to each other. The magnitude of the generated voltage is mathematically related to the temperature difference between the open end and closed end of the thermocouple and can therefore be used to calculate the temperature at the open end. The different models of thermocouples (type D, F, K etc.) are referring to the types of metals used in the thermocouple design as this affects the magnitude of the induced voltage. The type K thermocouples utilized in this project are constructed of Nickel Chromium and Nickel Aluminum wires [8].

The relationship between voltage and temperature is highly nonlinear and the generated voltage must be conditioned as illustrated by the diagram in Figure 3.3 to produce a linear 4-20mA signal suitable for input into the NEXUS RTU. The signal conditioner digitizes the thermocouple voltage signal, applies it to the appropriate temperature conversion equation, and outputs a 4-20mA signal that is directly proportional to temperature at the closed end of the thermocouple.

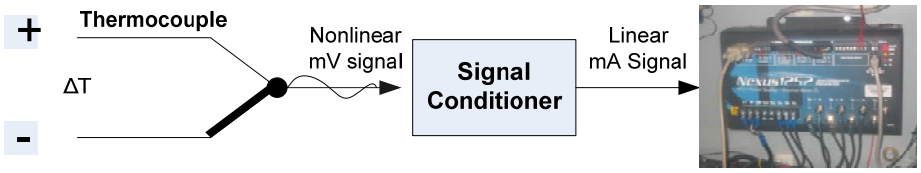

Figure 3.3: Process of acquiring data from a thermocouple.

Two Type K thermocouples are utilized to measure the input and output temperature of the glycol-water mixture used to cool the generator. The closed end of the thermocouple is inserted directly into the fluid using a "thermocouple well," basically a compression fitting that allows the thermocouple insertion to pass through a hole in the pipe. Knowing the input and output temperature of the generator coolant allows the heat transfer rate of the system to be calculated. Additional thermocouples are used to measure the engine block temperature of the generator and ambient temperature of the generator container. Knowing the temperatures of these parameters is useful to gauge the amount of energy being lost as engine heat.

3.2.3 Coolant Flow Meters

Coolant flow meters were evaluated independently in a test loop in the Duckering building as shown in Figure 3.4. Three types of flow meters were tested including: 1) inline turbulent flow, 2) inline electromagnetic, and 3) ultrasonic. The system consists of two tanks (supply and fill) and a ¾ HP pump. A series of tests were conducted at various coolant flow rates to determine the range and accuracy of the three types of flow meters used in this DEG application.

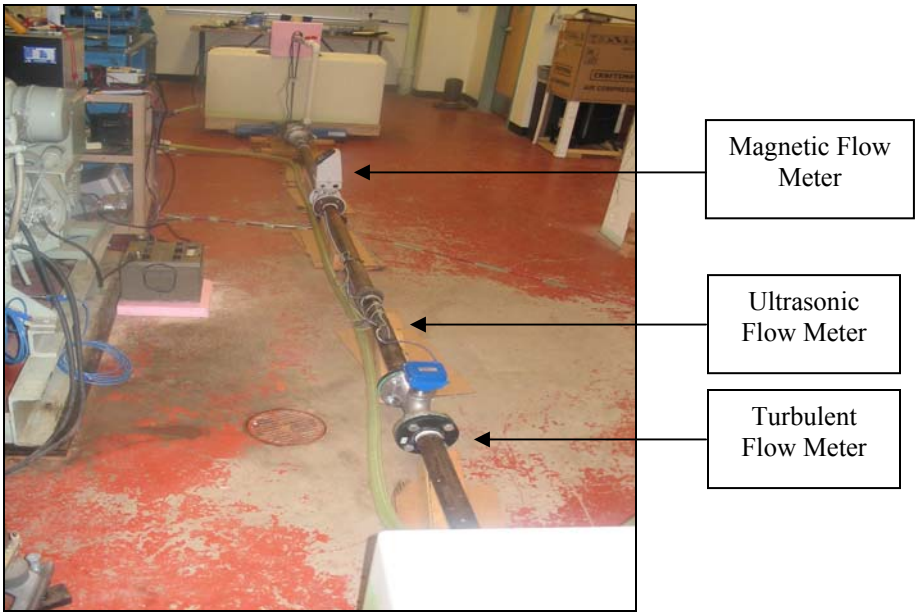

Figure 3.4: Apparatus constructed to test flow meters.

3.2.3.1 Turbine Flow Meter

The principle of operation of the turbine flow meter is quite straightforward. A probe is inserted directly into the coolant line through a tee section of pipe. The end of the probe is equipped with a small, plastic spinning wheel, better known as a turbine which is put into motion by the fluid flow through the pipe. There are magnets located at the end of four of the turbine blades and a

"high" voltage signal is emitted each time one of these magnets passes by a large magnet located at the end of the turbine shaft. The subsequent output of the meter is therefore a "pulse train" or a series of low and high voltage signals. The "K-factor" or conversion rate between the number of pulses and the volumetric flow rate is 60 pulses/gallon. The model of flow meter being used is the Omega FTB 720 [9].

The NEXUS RTU has the ability to count pulse signals and an attempt was made to utilize this feature. Recording the number of pulses over the time taken to create the pulses gives an accurate indication of flow rate. However, this attempt was unsuccessful and a signal conditioner had to be ordered that processed the pulse signal coming from the turbine meter and converted it to a 4-20 mA sign proportional to the flow rate. This signal could then be easily sent to the analog input module of the NEXUS RTU.

3.2.3.2 Magnetic Flow Meter

Magnetic flow meters, commonly known as electromagnetic flow meters, operate on the principle that fluids with charged particles moving at right angles to a magnetic field will induce an electric field or voltage. The voltage will be induced on a pair of electrodes mounted on the flow meter. There is a mathematical relationship between the magnitude of induced voltage and the velocity of the fluid. A fluid velocity is calculated by the microprocessor on the flow meter using the induced voltage and this relationship. A mass or volumetric flow rate can be calculated using the fluid velocity, density, and the cross sectional area of the fluid flow. A diagram showing the orientation of the magnetic fields used to operate the flow meter is shown in Figure 3.5. The model of flow meter used was the Siemens Magflo 7000 [10].

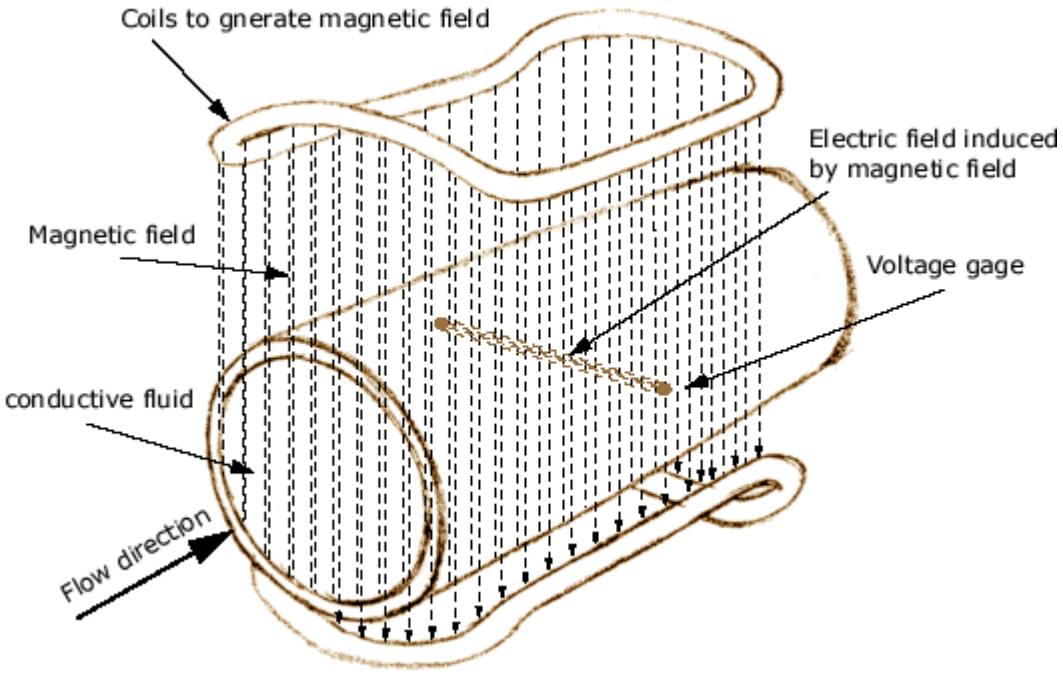

Figure 3.5: Principle of operation of magnetic flow meter [11].

3.2.3.3 Ultrasonic Flow Meter

The EESiFlo 5000 is an ultrasonic meter that is used to measure the coolant flow [12]. It consists of two sensors (upstream and downstream) that clamp around the coolant pipe for transmitting and receiving ultrasonic signals, therefore, it can be installed without cutting into the coolant loop. Ultrasonic flow meters present a distinct advantage over turbine or other in-line style meters as little time and effort is required for the installation process. The principle of the ultrasonic flow meter is centered on the apparent propagation velocity of the ultrasonic wave through a medium flowing through a pipe. If the medium is stationary and remains at a constant temperature and density, the time taken for an ultrasonic signal to be transmitted by one sensor, travel down the line a short distance, and then be received by another sensor will remain constant. However, if the medium is dynamic, the time taken for the transmitted signal to be received by a downstream sensor will be reduced proportional to the fluid speed. For the EESiFlo meters used in this project, the upstream sensor transmits an ultrasonic signal to a receiving sensor located approximately one to two inches downstream, the exact distance depending on the diameter of the pipe. The upstream sensor emits the testing signal 60 times per second, thus producing a very accurate profile of the fluid velocity. The microprocessor within the flow meter then compares the reception time for the dynamic fluid flow to the reception time if the fluid were static. This data provides sufficient information for the microprocessor to calculate the velocity and subsequent flow rate.

The EESiFlo 5000 meter is specifically designed to measure high volumetric fluid flows through pipes with a large cross sectional area. Due to the sizeable cross-sectional diameter of coolant line piping, the path of the ultrasonic signal will be distorted by a considerable amount as it travels through the medium. Therefore, a detailed set of information about the fluid parameters such as density and viscosity must be programmed into the flow meter. Also, the parameters regarding the pipe wall material, lining, and roughness are also very important for the meter to calculate appropriate correction factors and provide accurate flow rate data.

3.2.4 Instantaneous Fuel Flow

The amount of fuel consumed by the generator can be monitored in two ways: 1) on a real-time basis by using a flow meter to monitor the amount of fuel flowing through the supply and return fuel lines and 2) by measuring the known volume of fuel consumed from a day tank using a pressure transducer for timing. The momentary change in fuel consumption is useful to know as it allows the fuel consumption trend to be distinctly seen during times of changing electrical load on the generator.

3.2.4.1 Fuel Flow using Ultrasonic Flow Meter

The EESiFlo Inc. S-Series ultrasonic flow meter was used in this project to measure the flow of diesel fuel from a storage tank into the electric generator [13]. The operation of this ultrasonic flow meter for fuel is the same as that presented in section 3.2.3.3 for coolant accept for one major difference. This particular EESiFlo ultrasonic meter is designed to measure fluid flow in small pipes with a diameter of three-quarters of an inch or less. Also, according to the manufacturer, the EESiFlo ultrasonic meters are advantageous over other ultrasonic meters because there are no requirements as to the mounting location on the pipe. The inner cross sectional area of the fuel line is programmed into the flow meter by the user and the meter performs the necessary calculations and outputs a 4-20 mA signal that is proportional to the volumetric flow rate of fluid through the line. In addition, the meter has an accumulator function that records the total amount of fuel that has passed through the line.

3.2.4.2 Fuel Flow using Day Tank Volume

The actual fuel flow rates were measured from the small day tank which fuels the DEG. The monitoring system contains two different sensors that are capable of measuring the volume of fuel in the day tank. These sensors include an ultrasonic rangefinder and a pressure transducer.

The ultrasonic rangefinder emits a 4-20mA analog signal proportional to the depth of fuel in the tank. The rangefinder transmits a 26 kHz signal from its base and then receives this signal after it is reflected off the medium. The microprocessor contained inside of the rangefinder measures the time between the signal transmission and reception and translates this into a distance between the bottom of the rangefinder and the medium below. Once the depth of the fuel in the tank is known, the volume of fuel can be easily calculated by factoring in the dimensions of the tank. Proper selection of the mounting location is the most important parameter that must be taken into consideration to ensure proper operation of the rangefinder. The device emits an 8 degree conical beam meaning that the larger the distance between the bottom of the rangefinder and the medium below, the larger the radius occupied by the ultrasonic signal. If a portion of this signal is obstructed by the wall of the fuel tank, a portion of it will be reflected prematurely and will cause erroneous calculations to be made by the microprocessor in the device.

The second method of measuring the fuel consumption is through the use of a pressure transducer located in the bottom of the day tank. The pressure transducer emits a 4-20mA signal proportional to the weight of the fuel in the tank. The pressure exerted on the transducer by the fluid is sufficient to distort a plastic diaphragm located within the transducer a small amount. The amount of distortion in the diaphragm is proportional to the pressure at the bottom of the fuel tank measured in lbs/in^2 (PSI) and a 4-20 mA signal proportional to the PSI is emitted. This signal can then be converted to volume by multiplying it by the surface area and the density. The change in volume over time can be used to calculate the fuel consumption rate of the generator.

3.2.5 Exhaust Flow

The mass flow rate of the exhaust is measured using a thermal anemometer. The primary component of a thermal anemometer is two temperature sensors that are inserted directly into the flowing exhaust gas. One sensor measures the ambient temperature and the other is heated 120 °F to 200 °F above ambient temperature. The motion of the exhaust gas passing by the heated sensor will cause a cooling process to occur. A feedback control system within the thermal anemometer will attempt to keep this heated sensor at a constant temperature by supplying more power to compensate for the temperature decrease. The corresponding increase in current due to the greater power draw will be related to the exhaust velocity.

A microprocessor within the meter records the current increase and combines this information with other settings to calculate a value for exhaust gas velocity. Applying the same concepts that were described in the description of the flow meters, a volumetric or mass flow rate value can be found from velocity. This value is then outputted from the meter as a 4-20 mA signal. The meter also has the ability to output the temperature of the exhaust gas as a 4-20 mA signal. This is advantageous as it negates the need for a thermocouple fixture to measure the exhaust temperature.

3.2.6 Electrical Outputs

Monitoring the electric power output of a generator is relatively simple; all that needs to be found are the voltage and current values of each phase between the generator and load. If the sampling rate is sufficiently high, all of the subsequent calculations that are needed to calculate power parameters can be found through manipulation of the current and voltage data. The primary equipment needed to monitor the level and trends of the electrical power produced by the generator are three current transformers situated on the wiring between the generator and load. The purpose of the current transformers is to step the current down to an acceptable level to be read and digitized by the data recorder. The current transformers used by this project are 500:5, meaning that 5 A will be sent to the NEXUS RTU for every 500 A of actual current flowing from the generator to the load. The size of the current transformer is programmed into the NEXUS RTU and enables the original current reading to be digitally reconstructed. Probes are connected at the load terminals to monitor the voltage being supplied to the load. The NEXUS RTU is equipped to measure up to 300V, enabling the voltage signal to be directly measured without the need for transformers to step the voltage down. Once the current and voltage signals have been sent to the RTU, the signals can be digitized and calculations can be performed to find all of the pertinent electrical information. The real power, power factor, and energy usage (kWh) are just a few of the parameters that the NEXUS can calculate once the current and voltage are known. The sampling rate of the NEXUS RTU pertaining to the electrical data (512 samples/cycle) is sufficient to perform in-depth calculations of the power quality parameters that may be used later in subsequent phases of the project.

3.2.7 Energy Balance of DEG Plant

Data from all the flow meter and sensor tests was then used to calculate the energy balance of the plant (see Figure 3.6) and compared to the energy balance calculated using the manufacturer's performance data for the DEG. The energy balance, the total amount of energy leaving the system in different forms compared to the total amount of energy entering the system as fuel, was calculated for the given load profile. The energy input for the DEG is the fuel while the energy outputs are the aftercooler, coolant loop, exhaust gas, electrical power, and miscellaneous losses in the engine and generator such as friction. The partial purpose of the energy balance calculations was to provide a means to verify the accuracy of the collected data. Also, viewing the energy balance provided a great deal of information in a concise format.

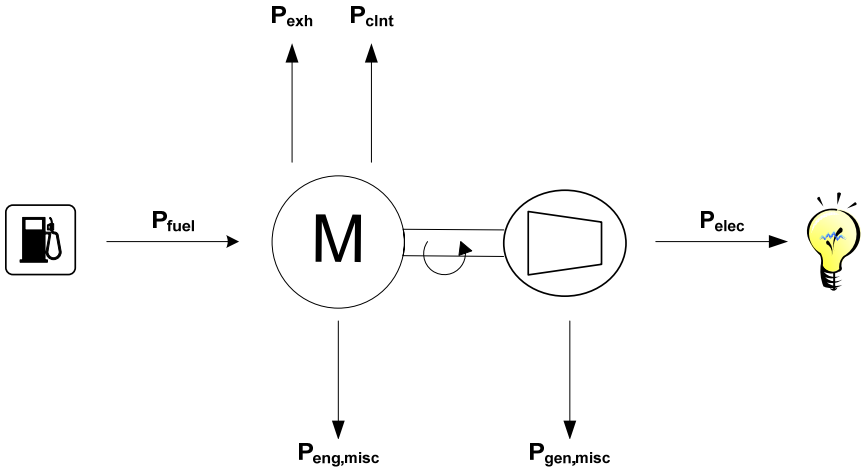

Figure 3.6: Power distribution within a diesel generator.

Sufficient data were recorded by the monitoring system to calculate the energy in the output coolant. The amount of energy being transported from the engine in the form of heated coolant, Q, can be found by the equation [14]:

$$Q = \overset{*}{m} * C_p * \Delta T \quad \text{(Eq. 3.1)}$$

The entities that need to be monitored to utilize this equation are $\overset{*}{m}$, the flow rate of the coolant through the system, and Δ*T*, the temperature difference between the coolant before and after it has passed through a radiator or heat exchanger. C_p, the specific heat of the coolant, can be obtained through lookup tables. Using 0.81 BTU/lb ºF for the specific heat of the 60/40 glycol-water mixture, the energy output through the generator coolant was calculated and equated to the amount of fuel lost due to the coolant.

The energy lost to the aftercooler and radiant heat along with the energy contained in the input fuel are the only items that remain to be found to complete the energy balance. Calculating the input fuel energy simply involved multiplying the heating value of the fuel by the instantaneous flow rate of the fuel into the engine. As the instantaneous fuel energy input was unknown due to the EESiFlo fuel flow meters malfunctioning, this information was obtained through sensors incorporated into the UAF Energy Center DEG.

Another element that needed to be calculated for the energy balance was the output energy from the aftercooler. The monitoring system built for this project did not have thermocouples in the necessary locations to perform this task and the data for these calculations had to be obtained from thermocouples that were installed as part of the Energy Center DEG. The energy output of the aftercooler was calculated by using Eq. 3.1 with 0.23 BTU/lb °F for the specific heat of air [15].

The final element that needed to be calculated for the energy balance was the radiant heat emitted by the generator. This was calculated by incorporating the engine block heat, T_b, with the temperature of the generator enclosure, T_{in}. This information was entered into Eq. 3.2 to calculate the amount of radiant heat.

$$\dot{Q} = \sigma A_b [T_b^{\,4} - T_{in}^{\,4}] \quad \text{(Eq. 3.2)}$$

The symbol σ is the Stefan-Boltzmann constant and has a value of 5.67 x 10-8 W/(K^4m^2). A_b is the surface area of the engine-generator set.

The energy output data from the aftercooler, the exhaust gas, electric generator, and coolant loop were all plotted and compared to the fuel input energy.

3.3 Village Power System Survey and Data Collection

Data was collected from a representative set of village power systems which have been instrumented with monitoring equipment by AEA. AEA provided the available power system data from a number of villages in its service territory. AEA also provided a plan of the current equipment used in some of the village power systems. Because of the variations in location,

population, and general village demographics, these villages were classified in terms of their average electric load requirement. This information was used to create a map which marks the location and average electrical load of each village represented in the survey.

3.4 Installation of Remote Monitoring Equipment

Remote monitoring equipment and switchgear upgrades were installed in 21 Alaska rural villages served by AEA using Denali Commission funding. Limited online access to the power systems including webcams in 16 of these villages was made available at (URL:http://www.aidea.org/aea/aearemotemon.html). A central server at AEA in Anchorage, Alaska and some basic remote monitoring equipment was installed in two more villages with the $60k project subcontract.

3.5 System Models

Two system models were developed in MATLAB® Simulink®: 1) for long-term performance assessment of hybrid village power systems, and 2) for economic dispatch analysis of multi-DEG systems. Our efforts were the first to include economic impacts in a simulation model of emissions from DEGs in Alaska villages.

3.5.1 Hybrid Power System Model

Integrating other energy sources into power systems in Alaska rural villages could significantly reduce fuel consumption and operating costs for DEGs. A power system model was developed specifically for Alaska rural village power systems taking into account temperature effects, rising fuel costs, and plant emissions to investigate the feasibility of integrating renewable energy sources such as wind turbines and solar PV.

3.5.1.1 Overall Hybrid Model

An overall block diagram of the model developed in MATLAB® Simulink® is shown in Figure 3.7. The details of the hybrid power system model for Alaska rural villages is presented by Ashish Agrawal in a Ph. D dissertation, *Hybrid Electric Power Systems In Remote Arctic Villages: Economic And Environmental Analysis For Monitoring, Optimization, and Control*, under the direction of the project PIs (see Ph. D. dissertation 1 under Project Publications).

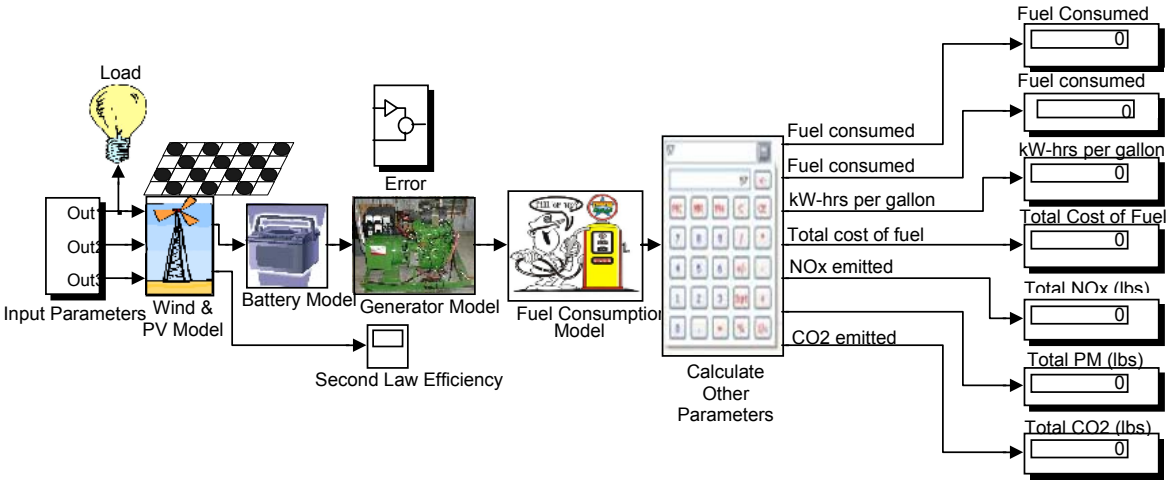

Figure 3.7: Overall PV-wind-diesel-battery hybrid power system model.

The model is used to perform an economic feasibility analysis for integrating renewable energy sources into existing DEG systems. Various hybrid power systems studied in this analysis include the diesel-battery system, the PV-diesel-battery system, the wind-diesel-battery system, and the PV-wind-diesel-battery system. Inputs to the model are the electrical load, wind, and solar profile for the village, and the manufacturer's performance curves for the DEGs, PV, wind turbines, and the battery bank. The outputs are the fuel consumption, efficiency (kW-hr/liter), total cost of fuel, and total emissions from CO_2, NO_x and PM_{10}. The life cycle costs (LCC) and sensitivity analysis of net present value (NPV), cost of energy (COE), and payback were also evaluated by porting data to Excel. The model was validated by comparing the results obtained from the Simulink® model, for supplying the annual load profile, with the available data obtained from the Hybrid Optimization Model for Energy Efficient Renewables (HOMER) software. At the time of this analysis HOMER was not set up to calculate payback period or NO_x and PM_{10} emissions.

3.5.1.1.1 DEG Model

The DEG consists of two parts: the electric generator and the diesel engine. The electric generator model consists of the efficiency curve that describes the relationship between the electrical efficiency and the electrical load on the generator. Figure 3.8 shows a typical electrical efficiency curve for a 21 kW Marathon electric generator. The performance curve data were obtained from the manufacturer of the electric generator.

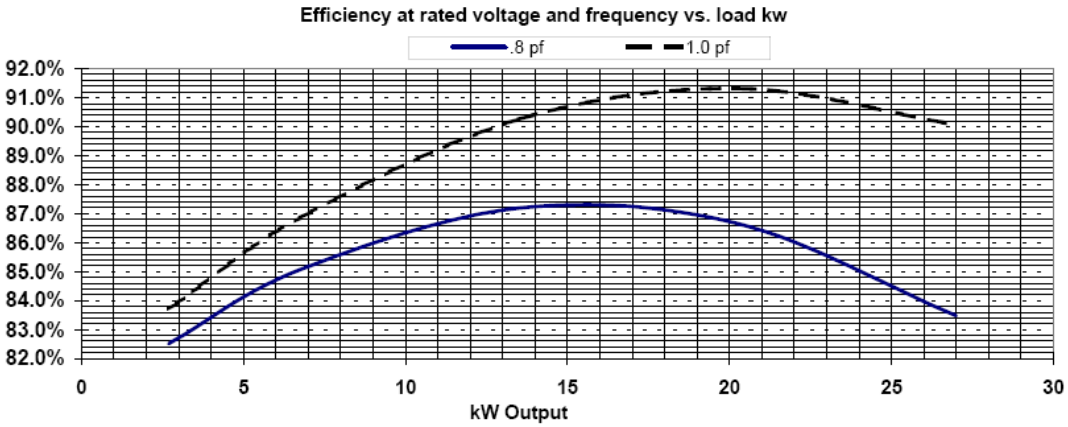

Figure 3.8: Electrical efficiency for a 21 kW Marathon electric generator [16].

A fourth order polynomial fit for the electrical efficiency curve at unity power factor and 0.8 power factor is given by Eq. 2-1 and Eq. 2-2, respectively,

$$\eta_{el1} = -6.953e-9 * L^4 + 2.932e-7 * L^3 - 9.858e-4 * L^2 + 0.201 * L + 81.372 \quad \text{(Eq. 3.3)}$$

$$\eta_{el2} = 1.540e-7 * L^4 - 4.424-5 * L^3 + 2.996e-3 * L^2 + 0.034 * L + 81.652 \quad \text{(Eq. 3.4)}$$

where 'L' is the load on the electric generator (%). The actual load on the electric generator is converted to its percentage value by dividing the actual load with the rating of the electric generator as given by Eq. 3.5,

$$\text{percentage load} = \frac{\text{actual load}}{\text{generator rating}} * 100\,. \qquad \text{(Eq. 3.5)}$$

This operation is performed so that the same efficiency equations are independent of the rating of the electric generators. The values from Eq. 3.3 and Eq. 3.4 are used to obtain the value for the electrical efficiency of the generator for any given power factor 'pf' by means of linear interpolation as follows:

$$\eta_{el} = \eta_{el2} + \left(\frac{(\eta_{el1} - \eta_{el2})}{0.2} * (pf - 0.8) \right) \qquad \text{(Eq. 3.6)}$$

where η_{el} is the electrical efficiency of the generator for a given power factor 'pf'.

The load on the diesel engine (the input to the electric generator) is obtained from the system load (the output of the electric generator) and the electrical efficiency of the generator as follows:

$$L_{eng} = \frac{L_{gen}}{\eta_{el}} \qquad \text{(Eq. 3.7)}$$

where 'L_{eng}' is the load on the engine, 'L_{gen}' is the load on the generator, and 'η_{el}' is the electrical efficiency of the generator.

The block diagram representation of Eq. 3.3 through Eq. 3.7 as developed in Simulink® is shown in Figure 3.9, and the subsystem for the electric efficiency model for the generator is shown in Figure 3.10. Inputs to the model are the percentage load on the DEG and the power factor data, while outputs from the model are the electrical efficiency (%) of the generator and the engine load (% of rated).

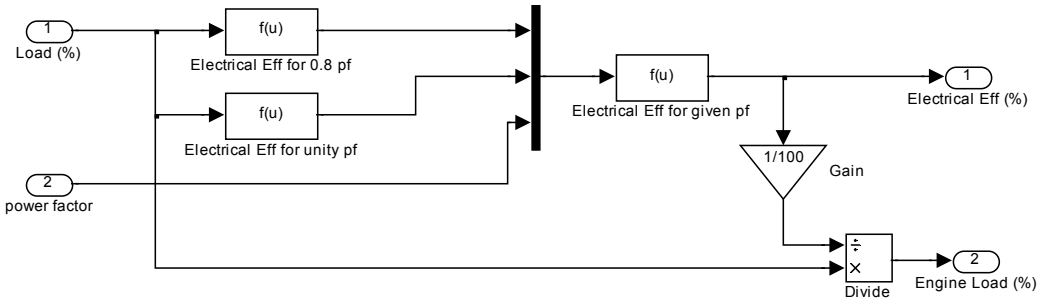

Figure 3.10: Details of the electrical efficiency model block.

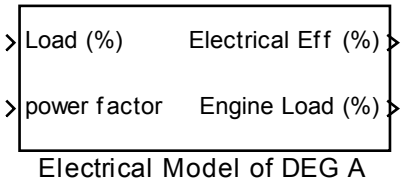

Figure 3.11: Subsystem of the electrical efficiency model for the generator.

The fuel curve for a diesel engine describes the amount of fuel consumed depending on the engine load. A typical engine fuel curve is a linear plot of load versus fuel consumption as shown in Figure 3.12 for the 24 kW John Deere DEG.

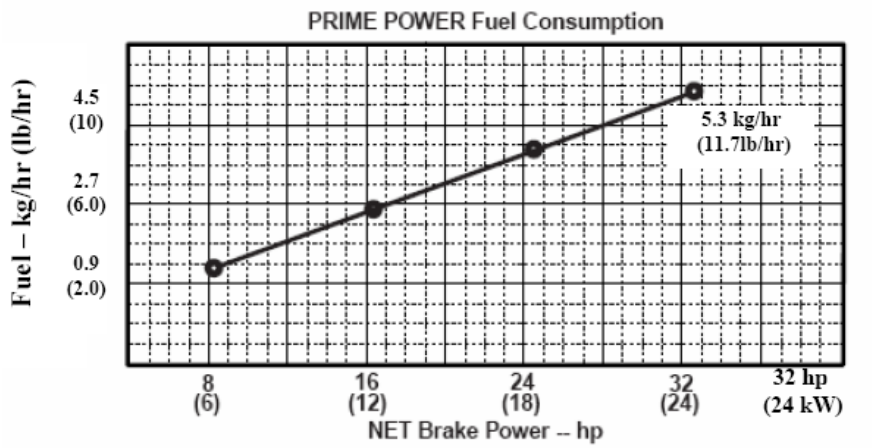

Figure 3.12: Fuel consumption curve of a 24 kW John Deere DEG [17].

The linear curve fit for the John Deere's engine fuel curve is given as:

$$\dot{F}_c = 0.5 * (L_{eng} * \frac{kW\_A}{100}) - 0.44 \qquad \text{(Eq. 3.8)}$$

$$\text{Total } F_c = \int_0^T \dot{F}_c \, .dt \qquad \text{(Eq. 3.9)}$$

where '$\dot{F}_c$' is the fuel consumption rate in kg/hr (lbs/hr), 'L_{eng}' is the percentage load on the engine, 'kW_A' is the rating of the electric generator, 'F_c' is the total fuel consumed in kg (lbs), 'dt' is the simulation time-step, and 'T' is the simulation period. The fuel consumed in kg (lbs) is obtained by multiplying the fuel consumption rate of kg/hr (lbs/hr) by the simulation time-step 'dt' (given in hours), and the total fuel consumption in kg (lbs) is obtained by integrating the term '$\dot{F}_c \, .dt$' over the period of the simulation.

The block diagram representation and the subsystem for the engine model block are shown in Figure 3.13 and Figure 3.14, respectively.

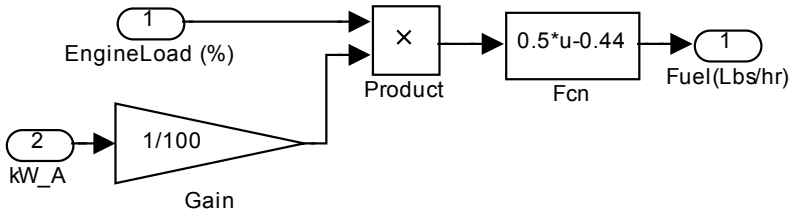

Figure 3.13: Details of the engine model block.

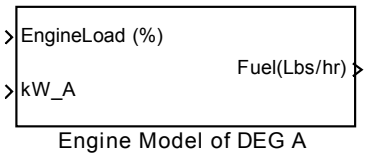

Figure 3.14: Subsystem for the engine model.

3.5.1.1.1.1 Optimization of DEG Model

When there are two DEGs to supply the load, it is important that DEGs operate optimally. In the Simulink® model, the data are supplied in such a way that DEG 1 is more efficient than DEG 2. The following steps are performed to find the optimal point of operation for DEG 2.

1) The electrical generator performance curve (Figure 3.8) and the diesel engine performance curve (Figure 3.12) are combined to obtain the overall fuel consumption for the given load profile.
2) The load on the DEGs is varied from 0 to 100%.
3) The fuel consumption for each DEG is noted at different load points.
4) The point of intersection of the two curves is the optimal point of operation for DEG 2. Beyond this point DEG 1 is more efficient than DEG 2.
5) If the two curves do not intersect, the optimal point is taken as 0. This situation implies that DEG 1 is efficient throughout the operating range of the load.

Figure 3.15 shows the overall fuel consumption curves for the two DEGs and the optimal point of operation for DEG 2. In order to avoid premature mechanical failures, it is important that DEGs operate above a particular load (generally 40% of rated). The long-term operation of DEGs on light loads leads to hydrocarbon built-up in the engine, resulting in high maintenance cost and reduced engine life [18]. In the Simulink® model, if the optimal point is less than 40% load, the optimal point is adjusted so that DEG 2 operates at or over 40% load.

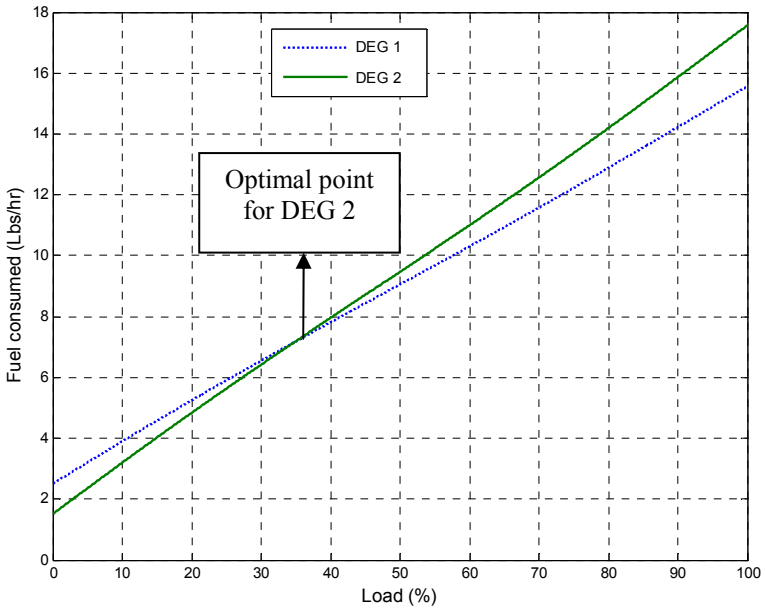

Figure 3.15: Optimal point of operation for DEG 2.

The block diagram representation and the subsystem for the optimization model are shown in Figure 3.16 and Figure 3.17, respectively. The 'DEG_Load' in Figure 3.17 is the s-function written in MATLAB® Simulink®. This s-function compares the load on two DEGs and divides the load based on the optimal point of operation.

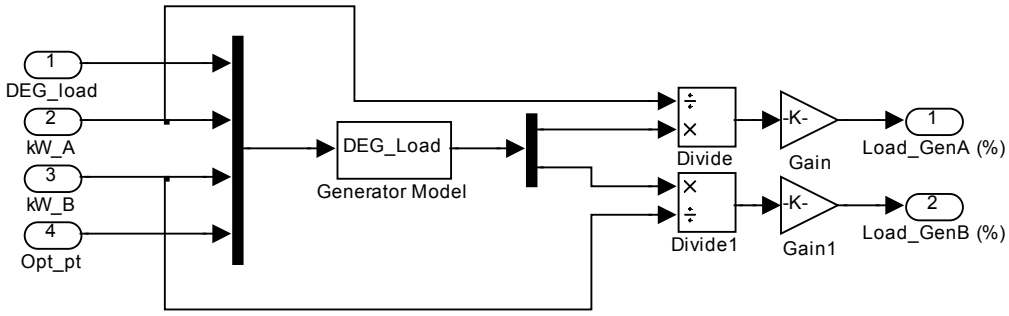

Figure 3.16: Details of the optimization model block.

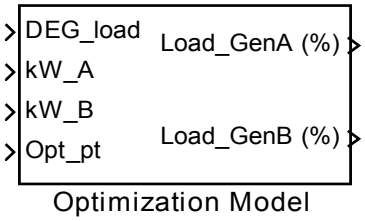

Figure 3.17: Subsystem for the optimization model

3.5.1.1.2 Heat Exchanger Model

The heat flux recovered from the jacket water of a DEG using a heat exchanger is calculated as follows [14]:

$$\dot{Q} = \eta_{HE} * \dot{m} * Cp * \Delta T \qquad \text{(Eq. 3.10)}$$

where '$\dot{Q}$' is the rate at which heat is transferred in Joules/sec (BTU/sec), 'η_{HE}' (eta_HE in Figure 3.18 and Figure 3.19) is the efficiency of the heat exchanger, '$\dot{m}$' is the mass flow rate of the coolant in kg/sec (lbs/sec), 'Cp' is the specific heat of the coolant in Joules/(kg °K) (BTU/(lb °F)), and 'ΔT' is the temperature difference in °K (°F) of the coolant in and out of the jacket. The total heat recovered 'Q' (kWh) is calculated by integrating the heat recovery rate over the entire time of the simulation and is calculated as follows:

$$Q = \int_0^T \dot{Q}.dt\,. \qquad \text{(Eq. 3.11)}$$

In addition to the total heat recovered, the heat exchanger model also calculates the total avoided pollutants including CO_2, PM_{10}, and NOx. The method used to calculate the avoided pollutants is discussed in Section 3.5.1.3.4.

The subsystem and the block diagram representation for a heat exchanger model block are shown in Figure 3.18 and Figure 3.19, respectively.

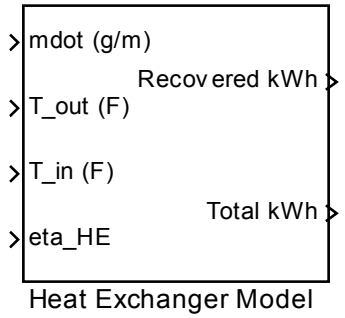

Figure 3.18: Subsystem for the heat exchanger model.

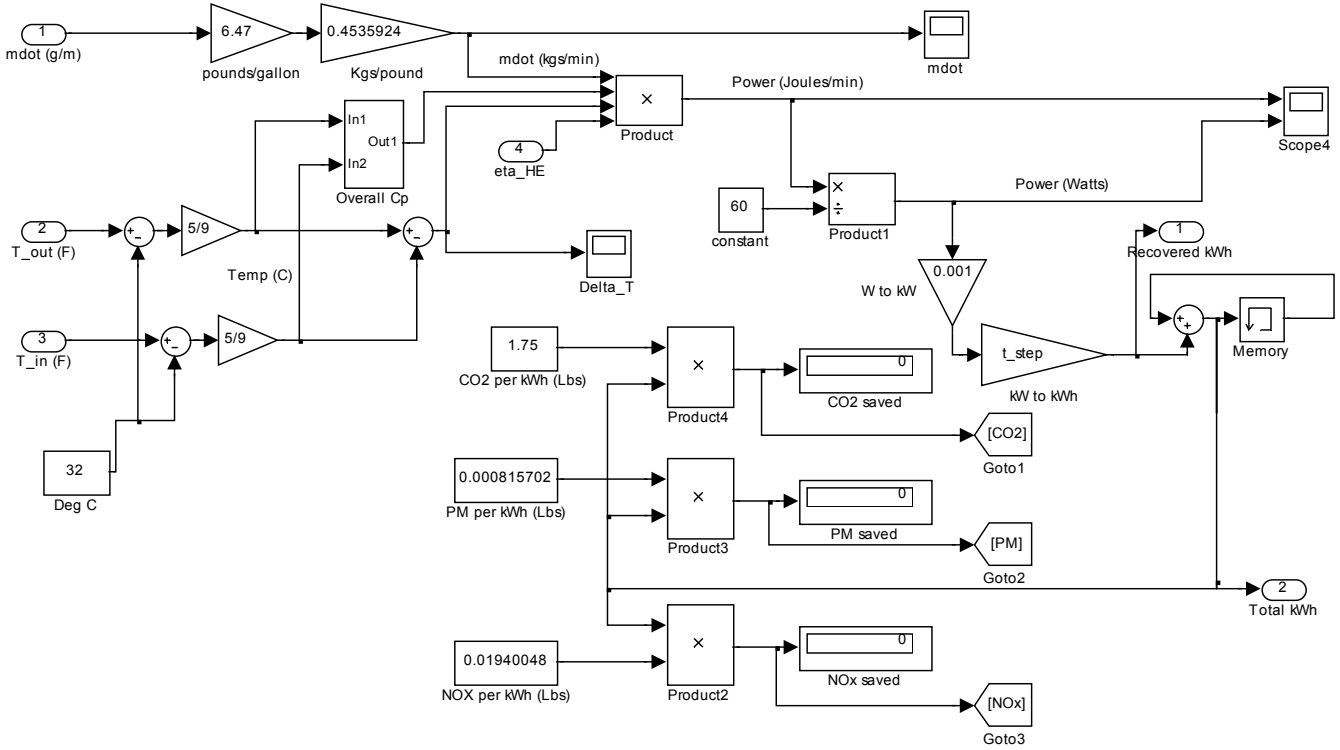

Figure 3.19: Details of the heat exchanger model block.

3.5.1.1.3 Boiler Model

The boiler model block calculates the fuel saved if the total heat recovered from the heat exchanger, given by Eq. 3.11, is supplied using a boiler. The total fuel saved is obtained using the following equation:

$$Fs = \frac{Q}{HV * \eta_b} \qquad \text{(Eq. 3.12)}$$

where 'Fs' in liters (gallons) is the total fuel saved due to the heat recovery, 'Q' is the total heat energy recovered (kWh), 'HV' is the heating value of the boiler fuel in kWh/liter (kWh/gallon), and 'η_b' (eta_boiler in Figure 3.20 and Figure 3.21) is the efficiency of the boiler.

The block diagram representation and the subsystem for the boiler model block are shown in Figure 3.20 and Figure 3.21, respectively.

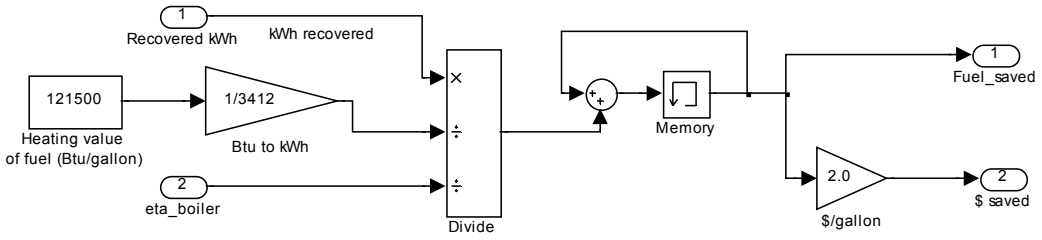

Figure 3.20: Details of the boiler model block.

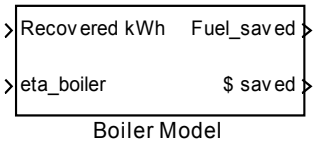

Figure 3.21: Subsystem for the boiler model.

3.5.1.1.4 WTG Model

The wind model block calculates the total power available from the wind turbines based on the power curve. The power curve gives the value of the electrical power based on the wind speed. Figure 3.22 shows the power curve for the 15/50 Atlantic Oriental Corporation (AOC) wind turbine generator [19].

The fifth order polynomial for the power curve is given as follows:

$$P_{WTG} = -4.12e-6 * S^5 + 7.58e-4 * S^4 - 5.22e-2 * S^3 + 1.59 * S^2 - 17.8 * S + 63.12 \qquad \text{(Eq. 3.13)}$$

$$E_{WTG} = \int_0^T P_{WTG}\, dt \qquad \text{(Eq. 3.14)}$$

where 'P_{WTG}' is the power output (kW) from the WTG, 'S' is the wind speed in m/s (miles/hour), 'E_{WTG}' is the energy obtained from the WTG (kWh), 'T' is the simulation time (hours), and 'dt' is the simulation time-step (hours).

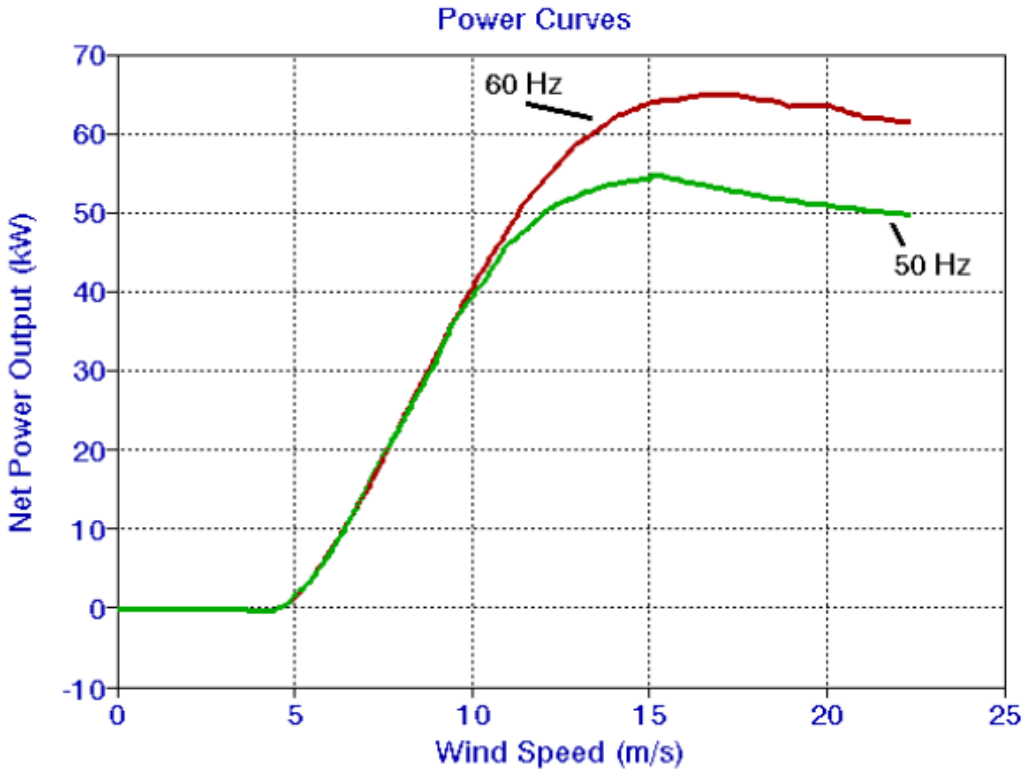

Figure 3.22: Power curve for 15/50 Atlantic Oriental Corporation WTG [[18]].

The wind model block also calculates the second law efficiency of the WTG. The second law efficiency of the WTG is given as follows:

$$\eta_{second\_law} = \frac{actual\_power}{max\_possible\_power} \qquad \text{(Eq. 3.15)}$$

where 'η_{second_law}' is the second law efficiency of the WTG, 'actual_power' is the actual power output from the WTG and 'max_possible_power' is the maximum possible power output from the WTG.

The actual power of the wind turbine is obtained from the manufacturer's power curve given by Eq. 3.13 and the maximum possible power is obtained from the Betz formula described in [20] and given as follows:

$$P_{max} = \frac{1}{2}\rho.A.V^3.0.59 \qquad \text{(Eq. 3.16)}$$

where 'P_{max}' is the maximum possible power, 'ρ' is the density of air taken as 1.225 kg/m^3 (0.076 lb/ft^3) at sea level, 1 atmospheric pressure i.e. 101.325 kPa (14.7 psi), and a temperature of 15.55°C (60°F), 'A' is the rotor swept area in m^2 (ft^2), 'V' is the velocity of wind in m/s (miles/hour), and the factor '0.59' is the theoretical maximum value of power coefficient of the rotor (Cp) or theoretical maximum rotor efficiency which is the fraction of the upstream wind power that is captured by the rotor blade.

The air density 'ρ' can be corrected for the site specific temperature and pressure in accordance with the gas law and is given as follows:

$$\rho = \frac{p}{RT} \qquad \text{(Eq. 3.17)}$$

where 'ρ' is the density of air, 'p' is the air pressure, 'R' is the gas constant, and 'T' is the temperature.

It should be noted from Eq. 3.16 that the wind power varies with the cube of the air velocity. Therefore, a slight change in wind speed results in a large change in the wind power.

The block diagram representation and the subsystem for the wind model are shown in Figure 3.23 and Figure 3.24, respectively.

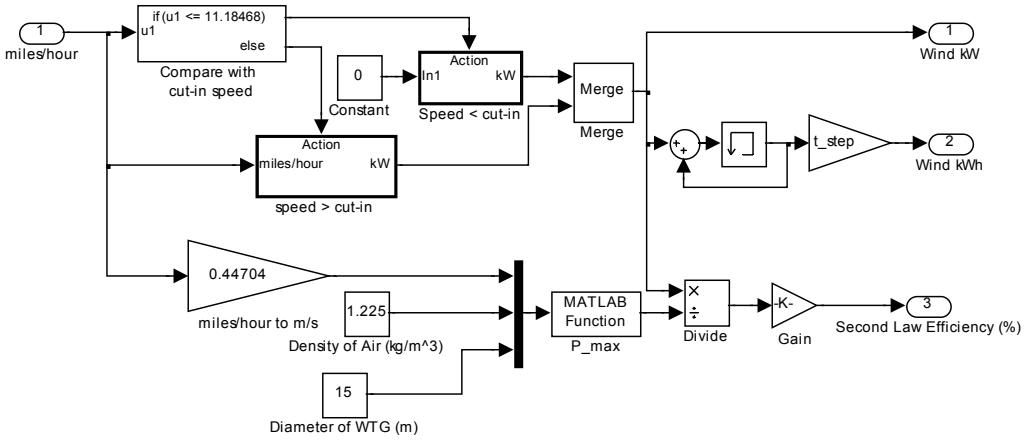

Figure 3.23: Details of the wind model block.

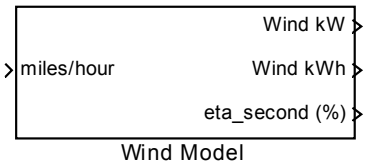

Figure 3.24: Subsystem for the wind model.

3.5.1.1.5 PV Model

The PV model block calculates the PV power (kW) and the total PV energy (kWh) supplied by the PV array using the following equations:

$$P_{PV} = \eta_{pv} * ins * A * PV \quad \text{(Eq. 3.18)}$$

$$E_{PV} = \int_0^T P_{PV}.dt \quad \text{(Eq. 3.19)}$$

where 'P_{PV}' is the power obtained from the PV array (kW), 'η_{pv}' is the efficiency of the solar collector, 'ins' is the solar insolation (kWh/m^2/day), 'A' is the area of the solar collector/kW, 'PV' is the rating of the PV array (kW), and E_{PV} is the total energy obtained from the PV array.

The efficiency of the solar collector is obtained from the manufacturer. The solar insolation values are available from the site data or can be obtained by using the solar maps from the National Renewable Energy Laboratory website [21]. The area of the solar collector depends on the number of PV modules and the dimensions of each module. The number of PV modules depends on the installed capacity of the PV array and the dimensions of each PV module are obtained from the manufacturer's data sheet.

The block diagram representation and the subsystem for the PV model block are shown in Figure 3.25 and Figure 3.26, respectively.

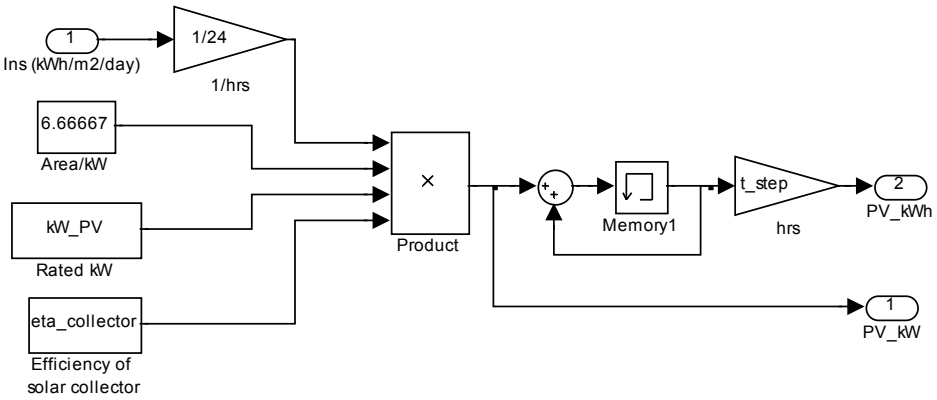

Figure 3.25: Details of the PV model block.

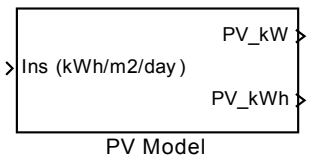

Figure 3.26: Subsystem for the PV model.

3.5.1.1.6 Battery Model

In the Simulink® model, the battery-bank is modeled so that the battery-bank acts as a source of power, rather than back-up power. The battery model block controls the flow of power to and from the battery bank. A roundtrip efficiency of 90% is assumed for the battery charge and discharge cycle. The battery model incorporates the effect of ambient temperature as described in [22] into the hybrid power system model. Therefore, the model can be used for cold region applications. The manufacturer's data sheet for the battery-bank is available in Appendix 5. The details of the battery model block are shown in Figure 3.27.

The details of the temperature dependent available battery energy model are shown in Figure 3.28 and the subsystem for the battery model is shown in Figure 3.29.

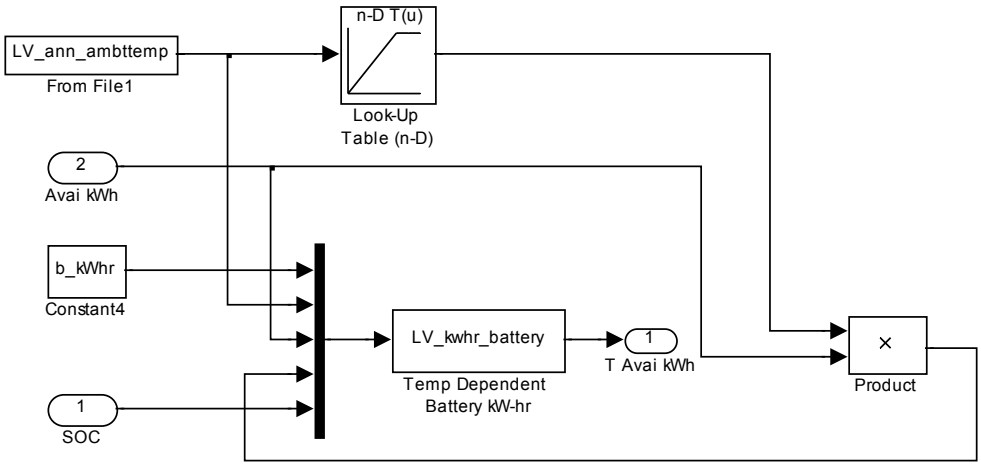

Figure 3.28: Details of the temperature dependent available battery energy model.

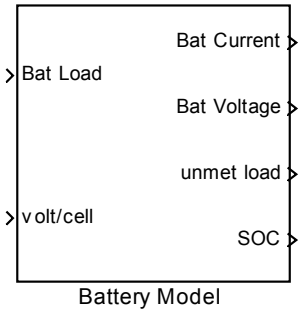

Figure 3.29: Subsystem for the battery model.

The life of the battery bank depends on the depth of discharge and the number of charge discharge cycles. In the Simulink® model the battery-bank is modeled so that it acts as a source of power rather than back-up power. Therefore, the depth of discharge of the battery-bank is assumed between 95% and 20% of the rated capacity. This higher depth of discharge reduces the number of battery operating cycles for the same energy output. It should be noted that the number of battery cycles plays a more significant role in the life of the battery-bank.

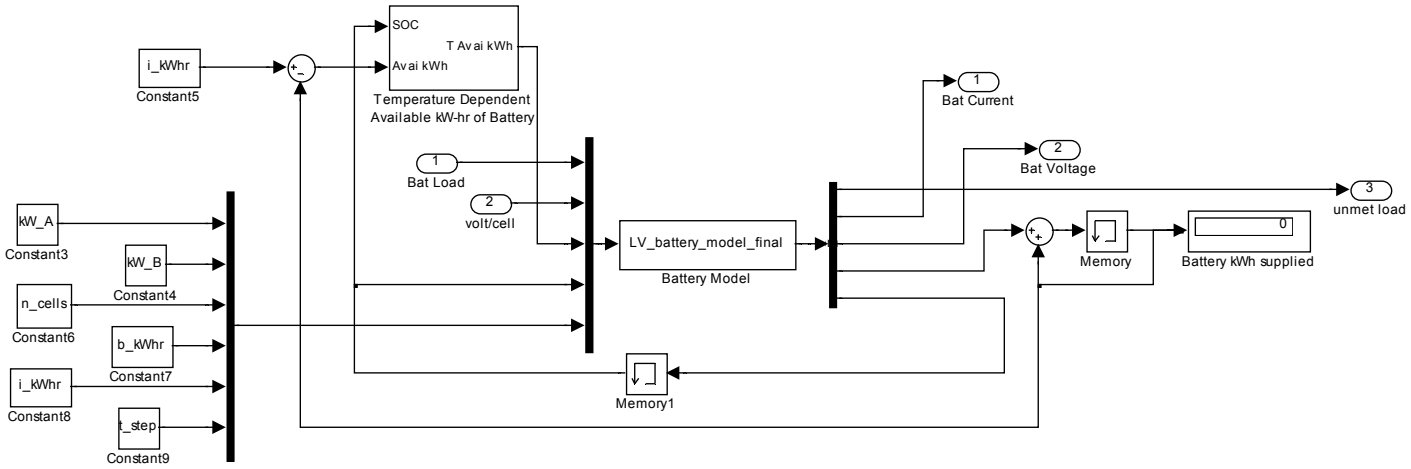

Figure 3.27: Details of the battery model block.

3.5.1.2 Economic Parameters Used in the Model

It is very important for the system designer to get acquainted with different economic parameters used in the modeling process of hybrid power systems. Economic parameters are used to calculate the COE, the payback period, and the life cycle cost of the system. The various economic parameters used in the hybrid power system model are discussed in the following sections [23].

3.5.1.2.1 Investment Rate, Inflation Rate, and Discount Rate

The investment rate is the percentage rate at which the value of money increases every year.

Inflation rate is the tendency of prices to rise over time. Inflation rate takes into account the future price rise in the project commodities including fuel and different power system components.

Discount rate is the difference between the investment rate and the inflation rate. Discount rate is generally used in life cycle cost analysis calculations.

$$\text{Discount rate} = \text{Investment rate} - \text{Inflation rate}. \quad \text{(Eq. 3.20)}$$

3.5.1.2.2 Life Cycle

The life cycle is the life-time of the project. It is the time at the end of which the system components require replacement.

3.5.1.2.3 Net Present Value

The net present value (NPV) is the money that will be spent in the future discounted to today's money. The NPV plays an important role in deciding the type of the system to be installed. The NPV of a system is used to calculate the total spending on the installation, maintenance, replacement, and fuel cost for the type of system over the life-cycle of the project. Knowing the NPV of different systems, the user can install a system with minimum NPV. The different equations used in the calculation of NPVs are given as follows:

$$P = \frac{F}{(1+I)^N} \quad \text{(Eq. 3.21)}$$

$$P = \frac{A[1-(1+I)^{-N}]}{I} \quad \text{(Eq. 3.22)}$$

where 'P' is the present worth, 'F' is the money that will be spent in the future, 'I' is the discount rate, 'N' is the year in which the money will be spent, and 'A' is the annual sum of money.

3.5.1.2.4 Life Cycle Cost

The life cycle cost (LCC) is the total cost of the system over the period of its life cycle including the cost of installation, operation, maintenance, replacement, and the fuel cost. The life cycle cost also includes the interest paid on the money borrowed from the bank or other financial institutes to start the project. The life cycle cost of the project can be calculated as follows:

$$LCC = C + M + E + R - S \quad \text{(Eq. 3.23)}$$

where 'LCC' is the life cycle cost, 'C' is the installation cost (capital cost), 'M' is the overhead and maintenance cost, 'E' is the energy cost (fuel cost), 'R' is the replacement and repair costs, and 'S' is the salvage value of the project.

3.5.1.2.5 Payback Period

Payback period is the time in which the total extra money invested in a project is recovered and is given as,

$$\text{Payback Period} = \frac{\text{Extra Investment}}{\text{Rate of Return}}. \qquad \text{(Eq. 3.24)}$$

Payback period is the major deciding factor for the feasibility of the project. If the payback period of the system is less than the life cycle of the system, the project is economically feasible.

3.5.1.3 Environmental Parameters in the Model

The different environmental parameters in the analysis of the Simulink® model include carbon dioxide (CO_2), nitrogen oxide (NOx), and particulate matter (PM_{10}). The environmental parameters are discussed in detail in the following sections.

3.5.1.3.1 Carbon Dioxide (CO_2)

CO_2 is released in the atmosphere due to the combustion of fossil fuels including coal, oil, natural gas, wood, and biomass. In the Simulink® model the total CO_2 was calculated based on the equation for the combustion of diesel fuel. For example, one empirical formula for light diesel $C_nH_{1.8n}$ is given in [24]. For this empirical formula, with 0 % excess air the combustion reaction is given as follows:

$$\begin{aligned} C_nH_{1.8n} + (1.45n)(O_2 + 3.76N_2) = \\ nCO_2 + 0.9nH_2O + (1.45N_2)(3.76N_2). \end{aligned} \qquad \text{(Eq. 3.25)}$$

For any n, the mass in kg (lb) of CO_2 per unit mass in kg (lb) of fuel = 44/(12 + 1.8) = 3.19. So, to get the emissions per unit electrical energy output, the above is combined with an engine efficiency of 3.17 kWh/liter (12 kWh/gallon) and a fuel density of 0.804 kg/liter (6.7 lb/gallon). Doing this results in specific CO_2 emissions of 3.1*(0.804/3.17) = 0.786 kg (1.73 lb) of CO_2 per kWh of electricity. This figure of 0.786 kg/kWh (1.73 lb/kWh) agrees closely with the data obtained from the manufacturer 0.794 kg/kWh (1.75 lb/kWh). The annual CO_2 amount was calculated from the lb CO_2/kWh and the annual kWh produced and is given as follows:

$$\text{Total pollutant in kg (lb)} = \frac{\text{pollutant}}{\text{kWh}} * \text{kWh}_{\text{Gen}} \qquad \text{(Eq. 3.26)}$$

where kWh_{Gen} is the total kWh supplied by the diesel generator during the simulation period.

3.5.1.3.2 Nitrogen Oxide

Nitrogen oxide (NOx) is one pollutant responsible for acid rain and is the major source for the formation of ground ozone. In the Simulink® model, the total NOx emitted is calculated based on

the value of 0.0088 kg (0.0194 lb) of NOx per kWh of electricity produced, as obtained from the manufacturer. The annual NOx was calculated using Eq. 3.26.

3.5.1.3.3 Particulate Matter

Particulate matter (PM) is the complex mixture of extremely small particles and liquid droplets. During the combustion of diesel fuel, PM may contain carbon particles and unburned hydrocarbons. In the Simulink® model, the total PM was calculated based on the value of 0.00037 kg (0.00082 lb) of PM_{10} per kWh of electricity produced as obtained from the manufacturer. The annual PM_{10} was calculated using Eq. 3.26.

3.5.1.3.4 Avoided Cost of Pollutants

Generally, a power plant incorporating renewable energy is more expensive than a non-renewable energy plant because of the high installation cost associated with the renewable energy systems. The avoided cost of pollutants is the extra cost associated with the low emissions power plant (the plant incorporating renewable energy sources) due to the use of renewable energy. The avoided cost of pollutants is given as follows [25]:

$$AC = \frac{COE_L - COE_H}{E_H - E_L} \qquad \text{(Eq. 3.27)}$$

where 'AC' is the avoided cost of pollutants in USD/metric ton (USD/US ton), 'COE_L' is the COE from the low emissions plant, 'COE_H' is the COE from the high emissions plant, 'E_H' is the amount of emissions from the high emissions plant in metric ton (US ton), and 'E_L' is the amount of emissions from the low emissions plant in metric ton (US ton).

3.5.2 DEG Model with Economic Dispatch

Rural utilities that do not have automated control and monitoring systems that perform economic dispatch (ED) must rely on operators to regulate system efficiency; however, an automated control system has the capability of accurately regulating system efficiency through economic dispatch and unit commitment [3]. In isolated villages with multiple generating units, the use of classical ED and normal unit commitment does not ensure a system is running at its most efficient point. In these villages where large fluctuations in load can occur, having the ability to bring units online or take units offline can help to ensure that the system is running efficiently. This type of automated control is a combination of economic dispatch and unit commitment running in real-time. An analysis tool was developed for economic load dispatch taking into account the fuel efficiency curves, the output power factor, and the thermodynamic model of each DEG.

3.5.2.1 Overall DEG Model

An overall block diagram of the thermodynamic model of the DEG developed in MATLAB® Simulink® is shown in Figure 3.30. This is a more detailed model than that presented in Section 3.5.1.1.1 for the hybrid power system model. The complete diesel generator model calculates the fuel consumed by a single diesel generator based on inlet air temperature, exhaust air temperature, diesel engine specifications, and the heating value of the fuel. The fuel consumed is also adjusted to meet manufacturer's fuel consumption data at standard operating temperatures. The details of the DEG model and the economic dispatch algorithm are presented by Larre Brouhard in a master's thesis, *Economic Dispatch and Control for Efficiency*

Improvements on Diesel Electric Power Systems in Alaska Rural Villages, under the direction of the project PIs (see MS Thesis 1 under Project Publications).

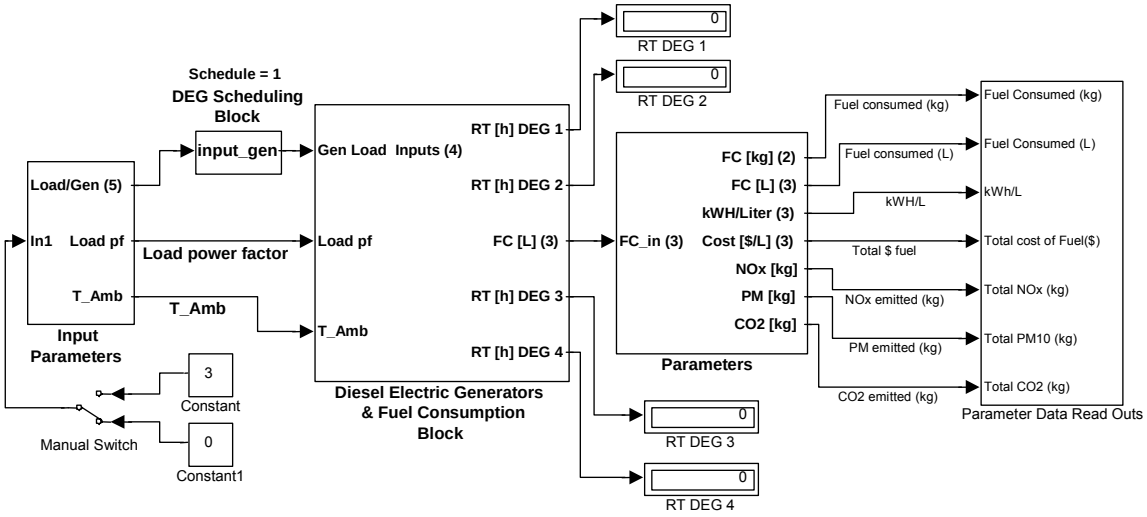

Figure 3.30: Overall Thermodynamic Model of DEG for Economic Dispatch

3.5.2.2 DEG Thermodynamic Model Block

The internal diagram and setup of the *DEG* block is illustrated in Figure 3.31. The *DEG* block consists of many sub-blocks which are described in detail in Chapter 4 of Larre Brouhard's M. S. thesis *Economic Dispatch and Control for Efficiency Improvements on Diesel Electric Power Systems in Alaska Rural Villages*. The inputs to the *DEG* blocks are data that come in from other blocks within the simulation or external data files.

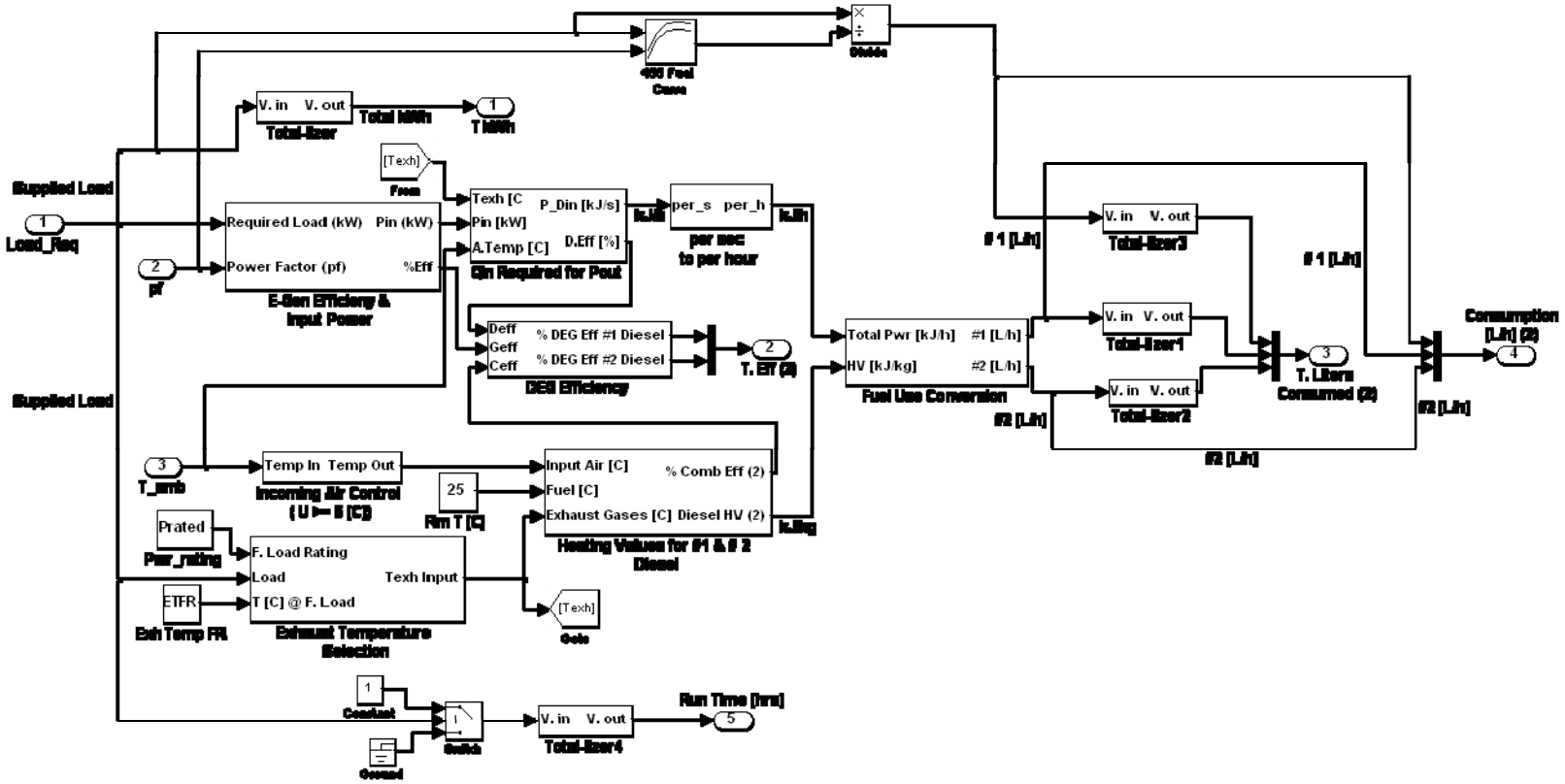

Figure 3.31: *DEG Model* internal diagram.

These other forms of input values are:

- Diesel Generator Power Rating [kW]
- Diesel Generator Power Factor Rating
- Diesel Engine Compression Factor – *Rc*
- Diesel Engine Exhaust Temp at Rated Power [C] – *ETFR*
- Fuel Rating: Temperature [C] – *Trated*
- DEG Performance Curves: Power Variables [Vector] – *Eff_pwr_G*
- DEG Performance Curves: Efficiency Variables [Vector] – *Eff_eff_G*
- DEG Performance Curves: Power Factor Variables [Vector] – *Eff_pf_G*
- Efficiency Adjustment Parameters for Power [Table Row] – *AdjEff_p*
- Efficiency Adjustment Parameters for Efficiency [Table Column] – *AdjEff*
- Fuel Curve Manufacturers Data: Power [kW] – *fulcrv_pwr*
- Fuel Curve Manufacturers Data: Power Factor – *fulcrv_pf*
- Fuel Curve Manufacturers Data: Fuel Efficiency[L/kWh] – *fulcrv_eff*

The input values above are either directly input or referenced by variables within a parameter window.

The outputs of the *DEG* block are *T kWh* total power in (kW) produced per hour, *T.Eff* overall efficiency for the generator, *T. Liters Consumed* total fuel consumed by fuel type, *Consumption [L/h]* fuel consumption rate of the generator by fuel type, *Run Time [hrs]* the amount of time that the generator was in operation, and *kWh/L* efficiency of generator at each time step in energy (kWh) per liter of fuel.

3.5.2.2.1 DEG Block: Exhaust Temperature Selection

From examining data on the UAF Energy Center diesel generator as the load on the generator changes there is a corresponding change in the exhaust temperature. Therefore, to more accurately show how exhaust temperature may affect the efficiency of the diesel a sub-block to calculate changes in the exhaust temperature from the rated value was created. Figure 3.32 shows the diagram of the *Exhaust Temperature Selection* block.

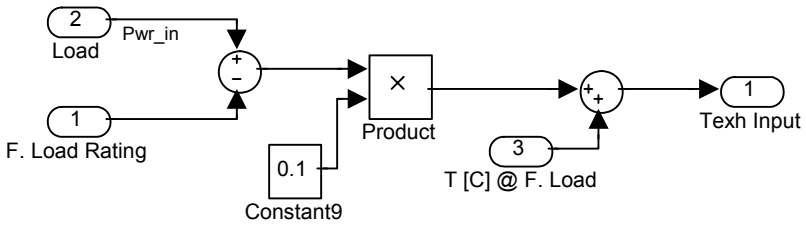

Figure 3.32: Diagram of the *Exhaust Temperature Selection* block.

The *Exhaust Temperature Selection* block subtracts the generators full load rating the full load exhaust temperature rating to establish a change in exhaust temperature with varying load requirements. Multiplying by $1/10^{th}$ was chosen due to the observation that the temperature for the UAF diesel's exhaust increased approximately one degree Celsius for every 10 kW. This value was based on an average change in temperature. The output of the *Exhaust Temperature Selection* block is then used by the *E-Gen Efficiency & Input Power* and *Heating Values For #1 & #2 Diesel* blocks.

3.5.2.2.2 DEG Block: E-Gen Efficiency & Input Power

Manufacturer's specification sheets contain information on the diesel engine and/or AC generator. This information usually includes the fuel consumption at various loads of the diesel generator as a set or on just the diesel engine. The fuel consumption data is often listed within a table. However, the fuel consumption data can also be given as a figure which requires conversion into a data set for implementation in this simulation model.

The fuel consumption of the diesel generator or diesel engine is usually based on steady state operating conditions at a specific temperature, pressure, and fuel type. The curve defined by this data, as seen in Figure 3.33, does not lend itself to calculation of fuel consumption with variable parameters such as intake air temperatures, fuel temperatures, and exhaust temperature. Since this simulation is to study the effects of how changing load and ambient temperature may affect the efficiency of the diesel generator set, an adaptation of the diesel cycle and diesel combustion formula is utilized for such analysis and is discussed in Section 3.5.2.2.2.1.

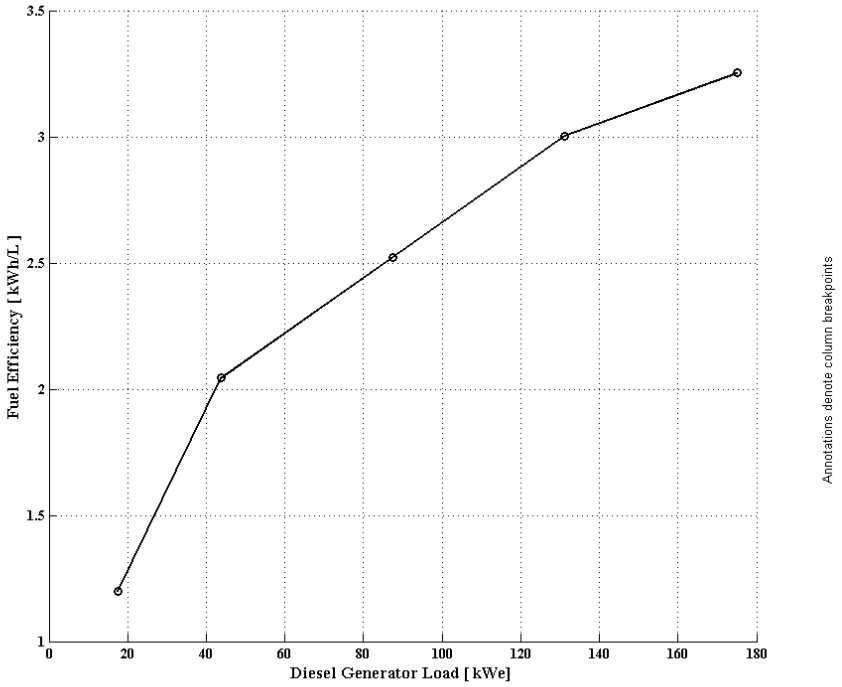

Figure 3.33: CATERPILLAR® 175 kWe diesel generator fuel consumption efficiency in kWh/L [26].

To analyze the temperature effects of both the inlet air and exhaust air on diesel efficiency, a model block of the diesel engine was necessary and is seen in Figure 3.34.

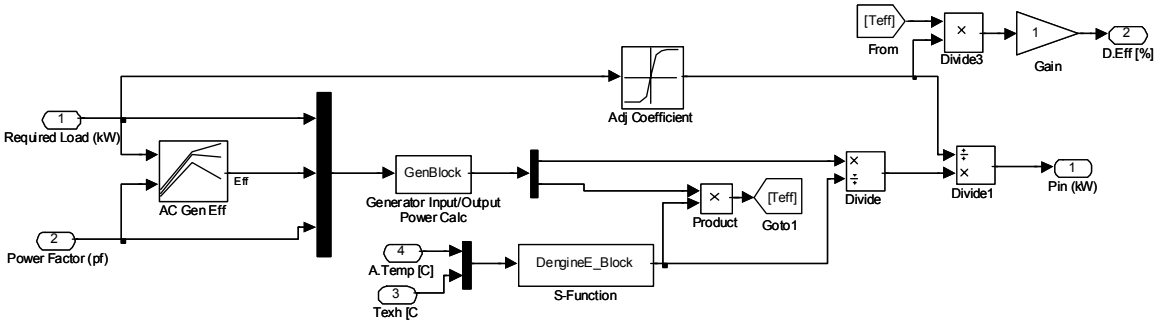

Figure 3.34: Internal structure of *DEG Efficiency* block.

3.5.2.2.2.1 Engine Efficiency Calculation Block: DengineE_Block

The model in Figure 3.34 utilizes the Diesel cycle to calculate the diesel engines efficiency. This calculation is programmed into the S-function *DengineE_Block*. Figure 3.35 illustrates the curves associated with the Diesel cycle.

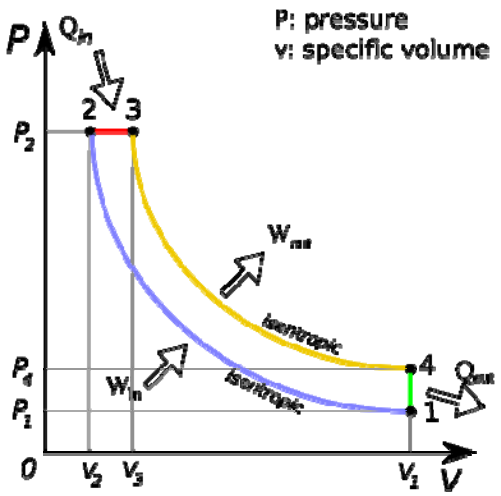

Figure 3.35: Diesel Cycle P-*v* diagram [27].

The equations that are derived from the Diesel cycle are as follows [24]:

$$r = \frac{V_1}{V_2}, \qquad \text{(Eq. 3.28)}$$

$$r_c = \frac{V_3}{V_2}, \qquad \text{(Eq. 3.29)}$$

$$V_4 = V_1, \qquad \text{(Eq. 3.30)}$$

where V_1, V_2, V_3, and V_4 are the volumes of the piston at each point in the cycle. Eq. 3.28 shows that r (compression ratio) is a ratio of volumes at points 1 and 2 of the diesel cycle and r_c (exhaust ratio) is a ratio of volumes between points 2 and 3 of the Diesel cycle.

Process 1-2 is isentropic compression of an ideal gas given constant specific heats:

$$T_2 = T_1\left(\frac{V_1}{V_2}\right)^{k-1}, \qquad \text{(Eq. 3.31)}$$

$$P_2 = P_1\left(\frac{V_1}{V_2}\right)^{k}, \qquad \text{(Eq. 3.32)}$$

where T_1 is the inlet temperature, T_2 is the temperature of the working fluid after compression, P_1 and P_2 is the pressure within the cylinder at points 1 and 2, and k is the specific heat ratio value of air at room temperature.

Process 2-3 is constant pressure heat addition to an ideal gas:

$$P_3 = P_2, \quad \text{(Eq. 3.33)}$$

$$\frac{P_2 V_2}{T_2} = \frac{P_3 V_3}{T_3} \rightarrow T_3 = T_2\left(\frac{V_3}{V_2}\right), \quad \text{(Eq. 3.34)}$$

where P_3 is the cylinder pressure and T_3 is the temperature at point 3.

Process 3-4 is isentropic expansion of an ideal gas given constant specific heats:

$$T_4 = T_3\left(\frac{V_3}{V_4}\right)^{k-1}, \quad \text{(Eq. 3.35)}$$

$$P_4 = P_3\left(\frac{V_3}{V_4}\right)^{k}, \quad \text{(Eq. 3.36)}$$

where P_4 (exhaust pressure) is the cylinder pressure and T_4 (exhaust temperature) is the temperature at point 4 of the Diesel cycle.

From the above equations diesel thermal efficiency can be calculated by the following equation:

$$\eta_{th,Diesel} = \frac{w_{net}}{q_{in}} = 1 - \frac{q_{out}}{q_{in}} = 1 - \frac{T_4 - T_1}{k(T_3 - T_2)}, \quad \text{(Eq. 3.37)}$$

where $\eta_{th,Diesel}$ is the thermal efficiency of the ideal Diesel cycle, w_{net} is the net work of the cycle, q_{in} is the heat transferred into the working fluid, and q_{out} is the heat transferred out of the working fluid.

The variables that are given for calculation of efficiency are: T_1, T_4, and r. T_4 and r are given by the manufacturer's data sheet and T_1 is a variable determined by the ambient air temperature. Calculation of the diesel engine efficiency requires knowing T_2 and T_3. T_2 is easily calculated using Eq. 3.31. The calculation of T_3 requires knowing r_c and the calculation of r_c can be accomplished by algebraic manipulation utilizing the relationships defined in Eqs. 3.28 - 3.30 as follows:

$$T_4 = T_3\left(\frac{V_3}{V_4}\right)^{k-1} = T_3\left(\frac{r_c V_2}{V_1}\right)^{k-1} = T_3\left(\frac{r_c}{V_1}\left\{\frac{V_1}{r}\right\}\right)^{k-1} = T_3\left(\frac{r_c}{r}\right)^{k-1}. \quad \text{(Eq. 3.38)}$$

Now, factoring the exponent and substituting the relationship between T_2 and T_3 we get:

$$T_4 = \frac{T_2 r_c (r_c)^{k-1}}{r^{k-1}} = \frac{T_2 r_c^k}{r^{k-1}}, \quad \text{(Eq. 3.39)}$$

Solving for r_c,

$$r_c = \left[\frac{T_4\left(r^{k-1}\right)}{T_2}\right]^{1/k} = \left(\frac{T_4}{T_1}\right)^{1/k}, \quad \text{(Eq. 3.40)}$$

T_3 can then be calculated using r_c and the four temperatures can be input into Eq. 3.37 to find the diesel thermal efficiency based on inlet and outlet temperatures. Another method to calculate thermal efficiency is to use the values of r, r_c, and *k* directly into the thermal efficiency equation re-arranged as a function of r, r_c, and *k* as seen in Eq. 3.41 below.

$$\eta_{th,Diesel_c} = \frac{1}{r^{k-1}}\left[\frac{r_c^{k-1}}{k(r_c - 1)}\right], \quad \text{(Eq. 3.41)}$$

However, it must be noted here that the value of r_c is calculated by using the exhaust temperature, T_4 rating of the DEG based on the manufacturer's data and an inlet temperature, T_1 at STP which is 25 °C. Since the values of T_1 and T_4 used in the calculation of r_c remain constant for a given diesel engine, r_c will remain constant for a given diesel electric generator. This means that the ratio T_4/T_1 must remain constant as well. This, combined with a constant r, results in a constant ideal cycle efficiency, since the efficiency becomes dependant only on r, r_c, and *k* seen in Eq. 3.41. For this thesis it is assumed that r and r_c are to remain constant. The changes in diesel generator efficiency that are seen in the simulation are not directly due to temperature effects on the diesel cycle, but are an effect of temperature on combustion discussed in a following section. However, if r_c was based on T_4, an increase in efficiency would be seen for an increase in inlet temperature. The S-function *DengineE_Block* contains a program script for the calculation of diesel thermal efficiency.

3.5.2.2.2.2 Adjustment Coefficient Table Construction

The thermal efficiency of the diesel generator calculated by the model does not take into account thermal losses. Therefore, to more accurately define the efficiency of the diesel generator at standard operating conditions the curves of diesel thermal efficiency and the efficiency based on the manufacturer's curves *Fuel Curve* block are compared to create a table that defines the percentage of losses, this table is the *Adj Coefficient* block in Figure 3.36 and is determined by the *Adjustment Coefficient Simulation* seen in Figure 3.37. This allows the simulation when run at standard operating conditions for the generators to calculate fuel consumption equal to that of the manufacturer's curves. Now, when there is a change in operating temperatures the final efficiency will account for thermal and mechanical losses within the generator.

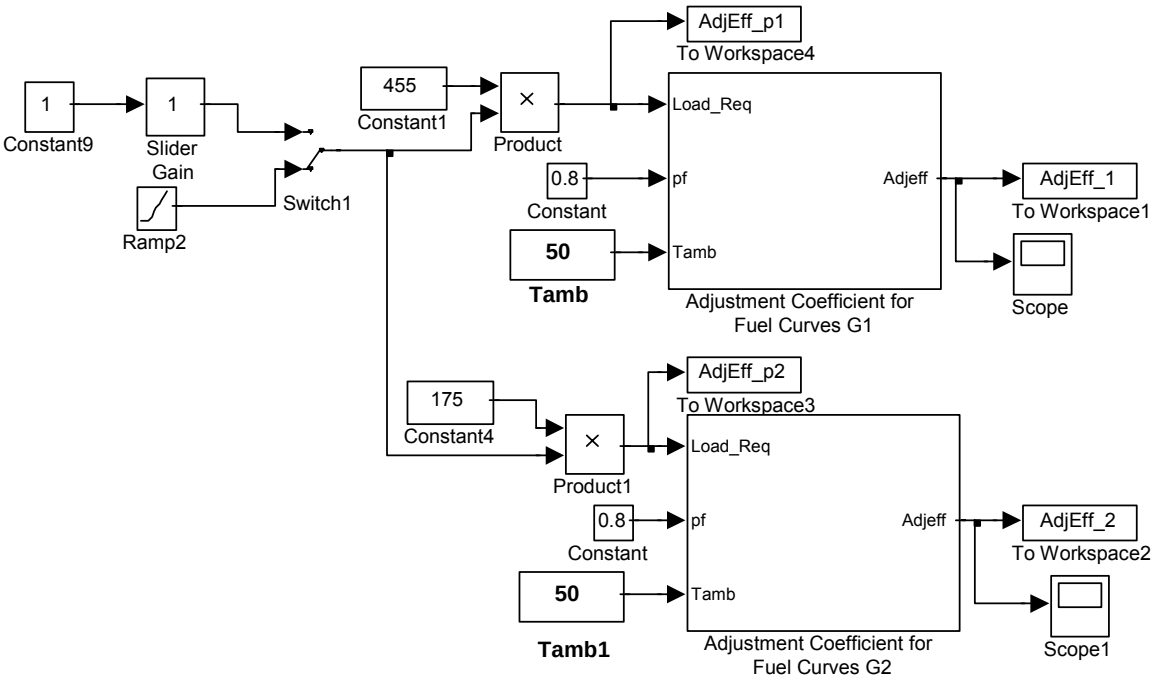

Figure 3.36: Efficiency adjustment calculation simulation diagram.

These thermal losses are affected by factors such as the difference between ambient room temperature and the generator's operating temperature. However, these factors affecting the thermal losses are not considered in this model for simplicity and computational time considerations. If we were to include these losses, we could say the convective heat loss rate from the engine to the surroundings decreases as T_{amb} increases. This is because this loss rate is proportional to $T_{eng} - T_{amb}$ which decreases as T_{amb} increases. Here, T_{eng} is the engine surface temperature and T_{amb} is the ambient temperature.

To calculate the diesel efficiency from the manufacturer's curves requires knowing what other parameters and conditions the data is based on. This information is included on the data sheets. For example, for the 445 kWe CATERPILLAR® diesel, the manufacturer's curves are based on steady state operating conditions of 25 °C and fuel rates based on #2 diesel fuel with a LHV of 42780 kJ/kg when used at 29 °C and weighing 0.08389 kg/L [28]. By taking this information and the fuel consumed for a value of output power in kWe, the overall percent efficiency between the fuel input and the electrical output for the diesel electric generator can be calculated based on manufacturer's data.

The following equation demonstrates these calculations and its representative Simulink® equivalent can be seen in the upper portion of Figure 3.34 showing the process diagram in the simulation.

$$\%Eff_{DEG} = Load(\frac{1}{Eff_{fuel}})\rho_{fuel} LHV_{fuel}\left(\frac{h}{3600s}\right), \qquad \text{(Eq. 3.42)}$$

where $\%Eff_{DEG}$ is the diesel generator efficiency in percent, $Load$ is the load to be supplied by the generator in kW, $\%Eff_{fuel}$ is the efficiency of the generator supplied by the manufacturer's curve in (kWh/L), ρ_{fuel} is the density of the fuel, and LHV_{fuel} is the heating value of the fuel supplied on the manufacturer's specification sheet.

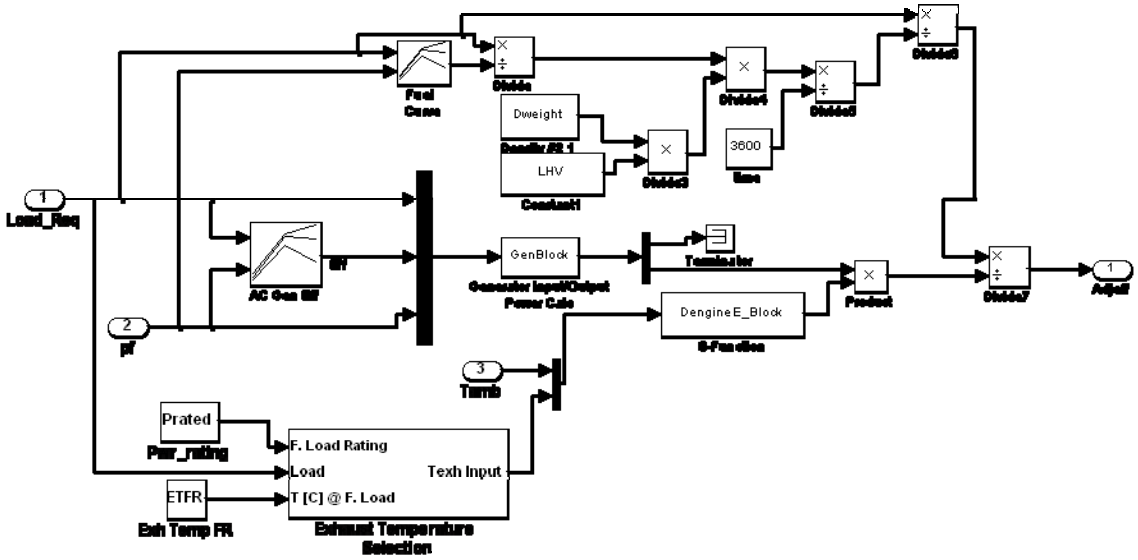

Figure 3.37: *Adj. Coefficient* block diagram calculating adjustment percentage for diesel thermal efficiency based on manufacturer's fuel consumption curves.

The following pieces of Figure 3.35 are identical to those found in the *E-Gen Efficiency & Input Power* block of the *Main System Simulation* and are discussed in Section 3.5.2.2.2.5:

- *Fuel Curve* Block
- *AC Gen Eff* Block
- S-Function *GenBlock*
- S-Function *DengineE_Block*
- Inputs & Constants:
  - *Prated*
  - *-C-*
  - *Load_Req*
  - *Tamb*

With the diesel generators calculated efficiency and the manufacturer's efficiency known then the manufacturer's efficiency can then be divided by the calculated efficiency to acquire an adjustment factor that can be used to create the adjustment *Adj Coefficient* block. To accomplish this, the *Adjustment Coefficient for Fuel Curves* block in Figure 3.36 which

represents the diesel generator has to be simulated at the standard operating condition given by the manufacturer's data sheet. The information of each generator was input manually at first, however, currently the information is transferred from the *Main System Simulation* to this *Adjustment Coefficient Simulation* prior to the main simulation running. The S*witch1* block seen in Figure 3.36 is normally set to route the *Ramp2* block output to the *Product* blocks. The range of values that the *Ramp2* block outputs is from 0 to 1 in steps of 0.1. This allows the *Adjustment Coefficient Simulation* to calculate the efficiency adjustment coefficient for any generator from zero load to full rated load. Upon completion of this pre-simulation the values for the adjustment coefficients for each generator are saved to the MATLAB® workspace for use in the *Adj Coefficient* block in the *E-Gen Efficiency & Input Power* block of the *Main System Simulation*.

3.5.2.2.2.3 Generator Input/Output Power Calculation Block

The *Generator Input/Output Power Calc* block located in the center of both Figures 3.34 and 3.35 is a MATLAB® S-Function block titled 'GenBlock'. The S-Function was originally written to allow for adjusting the AC generator curves of diesel generators that had their rotating speed reduced to 1,200-rpm from a rated speed of 1,800-rpm like the UAF Energy Center's generator. However, technological advancement in metallurgy, improved engine design, and better engine lubricants have narrowed the difference between 1,200-rpm and 1,800-rpm engines [3]. In addition, due to increasingly competitive markets in the size range of engines used in rural Alaska, the 1,800-rpm configuration provides more installed kW per dollar spent than the 1,200-rpm engine can provide. Therefore, it will be assumed that the approximately 23 percent of Alaska utilities having de-rated engines will in the future upgrade to 1,800-rpm engines. This will allow the program script in the S-function to be re-written to simplify the calculation and decrease computational time of the simulation. The new script is based on the following:

$$P_{in} = \frac{P_{sys}}{effr}, \qquad \text{(Eq. 3.43)}$$

where P_{sys} is the output power of the generator required to supply the load, $effr$ is the efficiency in percent of the AC generator at converting input power to output power as is a function of the required output power in kWe, and P_{in} is the input power from the diesel engine required to provide the required output power demanded by the load. This input power P_{in} in kW then goes to a *Product* block where it is multiplied by the engine efficiency. Due to the change in *Generator Input/Output Power Calc* block program script, the UAF diesel generators curves were adjusted prior to inclusion within the simulation.

3.5.2.2.2.4 AC Generator Efficiency Table

The *AC Gen Eff* block seen in Figures 3.34 and 3.36 are based on the manufacturer's specifications for the AC generator in the diesel generator unit. The manufacturer normally specifies the efficiency of the generator at a power factor (pf) of 0.8. After analyzing data from a number of villages, the power systems normally operate with a power factor that varies between 0.8 and close to 1.0. Therefore, to allow for the calculation of necessary input power with these higher power factors a 2.0 % increase in the data for the 0.8 pf was added to obtain the 1.0 pf curve. The 2.0 % increase was determined by taking the curves of an actual generator that provided curves for both 0.8 pf and 1.0 pf. Figure 3.38 shows the curves for a Marathon electric

generator. Four points have been labeled and are: point 1 (82.5%), point 2 (83.7%), point 3 (90.1%), and point 4 (83.4%).

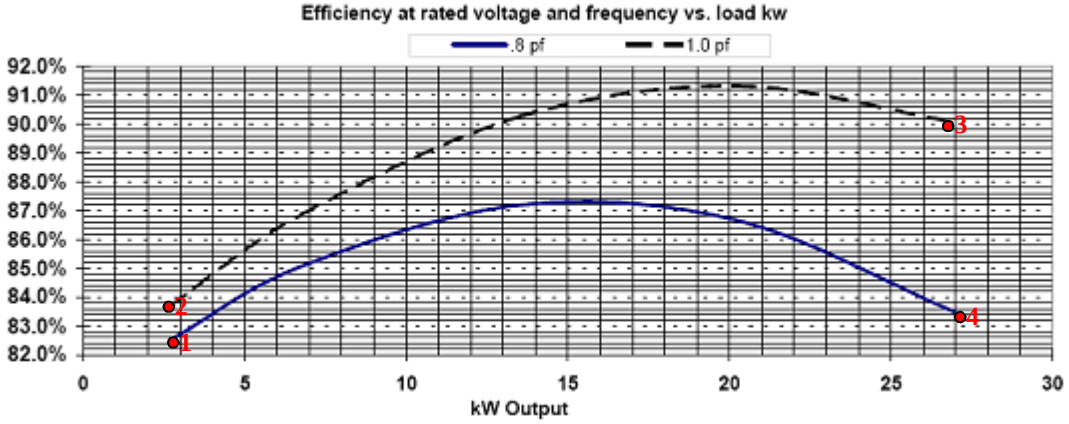

Figure 3.38: Electrical efficiency for a 21 kW Marathon electric generator [29].

$$Eff_{newavg} = \left[\frac{(pt2 - pt1) + (pt3 - pt4)}{2}\right] * 50\% = \left[\frac{(83.7 - 82.5) + (90.1 - 83.4)}{2}\right] * 50\% = 2.0\%, \qquad \text{(Eq. 3.44)}$$

The average difference between the points was calculated as illustrated in Eq. 4.24. The value was then multiplied by 50% to account for variations between different makes and models of generators. Figure 3.39 illustrates the AC generator efficiency curves at 0.8 pf and 1.0 pf for the UAF diesel generator.

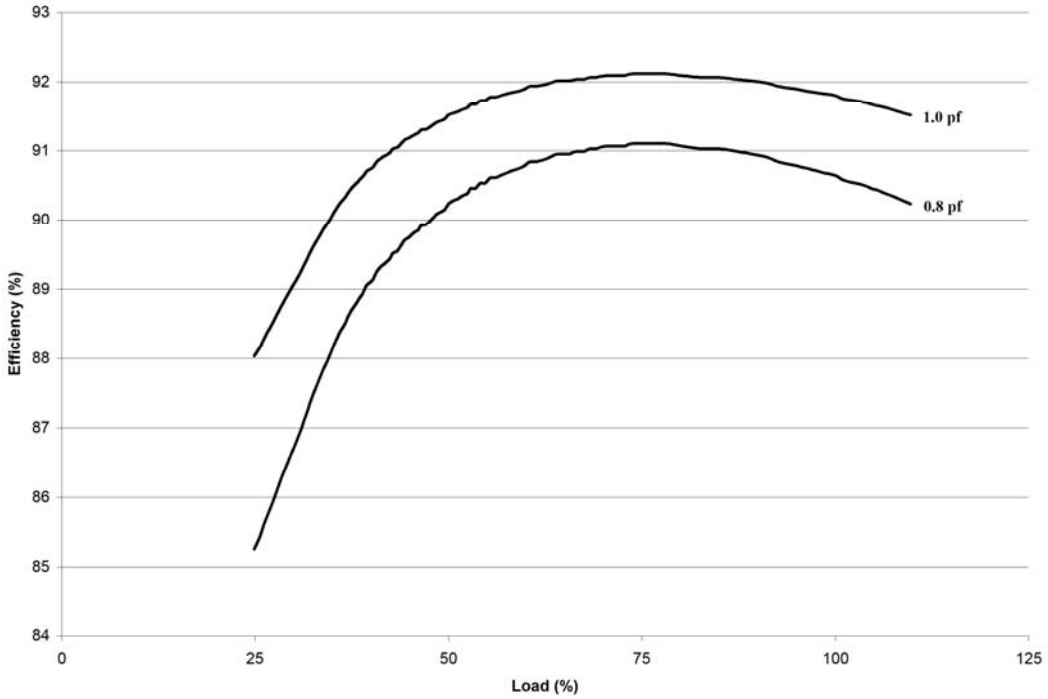

Figure 3.39: UAF Energy Center diesel generator unit's AC generator efficiency curves [30].

The UAF DEG curves in Figure 3.39 are in terms of percent load. These curves will be the basis for all other AC generators of DEGs used within the simulation. In addition, a 50% reduction was considered to be too conservative, therefore the 2% adjustment was applied to the 0.9 pf curve data and the base curve was readjusted. However, some of the manufacturers list the AC generator efficiencies only at rated power. Therefore, the data used to create the curves above are adjusted to match the specific AC generator efficiency at rated load. In addition, since the data pertaining to the curves in Figure 3.39 are in percent load, the percent load is multiplied by the generator's power rating to achieve a data set for the x-axis in kWe load. This process is repeated for all AC generators simulated in the system analysis and the data sets are utilized to create the table in the *AC Gen Eff* block. This data is then input into the *AC Gen Eff* block by use of the block parameters screen seen in Figure 3.40 where the load power data is the input to the block, the power factors are input in the column index, and the output values of efficiency are listed in the parameters output values as vectors.

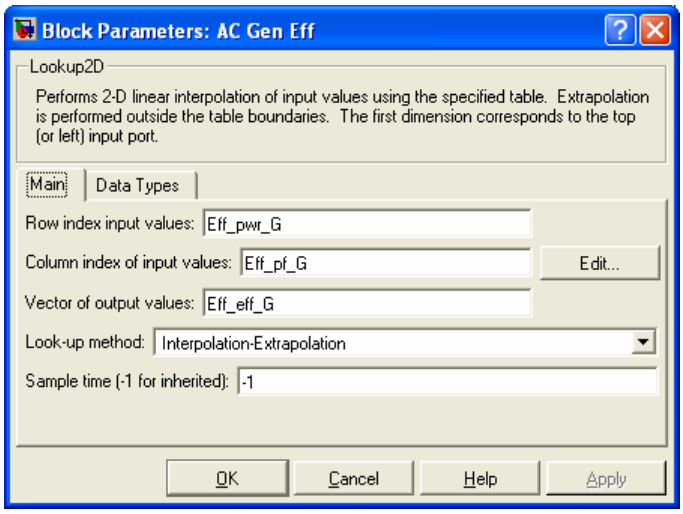

Figure 3.40: Block parameters screen for the *AC Gen Eff* block showing input data variables.

3.5.2.2.2.5 E-Gen Efficiency & Input Power: Inputs and Outputs

There are four direct inputs and two direct outputs to the *E-Gen Efficiency & Input Power* block, the inputs labeled *Required Load*, *Power Factor*, *A.Temp*, and *Texh* are tied to the direct inputs in the *DEG* blocks. *Required Load* is used as the input to the *AC Gen Eff* table block, the *Adj Coefficient* table block, and to the S-Function block *Generator Input/Output Power Calc* through a multiplexer block. *Power Factor* is only used as inputs to the *AC Gen Eff* table block and to the S-Function block *Generator Input/Output Power Calc* again through the multiplexer block. Both *A.Temp* and *Texh* inputs are directed through another multiplexer as inputs to the S-Function *DengineE_Block*.

The outputs of the *E-Gen Efficiency & Input Power* block are *D.Eff* and P_{in} which are inputs to other blocks within the *DEG* block. *D.Eff* is the total diesel generator efficiency after adjustment. It is the multiplication of the AC generator efficiency, the diesel engine efficiency, and the adjustment coefficient shown in Eq. 3.45.

$$D.Eff = AC\ Gen\ Eff\left(DengineE\_Block\ Eff\right)\left(Adj\ Coefficient\right), \qquad \text{(Eq. 3.45)}$$

P_{in} is the total power in kW required as an input to achieve the desired output to meet the load. The value of P_{in} is calculated as

$$P_{in} = \frac{P_{sys}}{AC\ Gen\ Eff}\left(\frac{1}{DengineE\_Block\ Eff}\right)\left(\frac{1}{Adj\ Coefficient}\right). \qquad \text{(Eq. 3.46)}$$

3.5.2.2.3 DEG Block: Manufacturer's Fuel Curve

The manufacturer's data on fuel consumption in kWh/L as a function of output load in kWe as specified in the data sheets in graphical format is illustrated in Figure 3.41 for two diesel generators. As can be seen there is only one curve for each generator using #2 diesel with a 0.8 pf load. Higher power factor will lead to a higher efficiency, and therefore, lower fuel consumption. The fuel consumption efficiencies in kWh/L at higher power factors are calculated

by taking the data for the curves at 0.8 pf and adding approximately 0.2 kWh/L to the values for 0.8 pf to arrive at values for a 0.9 pf rating.

The 0.2 kWh/L was determined by using the 2% increase in the AC efficiency determined in a previous section, standard heating value (HV) of #2 diesel fuel (42780 kJ/kg), and the density of #2 diesel fuel (0.838 kg/L). First convert fuel HV from kJ/kg to kWh/L using fuel density and appropriate conversion factors, Eq. 3.47 illustrates this step.

$$HV = \frac{42780\,kJ}{kg}\frac{0.838\,kg}{L}\frac{kW\cdot s}{kJ}\frac{h}{3600\,s} = \frac{9.958\,kWh}{L}. \qquad \text{(Eq. 3.47)}$$

Now, assuming an AC generator efficiency within the range of normal generators at 0.8 pf of 90% and now add 0.2% for an efficiency of 92% at 0.9 pf. Multiplying these two efficiencies with the value of the fuels HV converted above results in

$$\begin{aligned} 0.8\,pf: &\quad \frac{9.958\,kWh}{L}(0.90) = \frac{8.962\,kWh}{L} \\ 0.9\,pf: &\quad \frac{9.958\,kWh}{L}(0.92) = \frac{9.161\,kWh}{L} \end{aligned}. \qquad \text{(Eq. 3.48)}$$

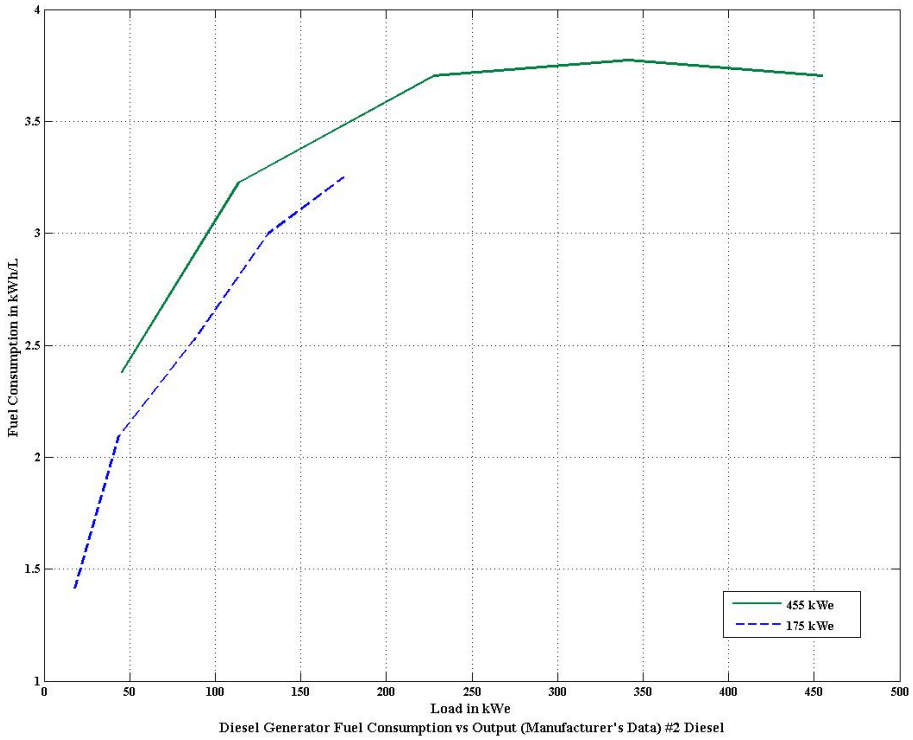

Figure 3.41: Manufacturer's fuel curve for CATERPILLAR® 175 kWe and 455 kWe diesel electric generators [26] [28].

Finally, the difference between the values above in Eq. 3.48 is 0.19936 kWh/L. This value is rounded up to 0.2 kWh/L and added to the value of efficiency at 0.8 pf to arrive at the value of fuel efficiency at 0.9 pf.

The data from the manufacturers is organized in vector form for input into the *Fuel Curve* table block parameter window in MATLAB® as seen in Figure 3.42 below. By listing this data as variables it allows multiple generators with their own fuel curves to be associated with just one *Fuel Curve* table block located within each *DEG* block.

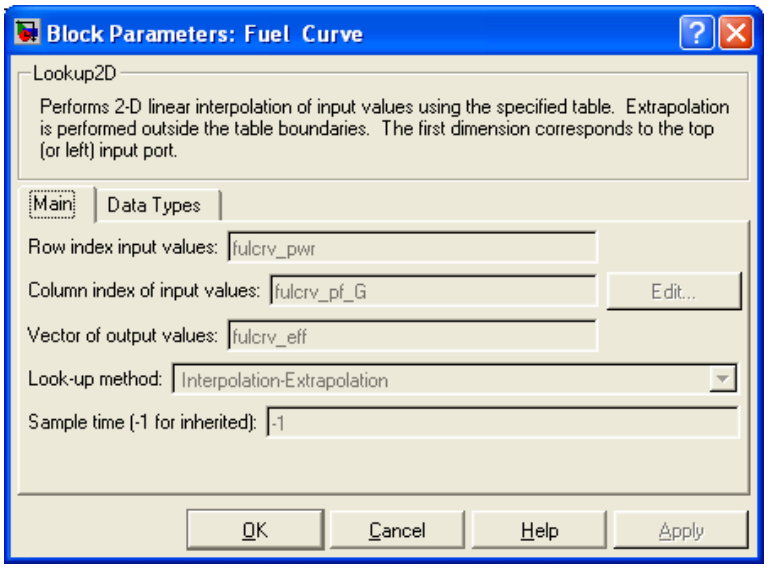

Figure 3.42: *Fuel Curve* table block parameter screen for manufacturer's fuel curve data variables.

3.5.2.2.4 DEG Block: Value Integration Total Block

The *Total-lizer* block shown in Figure 3.43, allows for the integration of a variable over time and is placed within the library for use throughout the *Main System Simulation* and the *Adjustment Coefficient Simulation*. The way the *Total-lizer* block works is that the *Memory* block stores the value output by the *sum* block for reuse as an input to the *sum* block on the next simulation time step. The *sum* block then adds the current value with the previous value and outputs the summed value to be held by the *Memory* block. The output of the *Memory* block is also multiplied by the simulation's sampling rate and the value 24 found within the *Gain* block. The value 24 represents 24 hours in a day, thereby converting the incoming hourly data into a daily value. The *Gain* block converts the current *Memory* block output value into a value based in hours.

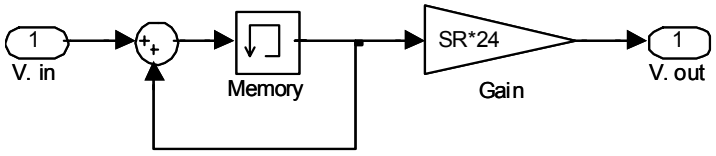

Figure 3.43: Inner diagram of the *Total-lizer* block.

3.5.2.2.5 DEG Block: Diesel Electric Generator Overall Efficiency Block

The *DEG Efficiency* block shown in Figure 3.44 multiplies the diesel generator units efficiency by the efficiency of the fuel which is based on the heating value of the fuel at the specified temperature divided by the heating value of the fuel at STP. The efficiency of the fuel is an output of the *Heating Values for Diesel* block. The outputs of the *DEG Efficiency* block are the diesel generator unit's efficiency and the diesel generator's overall efficiency for both fuel types.

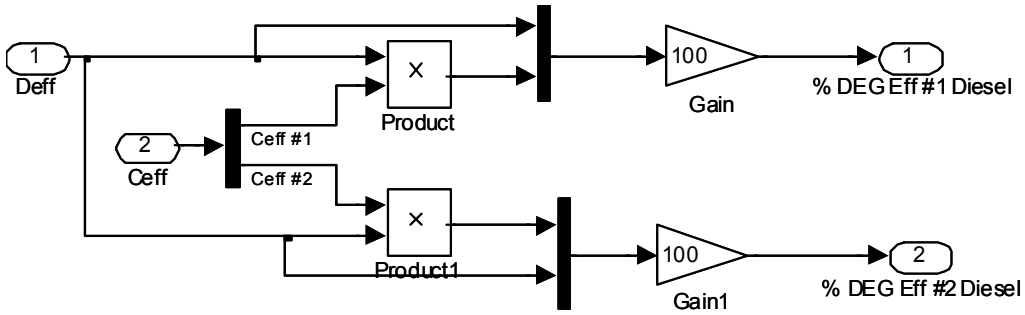

Figure 3.44: Inner diagram of the *DEG Efficiency* block within the *DEG* block.

3.5.2.2.6 DEG Block: Incoming Air Control Block

The *Incoming Air Control* block allows for the specification of the incoming air not to drop below a specific threshold. In Figure 3.45, the threshold specified is 5° C (41° F).

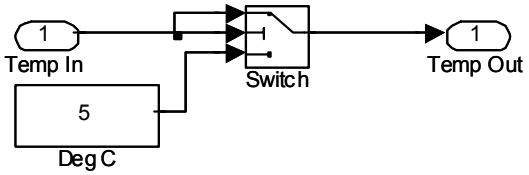

Figure 3.45: *Incoming Air Control* block diagram.

This value of the threshold will be maintained if the value of the incoming ambient air temperature is below the threshold value. The simulation is run at this value based on the following assumptions:

- Extreme cold temperature effects on diesel fuel combustion is difficult to model [31], [32].
- Optimal diesel engine efficiencies have been found to occur with inlet air temperatures above 5 °C.
- The model does not properly predict possible effects that icing and extreme cold air may have on the diesel engine internal components or on the combustion process, therefore in conjunction with the previous assumption a value of 5 °C was chosen.

3.5.2.2.7 DEG Block: Heating Values for Diesel Fuel Block

3.5.2.2.7.1 Fuel Energy Component Development

A combustion chamber typically has large amounts of heat output, and little or no heat input. In this case, the energy balance for a *typical steady-flow combustion process* becomes

$$Q_{out,comb} = \sum N_r \left(\overline{h}^{\circ}_f + \overline{h} - \overline{h}^{\circ} \right)_r - \sum N_p \left(\overline{h}^{\circ}_f + \overline{h} - \overline{h}^{\circ} \right)_p , \qquad \text{(Eq. 3.49)}$$

where $Q_{out,comb}$ is the heat output during combustion, N_r and N_p are the number of moles of the reactant *r* and the product *p*, respectively, per mole of fuel, and h^o_f is the enthalpy of formation at the standard reference *state*. The reference *state* refers to the temperature in degrees Kelvin for the enthalpy in question. The N_r and N_p values are picked directly from the balanced combustion equations.

Eq. 3.49 expresses that the heat output or heating value of a fuel during the combustion process is simply the difference between the energy of the reactants entering and the energy of the products leaving the combustion chamber [24]. The heating value of a fuel is equal to the absolute value of enthalpy of combustion of the fuel. Therefore, in a reacting system the heating value of a fuel is represented by the difference between $\overline{h}$ (sensible enthalpy at a specified *state*) and $\overline{h}^{\circ}$ (sensible enthalpy at the standard reference *state*) and is expressed in kJ/kmol (Btu/lbmol) of fuel. A simplified form of Eq. 3.49 is illustrated in Eq. 3.50 below:

$$Q_h = H_r - H_p , \qquad \text{(Eq. 3.50)}$$

where Q_h represents the energy input into the system by fuel combustion, H_r is the enthalpy of the reactant (intake air/fuel mixture), and H_p is the enthalpy of the product (exhaust gases). Examining Eq. 3.49 shows that, as the specified *state* changes so will the heating value. In simple terms efficiency is defined by the electrical work out produced W_{el}, divided by Q_h, Eq. 3.50. The simplified efficiency equation can be seen in Eq. 3.51.

$$\eta = \frac{W_{el}}{Q_h} , \qquad \text{(Eq. 3.51)}$$

Now, if the temperature of the reactants was to increase, enthalpy of those reactants would likewise increase, thereby increasing the energy input into the system from the combustion output of the fuel, Eq. 3.50. This would result in a decrease in efficiency, assuming that electrical work out does not increase proportionally. However, this is assuming that the enthalpy of the products does not increase with the increase in the reactants temperature. A change in inlet temperature affects the exhaust temperature. However, since it is expected that small changes in inlet air temperature will have little effect on efficiency and since many variables relate inlet air temp to exhaust temperature, changes in exhaust temperature maybe even

smaller. Therefore, we will not attempt to incorporate changes in exhaust temperature for this study. This effect is examined by simulation in the results section of this thesis.

To examine the possible effects of temperature on fuel consumption and DEG efficiency, table blocks were developed in Simulink® that use NASA's 9-constants polynomials to calculate individual products and reactants change in sensible enthalpy over a range of temperatures, this calculation is represented by Eq. 3.52 [33-35].

$$\frac{H^{\circ}_T}{RT} = -a_1 T^{-2} + \frac{a_2 \ln T}{T} + a_3 + \frac{a_4 T}{2} + \frac{a_5 T^2}{3} + \frac{a_6 T^3}{4} + \frac{a_7 T^4}{5} + \frac{b_1}{T}, \quad \text{(Eq. 3.52)}$$

where a_1, a_2, a_3, a_4, a_5, a_6, a_7, and b_1 are polynomial constants, T is the reference temperature, R is the gas constant, and H°_T is the enthalpy of a component on a unit-mole basis.

Thermobuild an interactive tool which uses the NASA Glenn thermodynamic database was used to create a table of thermodynamic properties at specified temperatures that then could be input into the table blocks for use in the Simulink® model of Eq. 3.48 as shown in Figure 3.46 for # 1 diesel and Figure 3.47 for #2 diesel [24], [33]. The chemical formulas for #1 and # 2 diesel fuel chosen are $C_{10}H_{22}$ and $C_{12}H_{26}$, respectively.

Using the chemical formulas and the associated balance combustion, Eqs. 3.53 and 3.54, the molar units could be added to Eq. 3.48 as gain blocks in Figure 3.47.

$$C_{10}H_{22} + 23.8*\left(O_2 + 3.76*N_2\right) \rightarrow 10*CO_2 + 11*H_2O + 8.261*O_2 + 89.3*N_2, \quad \text{(Eq. 3.53)}$$

and

$$C_{12}H_{26} + 28.4*\left(O_2 + 3.76*N_2\right) \rightarrow 12*CO_2 + 13*H_2O + 9.9*O_2 + 106.7*N_2. \quad \text{(Eq. 3.54)}$$

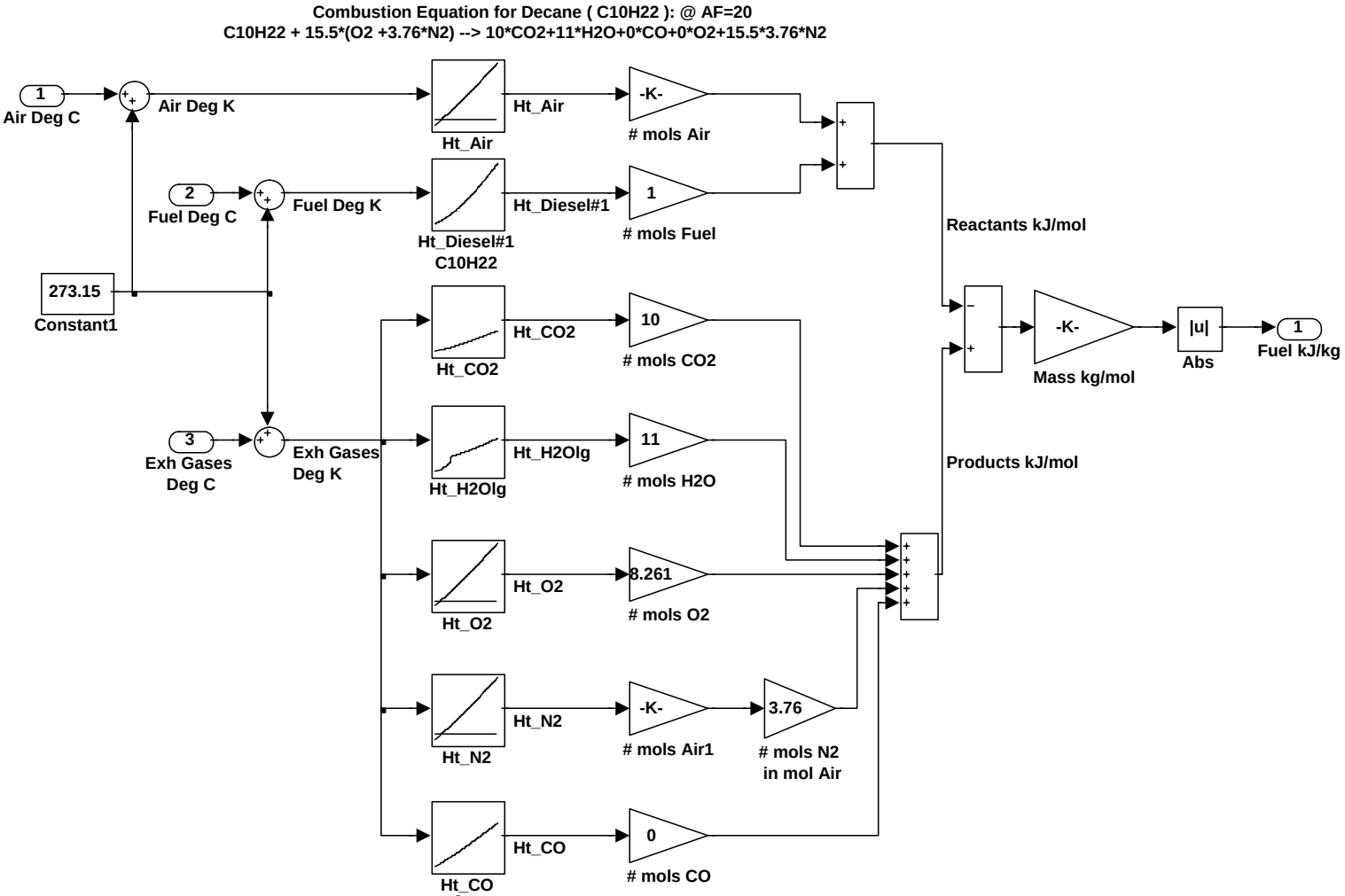

Figure 3.46: Simulink® model of the combustion equation (Eq. 3.53) for #1 diesel fuel.

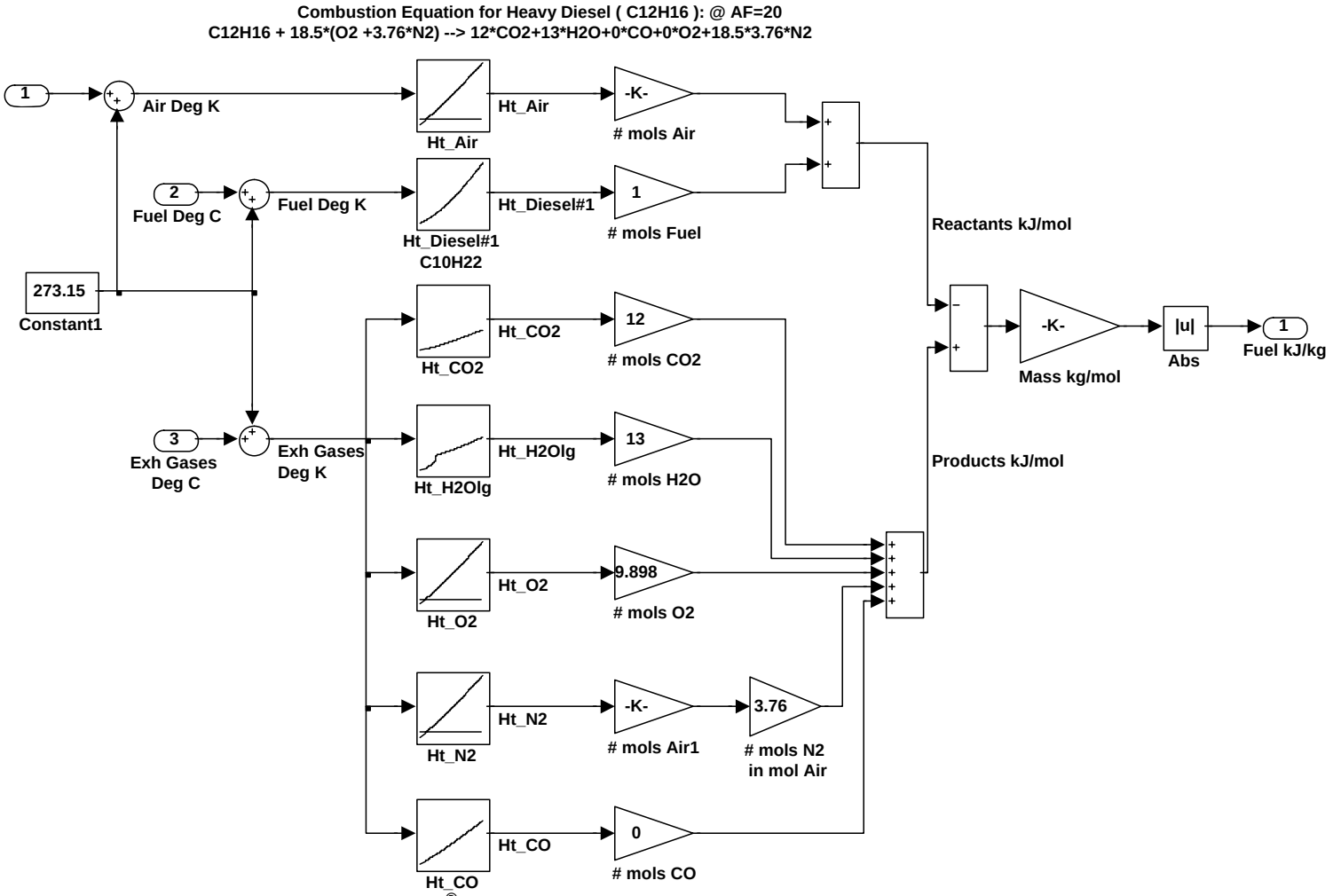

Figure 3.47: Simulink® model of the combustion equation (Eq. 3.54) for #2 diesel fuel.

3.5.2.2.7.2 Fuel Energy Component Testing

The systems in Figures 3.46 and 3.47 were simulated at STP to examine possible error between the simulated heating values for #1 and #2 diesel fuels. Table 3.1 shows the simulated values for both fuels at STP, compared to the higher heating value (HHV) and lower heating value (LHV) given in [24]. The simulated values for both diesel fuels are within the range of HHV and LHV from [24].

Table 3.1: Comparison table of simulation heating values to referenced values.

Parameter	Reference Heating Value kJ/kg (Btu/lbm) [13]		Simulated Heating Value (@ STP) kJ/kg (Btu/lbm)
	Higher	Lower	
# 1 Diesel	47640 (20490)	44240 (19020)	44580 (19166.2)
#2 Diesel	45500 (19600)	42800 (18400)	44450 (19109.3)

3.5.2.2.8 DEG Block: Fuel Use Conversion Block

The input energy divided by the fuel's heating value will result in the amount of fuel energy in (L/h) required to meet the load demand. This is illustrated by Eq. 3.55 and in the Simulink® version of the equation seen in Figure 3.48.

$$FuelConsumed\left[\frac{L}{h}\right] = \frac{Energy_{input}\left[\frac{kJ}{h}\right]}{HV_{fuel}\left[\frac{kJ}{kg}\right]\left(Fuel\ \ Density\left[\frac{kg}{L}\right]\right)}, \qquad \text{(Eq. 3.55)}$$

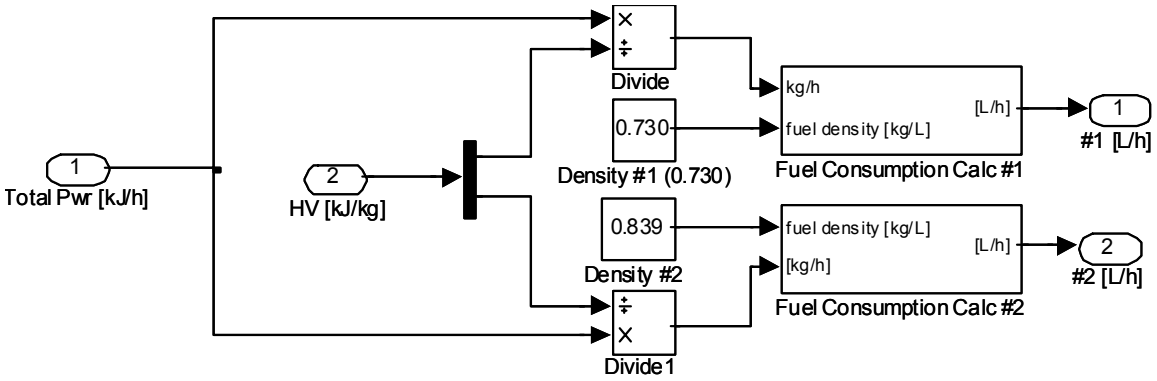

Figure 3.48: Diagram of *Fuel Use Conversion* block representing Eq. 3.55.

3.5.2.3 Dispatch Techniques

The model is used to perform an economic feasibility analysis for integrating economic dispatch control systems into existing DEG systems. Inputs to the model are the electrical load and power factor profile for the village, and the manufacturer's performance curves for the DEGs. The outputs are the fuel consumption, efficiency (kW-hr/liter), total cost of fuel, and total emissions of CO_2, NO_x and PM_{10}. The fuel efficiency curves for the DEGs in each system tested

were constructed from manufacturer's data and three different load dispatch schemes were implemented: 1) even load distribution (ELD) 2) pre-configured control (PCC) and 3) economic dispatch. ELD assumes all generators are operating to the supply the load with the demand distributed evenly based on each DEGs capacity. PCC (see Figure 3.49 and Table 3.2 for Kongiganak, Alaska) turns on and off generators in order of their maximum rating to meet the total demand neglecting efficiency. In this case one of the 190 kWe DEGs is used strictly as a back up. ED (see Figure 3.50 for Kongiganak, Alaska) finds the optimal operating point to satisfy the demand at the best possible efficiency. Although ELD is used as the base case, this is not necessarily the general operating condition in the village, as all generators would normally not be running unless there was a very high demand. So for comparison to ED, PCC was used to represent the closest possible scenario to the actual operating condition in the village where only the generators that need to be operated to supply the load are used.

This same economic dispatch program was also used to incorporate the effects of ambient temperature variations and was tested on ambient temperature and load data from Kongiganak, Alaska. A 3 °C rise in ambient air temperature over the next 50 years as predicted by scientist at the UAF Geophysical Institute's Alaska Climate Research Center was used in the model to determine the effect on DEG efficiency.

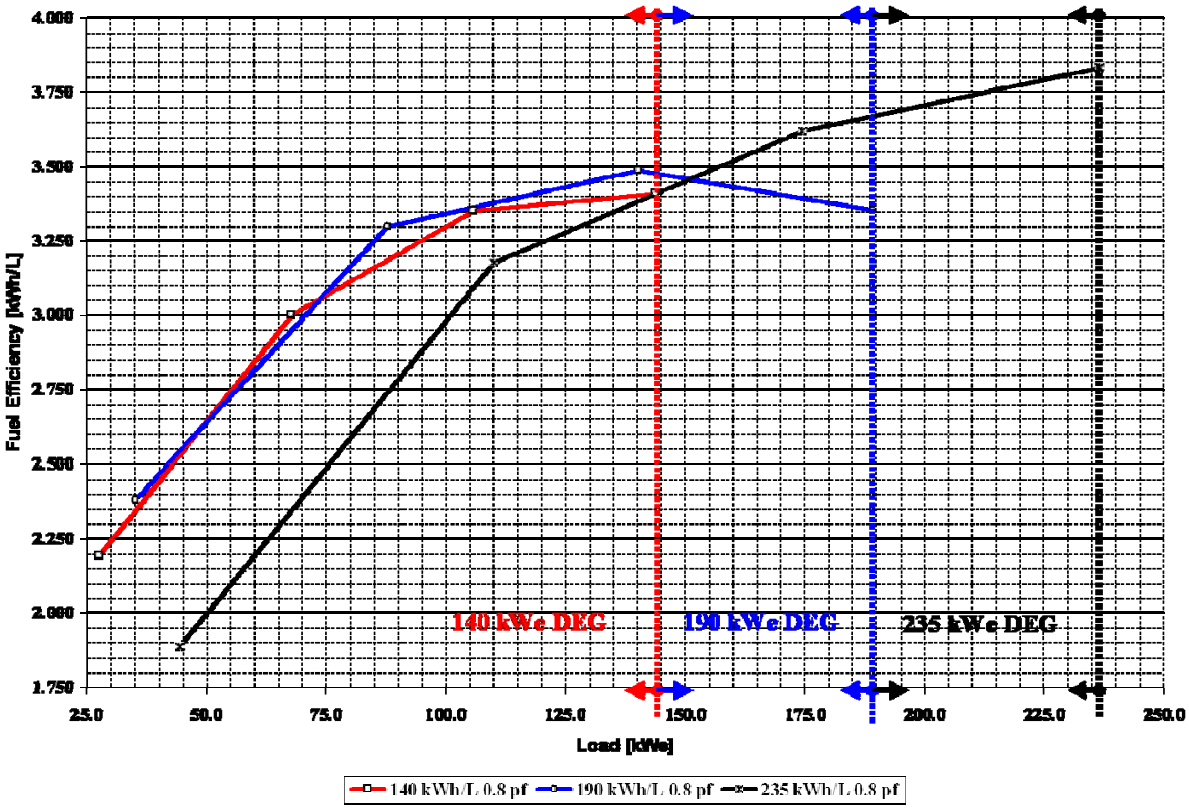

Figure 3.49: PCC zoned manufacturer's fuel curves for the Kongiganak DEGs.

Table 3.2: PCC control scheme for Kongiganak DEGs.

DEG	Load Demand (kWe)						
	< 140	**140 – 190**	**190 – 235**	**235 – 375**	**375 – 425**	**425 - 565**	**565-755**
235 kWe	Off-line	Off-line	**On-line**	**On-line**	**On-line**	**ELD** mode w/ All 3 DEGs	**ELD** mode w/ All 3 + Back-up DEGs
190 kWe (1)	Off-line	**On-line**	Off-line	Off-line	**On-line**		
140 kWe	**On-line**	Off-line	Off-line	**On-line**	Off-line		
190 kWe (2)	Back-up	Back-up	Back-up	Back-up	Back-up		

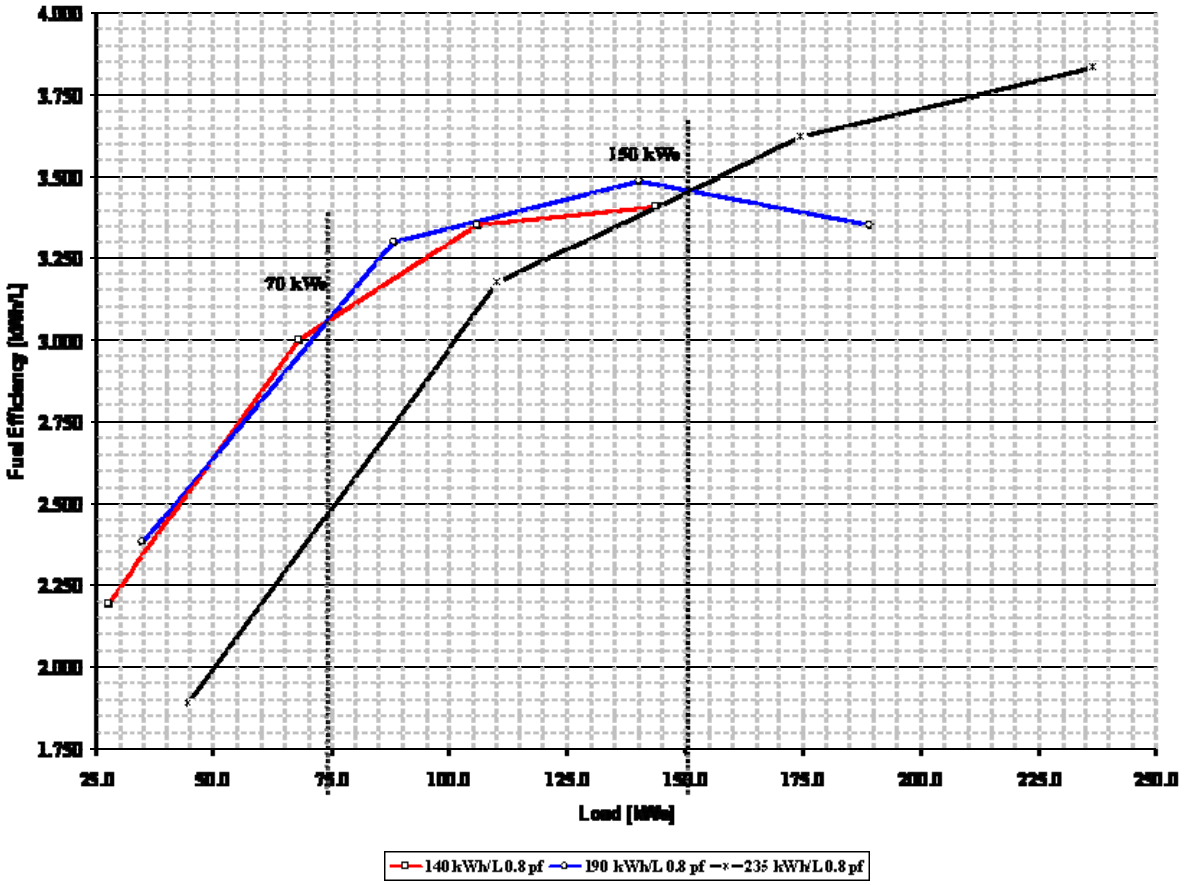

Figure 3.50: ED zoned manufacturer's fuel curves for the Kongiganak DEGs.

3.5.2.4 Classical Economic Dispatch Algorithm

The algorithm for classical economic dispatch is a minimized cost function for plant operation that includes all operating plants as follows in [36]. Given a system with m generators committed, pick the P_{Gi} to minimize the total cost

$$C_T = \sum_{i=1}^{m} C_i(P_{Gi}), \quad \text{(Eq. 3.56)}$$

such that

$$\sum_{i=1}^{m} P_{Gi} = P_D, \quad \text{(Eq. 3.57)}$$

and

$$P_{Gi}^{\min} \le P_{Gi} \le P_{Gi}^{\max} \quad i = 1,2,...,m. \quad \text{(Eq. 3.58)}$$

where power output is P_{Gi}, fuel cost as a function of power output is $C_i(P_{Gi})$ in the form

$$C_i(P_{Gi}) = \alpha + \beta P_G + \gamma P_G^2, \quad \text{(Eq. 3.59)}$$

with positive coefficients, C_T is the total cost, P_D is the total load demand, $P_{Gi}^{\min}$ is the minimum power capability of the generating unit, $P_{Gi}^{\max}$ is the maximum power capability of the generating unit and m is the number of units committed [36].

Now, take the derivative of the fuel cost function with respect to power out to reach a solution in terms of *incremental costs* (*ICs*)

$$IC_i = \frac{dC_i(P_{Gi})}{dP_{Gi}} \text{ = slope of fuel-cost curve,} \quad \text{(Eq. 3.60)}$$

assuming the incremental cost curves are linear to arrive at

$$IC_i = \beta + \gamma P_G. \quad \text{(Eq. 3.61)}$$

Now, apply the above equations to a known fuel-cost curve and a known total load to be supplied. Figure 3.51 shows an example of two generators with differing fuel-cost curves at different incremental costs. Assuming that the same incremental cost can be achieved by every generator, choose a value for IC_i, and solve for each P_{Gi}, check if Eq. 3.56 is satisfied. If not increase (decrease) IC_i until Eq. 3.56 is satisfied.

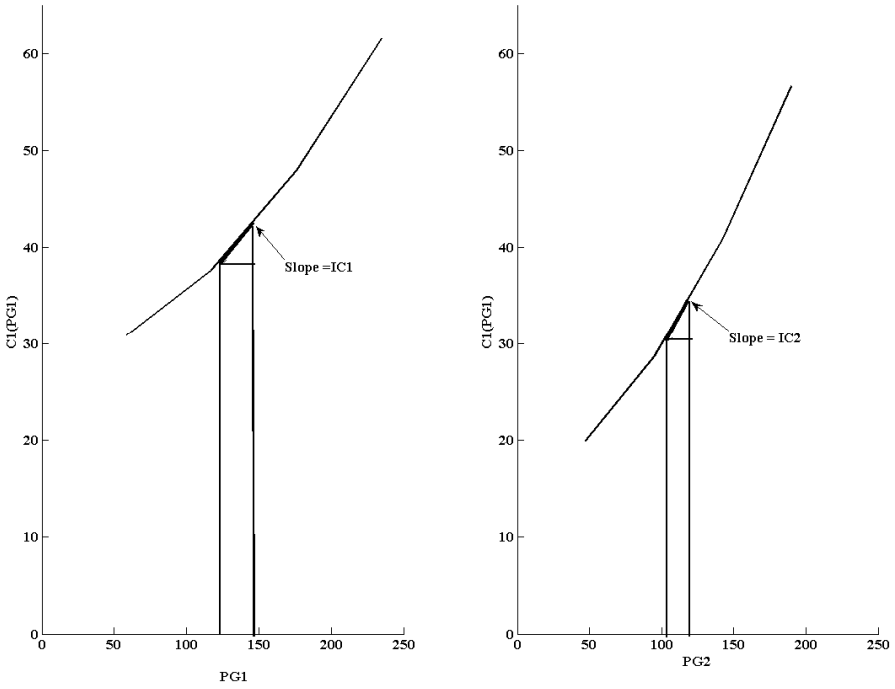

Figure 3.51: Two generator cost curves with both operating at different incremental costs [7], [8].

One significant difficulty in performing classical economic dispatch on any standalone DEG system in rural villages is the fact that not all DEGs are available to operate all the time. Therefore, unit commitment must be established before performing economic dispatch. In other words, the available units need to be determined and committed for operation before the economic dispatch problem can be solved and the program needs to allow for any DEG to go to the off state.

3.5.2.5 Unit Commitment Development

Unit commitment involves finding the combinations of DEGs that will most efficiently supply the given load using economic dispatch. Simply defined, a unit combination is feasible if it meets the following two criteria [37]:

1) The sum of all maximum power ratings (MW, kW, etc) for the units committed is greater than the load.
2) The sum of all minimum power ratings (MW, kW, etc) for the units committed is less than the load.

In equation format:

$$\sum_{i=1}^{m} P_{Gi}^{\min} \le P_D \le \sum_{i=1}^{m} P_{Gi}^{\max} \quad i = 1,2,...,m\,. \qquad \text{(Eq. 3.62)}$$

Therefore, if the system is to be optimized, units must be shut down as the load goes down and then recommitted as the load goes back up.

The unit commitment problem can be very difficult as discussed in [37]. Very large numbers for enumerations can be required. This results in practical barriers in the optimized unit commitment problem with high dimensionality and a number of possible solutions. The following three techniques are the most commonly used to overcome the unit commitment problem:

- Priority-list schemes,
- Dynamic programming (DP),
- Lagrange relation.

However, after evaluating the three above techniques, the dynamic programming technique was utilized within the MATLAB® environment for modeling. Since the DP technique can create similar priority lists as a priority-list scheme, only the priority list and DP technique will be discussed here.

A simple shut-down rule or priority-list scheme could be obtained after an exhaustive enumeration of all unit combinations at each load level. However, a much simpler approach can be applied by noting the full-load average production cost of each unit, where the full-load average production is simply the net heat rate at full load multiplied by the fuel cost. Table 3.3 is an example of a simple priority list.

Table 3.3: Example priority list for a three generating unit system [37].

Unit Combination	Min kW from Combination	Max kW from Combination
2 + 1 + 3	300	1200
2 + 1	250	1000
2	100	400

A chief advantage of dynamic programming over the enumeration scheme is a reduction in the dimensionality of the problem [37]. For example suppose we have a system with four units and any combination of them could serve the load. There would be a maximum of $2^4 - 1 = 15$ combinations to test. However, if a strict priority order was imposed, there would only be four combinations to try:

Priority 1 unit
Priority 1 unit + Priority 2 unit
Priority 1 unit + Priority 2 unit + Priority 3 unit
Priority 1 unit + Priority 2 unit + Priority 3 unit + Priority 4 unit

Theoretically, a priority list arranged in order of the full-load average-cost rate would result in a correct dispatch and unit commitment only if [37]:

1. No load costs are zero.
2. Unit input-output characteristics are linear between zero output and full load.
3. There are no other restrictions.

4. Start-up costs are a fixed amount.

In the following approach, assume that:

- A *state* consists of an array of units with specified units operating and the rest off-line.
- The start-up cost for a unit is a fixed amount.
- There are no costs for shutting down a unit.
- There is a strict priority order, and in each interval a specified minimum amount of capacity must be operating.

A feasible state is one where the committed units can supply the required load and meet the minimum amount of capacity each period.

A forward dynamic programming algorithm is shown by the flowchart in Figure 3.52 [37]. The recursive algorithm to compute the minimum cost in hour *K* with combination *I* is as follows,

$$F_{\cos t}(K,I) = \min_{\{L\}} [P_{\cos t}(K,I) + S_{\cos t}(K-1,L{:}K,I) + F_{\cos t}(K-1,L)] \qquad \text{(Eq. 3.63)}$$

where

State (K,I) is the I^{th} combination in hour *K*,
$F_{\cos t}(K,I)$ = least total cost to arrive at state (K,I),
$P_{\cos t}(K,I)$ = production cost for state (K,I), and
$S_{\cos t}(K-1,L:K,I)$ = transition cost from state $S_{\cos t}(K-1,L:K,I)$ to state (K,I)

For the dynamic programming approach shown in Figure 3.52, a *strategy* is defined as the transition from one state at a given hour to a state at the next hour. In addition the two variables, *X* and *N*, in Figure 3.52 are as follows:

X = number of states to search each period
N = number of strategies to save at each step.

These variables allow control of the computational effort. For example, with a simple priority-list ordering, the upper bound on *X* is *n*, the number of generating units. Reducing the number of *N* means that the highest cost schedules at each time interval are discarded and only the lowest *N* strategies are saved. However, there is no reassurance that the theoretical optimal schedule will be found using a reduced number of strategies and search range (the *X* value); experimentation with a particular program is the only way of indicating any potential error associated with limiting the values of *X* and *N*.

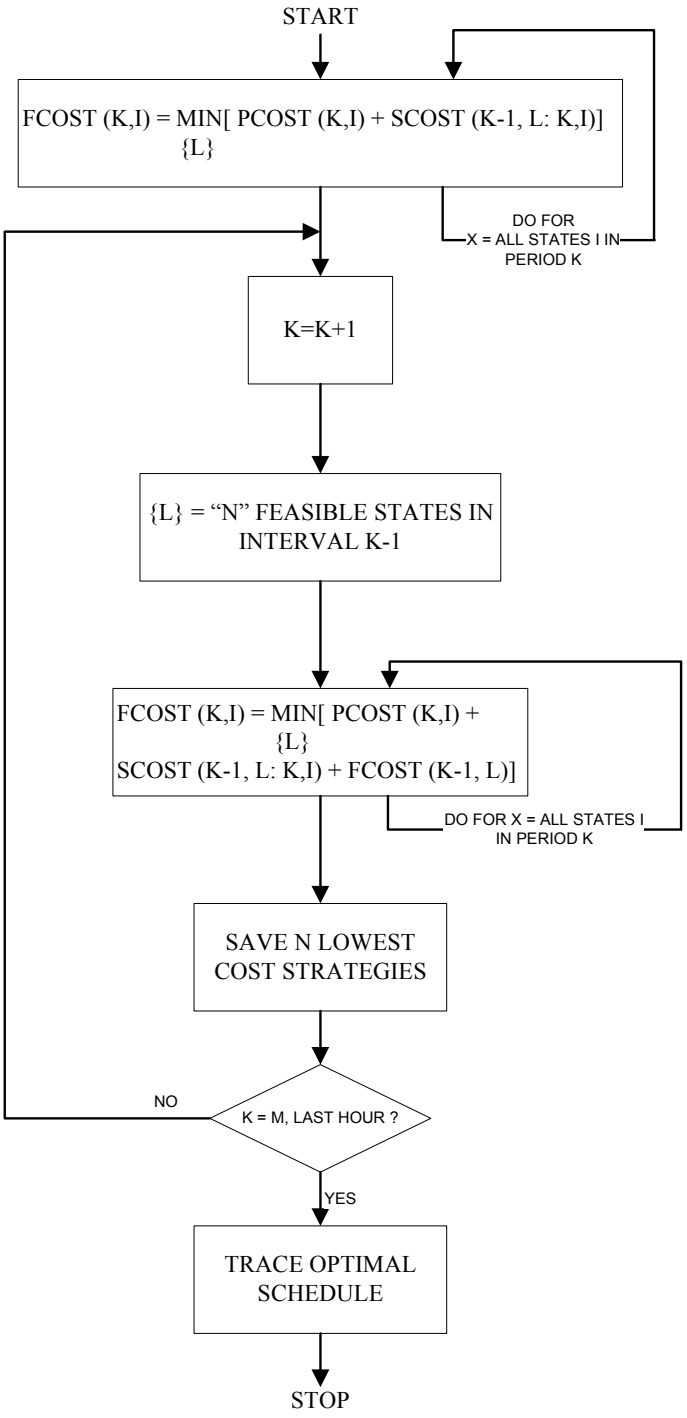

Figure 3.52: Forward dynamic programming flowchart recursive algorithm for unit commitment [37].

4. Results and Discussion

The results of studies conducted in this project have centered around the in-house (at UAF) testing of RTUs, flow meters and sensors for DEGs like those found in Alaska village communities, the development of a consortium of Alaska rural utilities, the deployment of remote monitoring systems in 25 villages in AEAs service territory, and the development of software programs and system models in MATLAB® Simulink® to determine the optimal mix of DEGs and renewable sources of power as well as the economic dispatch of power from these sources to serve the village loads.

4.1 UAF Energy Center Diesel

Results of testing a remote terminal unit, various types of fuel and coolant flow meters, and temperature and pressure sensors on the125 kWe Detroit DEG at the UAF Energy Center showed the importance of remote metering and the proper selection of flow meters and sensors. The detailed results of these tests are presented by Tyler Chubb in a master's thesis, *Performance Analysis for Remote Power Systems in Rural Alaska*, under the direction of the project PIs (see MS Thesis 2 under Project Publications).

4.1.1 Flow Meter Test Loop

The results of the independent test on a magnetic and ultrasonic flow meter in a small coolant flow loop are illustrated in Figures 4.1 and 4.2 for a high and low flow rate, respectively. These results showed that electromagnetic flow meters are more accurate across the measurement range than the ultrasonic flow meters. The ultrasonic meter suffered from the effects of air within the coolant loop at lower flow rates which could be attributed to the pump and was also simply less accurate in this measurement range. Consequently, the range of flow rates to be measured is important in selecting the proper flow meter. In other words, if we know the coolant flow rate is nominally 45 liters/minute (12 gallons/minute) and varies by +/- 40 liters/minute during generator operation, then we would need to select a fuel flow meter that exhibits the highest degree of accuracy in the range from 5 to 85 liters/minute.

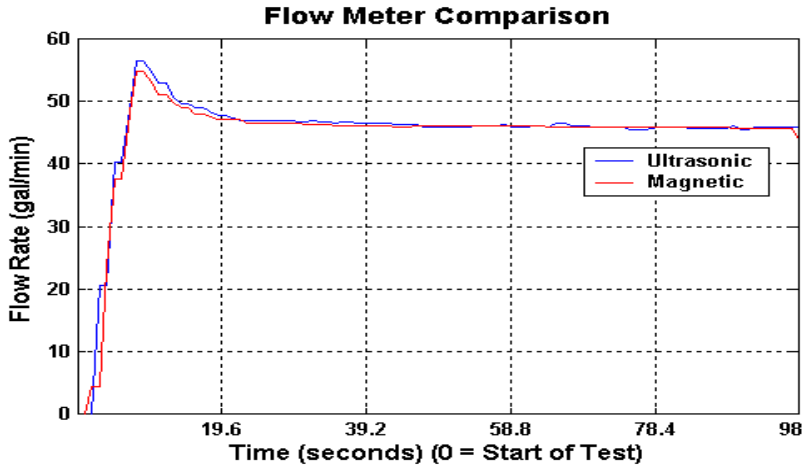

Figure 4.1: Magnetic and ultrasonic flow meter performance for high coolant flow rate.

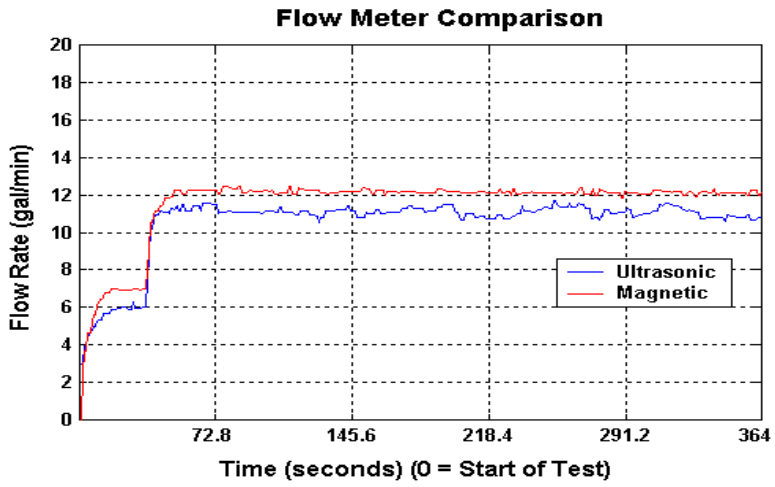

Figure 4.2: Magnetic and ultrasonic flow meter performance for low coolant flow rate.

4.1.2 Flow Meter and Temperature Sensor Tests on UAF DEG

A number of tests were conducted with flow meters on the UAF DEG coolant loop and fuel input line. The ultrasonic fuel flow meter that clamps around the fuel line was tested and found to be problematic because of generator vibration causing consistent errors with the fuel flow measurements as shown in Figure 4.3. The actual fuel flow rates were measured by timing the removal of fuel from a small day tank with a known volume using a pressure transducer and a level sensor as illustrated in Figure 4.4. An example of the increase in fuel flow rate with the increase in electrical load is shown in Figure 4.5.

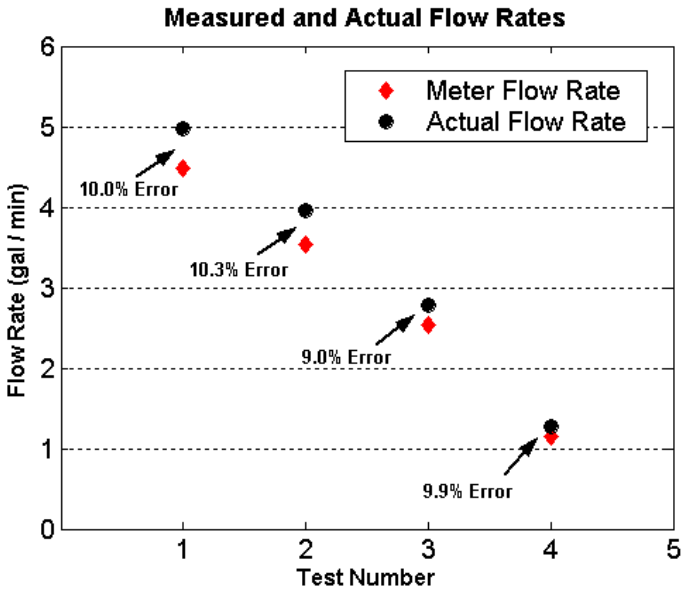

Figure 4.3: Ultrasonic fuel flow meter tests.

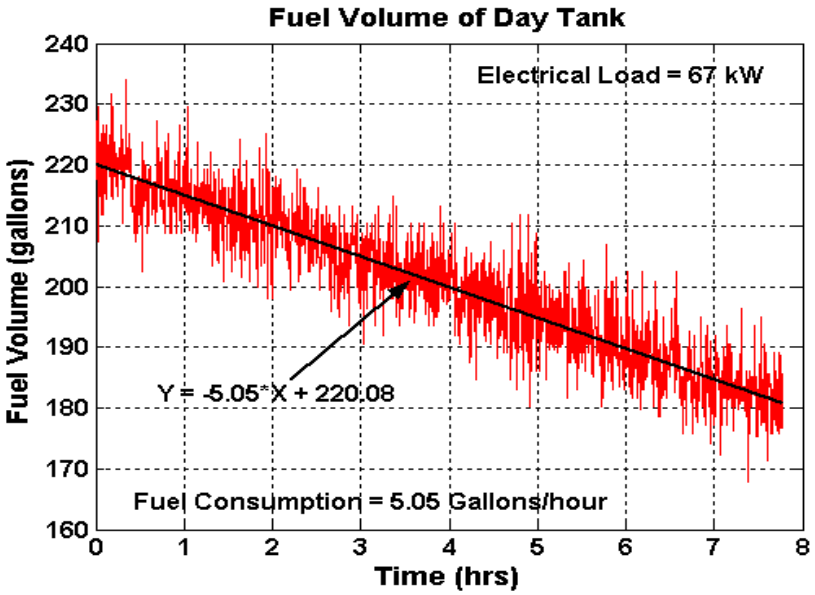

Figure 4.4: Using pressure transducer data to find fuel consumption rate.

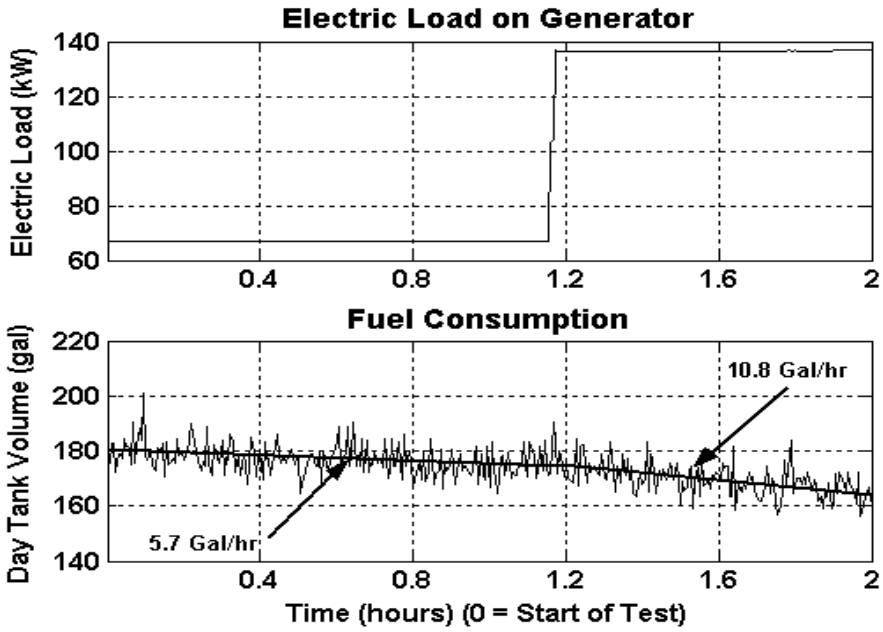

Figure 4.5: Changing fuel consumption rate for UAF DEG.

The magnetic and ultrasonic coolant flow meters were tested with the following results. Figure 4.6 shows the coolant flow rates (gal/min) for each meter and the electrical output (kWe) of the DEG over time. This illustrates that the coolant flow rate is directly proportional to electrical power output of the DEG. The ultrasonic flow meter suffers from high frequency noise (jitter) due to the generator vibration.

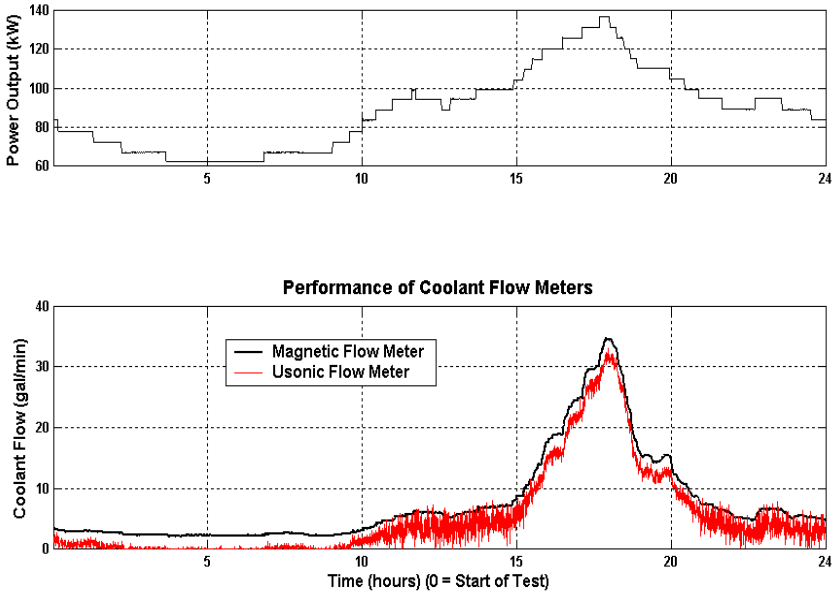

Figure 4.6: Magnetic and ultrasonic coolant flow meter comparison on UAF DEG.

Exhaust and coolant temperature sensors were also tested with the following results. Figure 4.7 shows the exhaust temperature (°F) and the electrical output of the DEG (kWe) over time. The exhaust temperature is directly proportional to the electrical power output of the DEG.

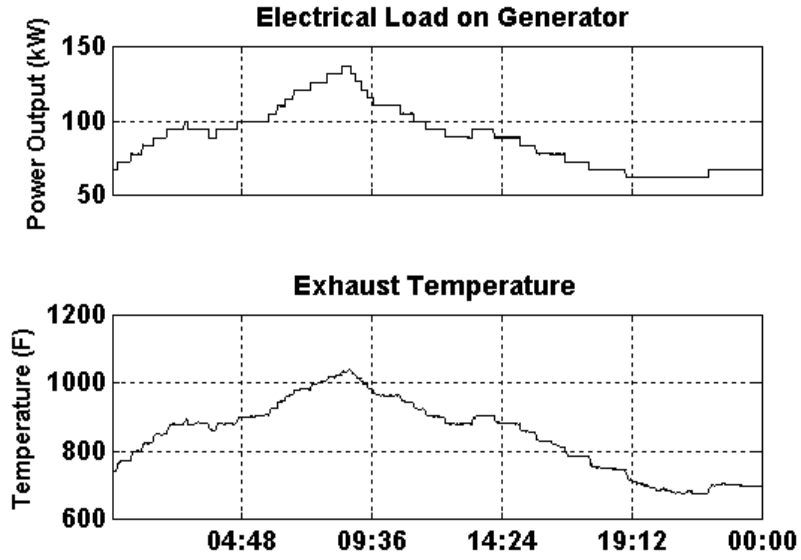

Figure 4.7: Exhaust system temperature and electrical power output over time for UAF DEG.

Figure 4.8 shows the coolant temperature (°F) and the electrical output (kWe) of the DEG over time. The coolant temperature is directly proportional to the electrical power output of the DEG.

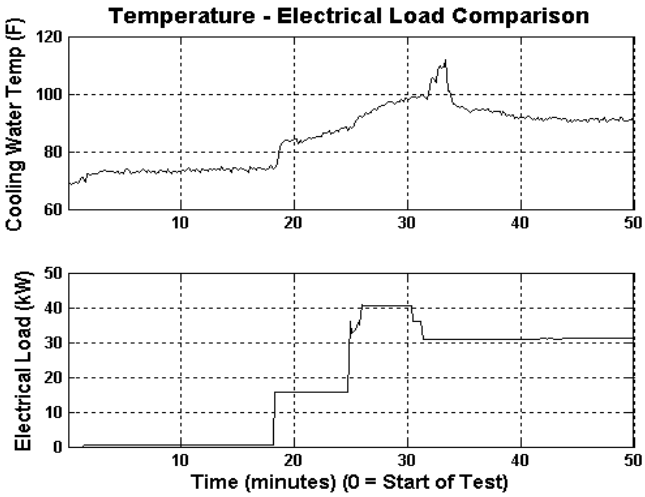

Figure 4.8: Coolant temperature and electrical power output over time for UAF DEG.

A significant result (see Figure 4.9) with regards to coolant temperature occurred when forest fire ash in the summer of 2004 clogged the cooling system radiator and the coolant operating temperature increased by 20 °C. In a village system without remote monitoring this situation might have led to a costly generator failure if left unchecked.

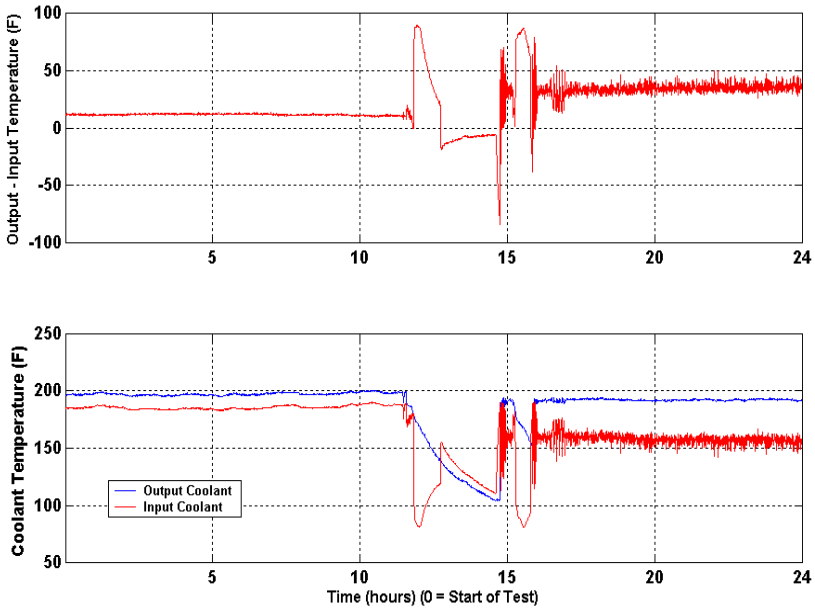

Figure 4.9: Effects of particle build-up in generator radiator.

The flow meter and temperature sensor measurements were used to develop the energy balance for the DEG plant. Using Eq. 3.1, the amount of energy contained in the coolant was calculated at 2,245,000 BTUs (658 kWh) over the course of the 24 hour load profile. Using the heating value of the Syntroleum fuel, 121,500 BTU/gallon [38] the lost energy in the coolant equates to 18.5 gallons of fuel per day. If a heat exchange system that were 80% efficient were utilized in this application, harnessing this wasted energy would be equivalent to saving 14.8 gallons of fuel per day or 5395 gallons of fuel over the course of a year. Using an estimated price for diesel fuel in rural Alaska, $3.00/gallon, this is equivalent to $16,185 over the course of a year in lost energy. Using Eq. 3.2, the average radiant heat emitted by the diesel engine was approximately 1.5 – 2.0 kW, or 2-3% of the input fuel energy. A value of 2.5% is used in the following energy balance calculations.

The overall energy balance plot is shown in Figure 4.10.

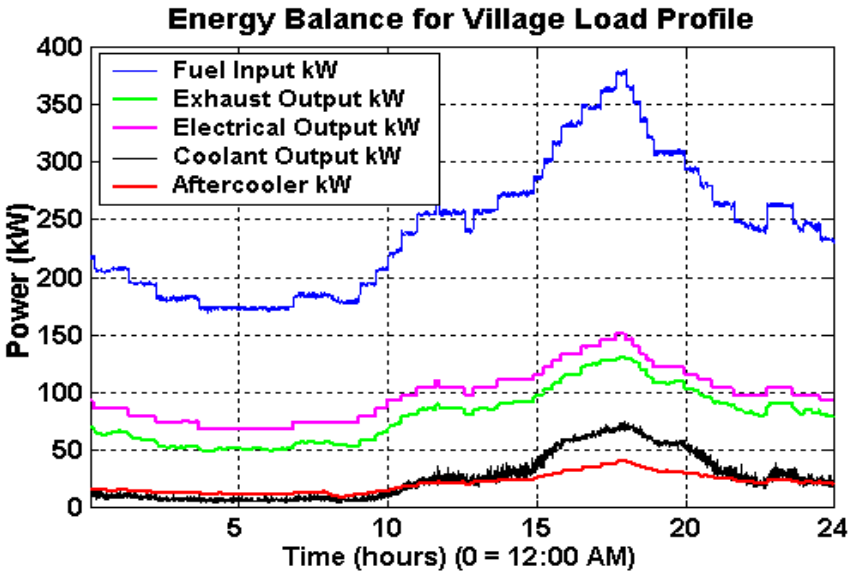

Figure 4.10: Energy output broken into individual forms.

Comparing the total output energy with the total input energy gives a means to verify the overall accuracy of the monitoring system as these two entities should ideally be equal. The comparison is shown in Figure 4.11. The accuracy of the energy balance was not perfect, but it must be taken into consideration that there were 11 sensors used to compile the information. Given that there was inaccuracy inherent with each sensor, an overall error of this magnitude should not be unexpected. At high electrical loads on the generator, the output energy exceeded the input energy by up to 30 kW (maximum 10% error) and at lower electrical load this situation was reversed by 35 kW (maximum 12% error). The output and input energies seemed to optimally correspond when the electrical load on the generator was 80 kW to 100 kW. It can be deduced from the energy balance that several of the sensors were in their optimal operating range when loads of 80 – 100 kW were placed on the generator.

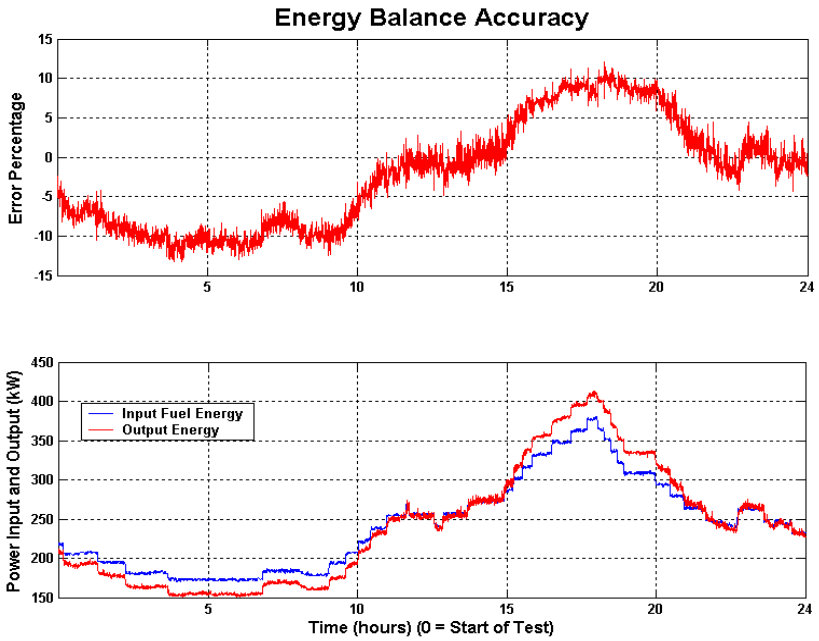

Figure 4.11: Energy balance input compared to energy balance output.

Figure 4.12 shows pie charts of the energy balance calculated for the DEG from the measured data (a) and generator specifications (b). A significant portion of the energy is lost in the exhaust and heated coolant. The heated coolant is used to heat buildings in the village by piping the heated coolant from the generator house to buildings in the village.

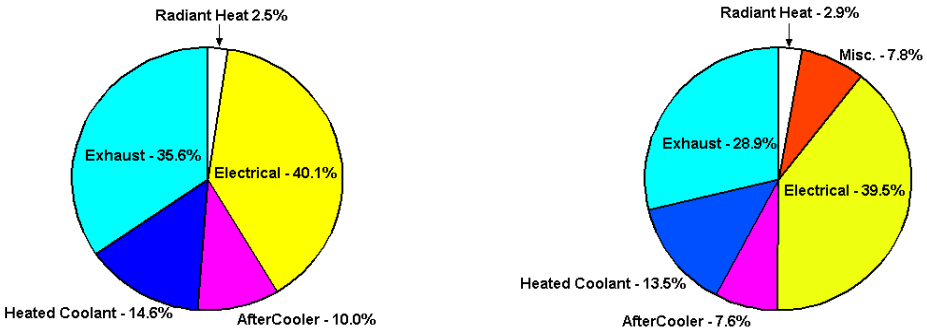

(a) (b)

Figure 4.12: Average energy outputs of UAF DEG operating near full load using a) data from tests and b) generator specifications.

4.2 Village Power Survey and Data Collection

A number of villages in AEAs service territory were surveyed to collect current system information and existing data. These villages were classified in terms of their average electric load requirement as illustrated in Figure 4.13. However, much of the existing load data is of poor

quality, consisting of missing time windows, sampling errors, or only small time windows of data when service technicians were on site for a few days. An example plot of load profiles for five random villages in Figure 4.14 illustrates this point.

Both AEA and AVEC have partnered to install standard remote monitoring equipment in a number of villages in their service territories in order to work towards creating a standard data collection system. AEA currently has limited online access to real-time monitoring in many of its villages at http://www.aidea.org/aea/aearemotemon.html. The 21 villages included in this study are: Atka Diesel Powerhouse and Hydro Facility, Arctic Village, Buckland, Chefornak, Chuathbaluk, Crooked Creek, Diomede, Golovin, Hughes, Kongiganak, Koyukuk, Kwigillingok, Pedro Bay, Larsen Bay Hydro Facility, Manokotak, Nikolski, Ouzinkie Diesel Powerhouse and Hydro Facility, Sleetmute, Stevens Village, Stony River, and Takotna. This includes password access to the actual computer terminal in the village power house as well as video cameras in the power house. The problem has been collecting information from all of these communities in a standard format that can be stored and processed at a central server. Two more villages, Chitina and Chignak, in AEAs service territory received basic remote monitoring upgrades and were included in this study.

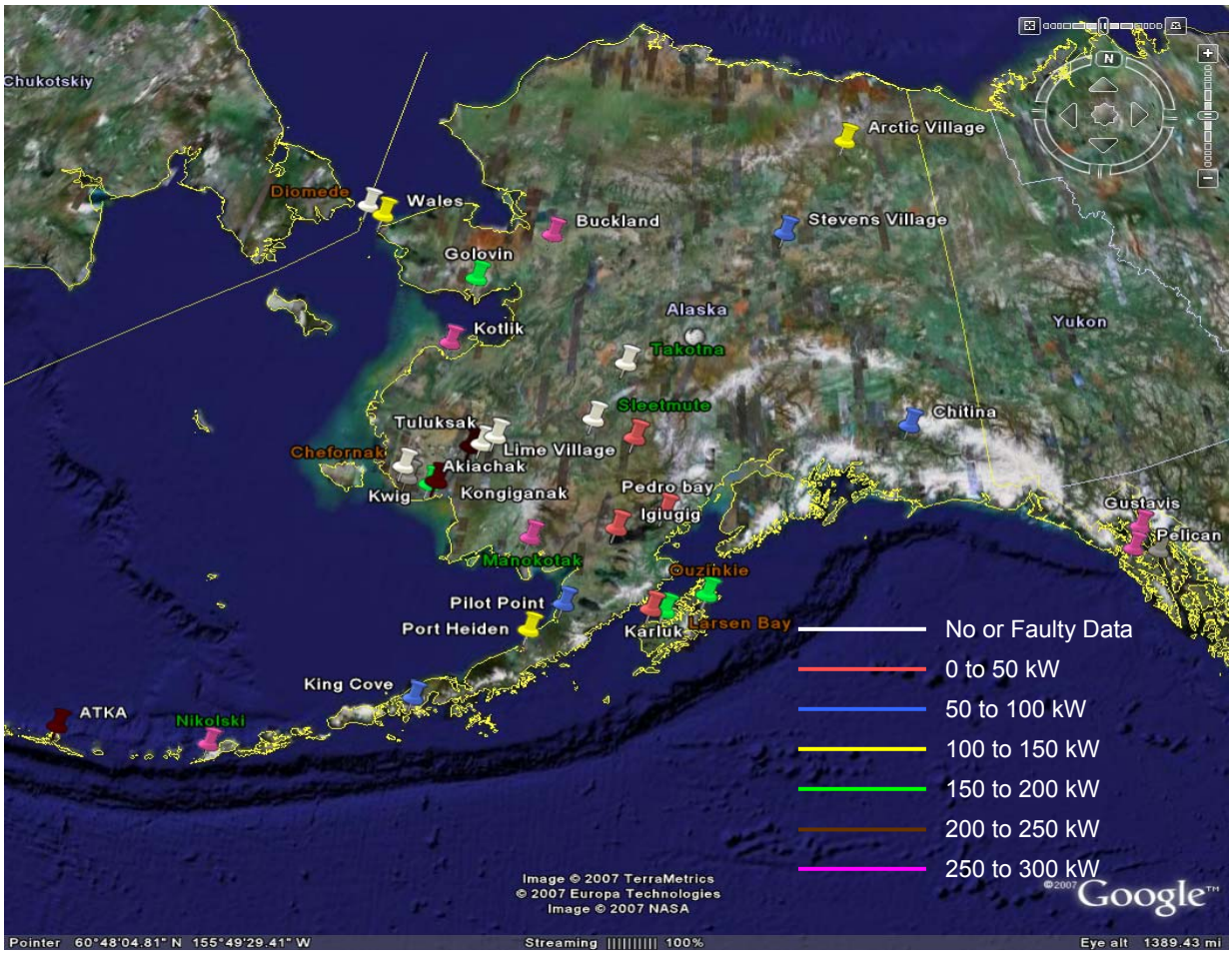

Figure 4.13: Map of select villages in AEAs service territory grouped by average load.

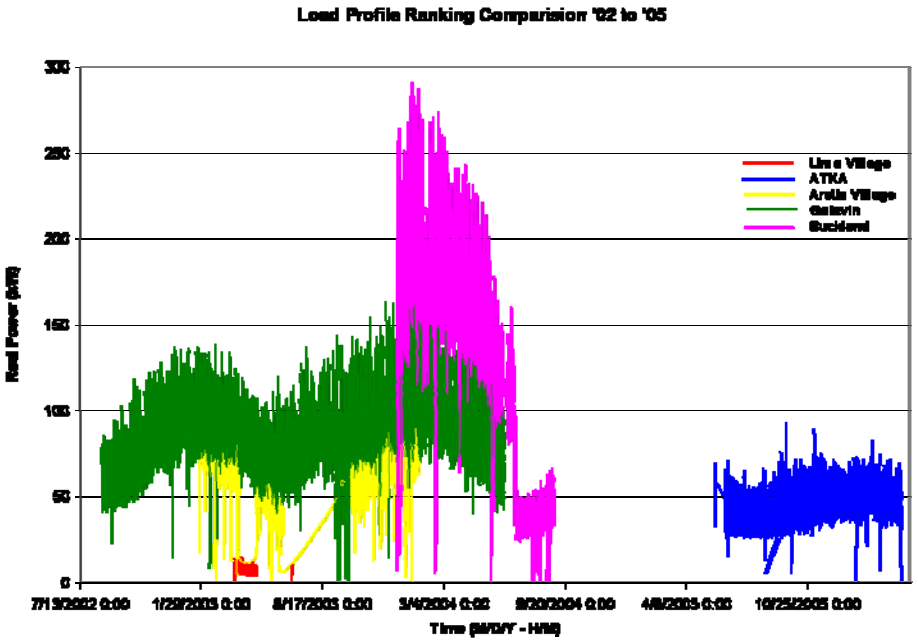

Figure 4.14: Sample load profiles from five Alaska rural villages.

4.3 Village Hybrid Power Performance Analysis

UAF evaluated the performance of systems at Kongiganak, Lime Village, Stevens Village, and Wales Village, Alaska using the hybrid power system model developed in MATLAB® Simulink® specifically for the Alaska rural village power systems. The model is used to perform an economic feasibility analysis for integrating renewable energy sources into existing DEG systems.

4.3.1 Performance Analysis for Kongiganak, Alaska

The hybrid power system model was used to study the performance of the system at Kongiganak, Alaska. Our model was used to study the feasibility of integrating a PV array, a WTG, and a battery bank with the existing DEGs to meet the village load demand. Currently, DEGs are the only source of power for the load demand. Load demand for the village of Kongiganak is supplied by Puvurnag Power Company which operates four diesel generator units: one 235 kWe John Deere® 6125AF, two 190 kWe John Deere® 6081AF, and one 140 kWe John Deere® 6081TF.

The annual synthetic load profile from January 1st, 2003 to December 31st, 2003 with one hour samples, the annual synthetic wind speed profile, and the annual solar flux profile used for analyzing the performance of the Kongiganak Village are shown in Figure 4.15, 4.16, and 4.17, respectively. The clearness index data for the solar insolation profile is obtained using the solar maps developed by the National Renewable Energy Laboratory (NREL) [39]. It can be observed from Figure 4.15 that the maximum load of the system is about 150 kW, the minimum load is about 45 kW and the average load is about 95 kW. From Figure 4.16 it can be observed that the annual average wind speed is about 7 m/s (15.66 miles/hr). From Figure 4.17 it can be observed that the village has low solar flux during winter months and high solar flux during summer months.

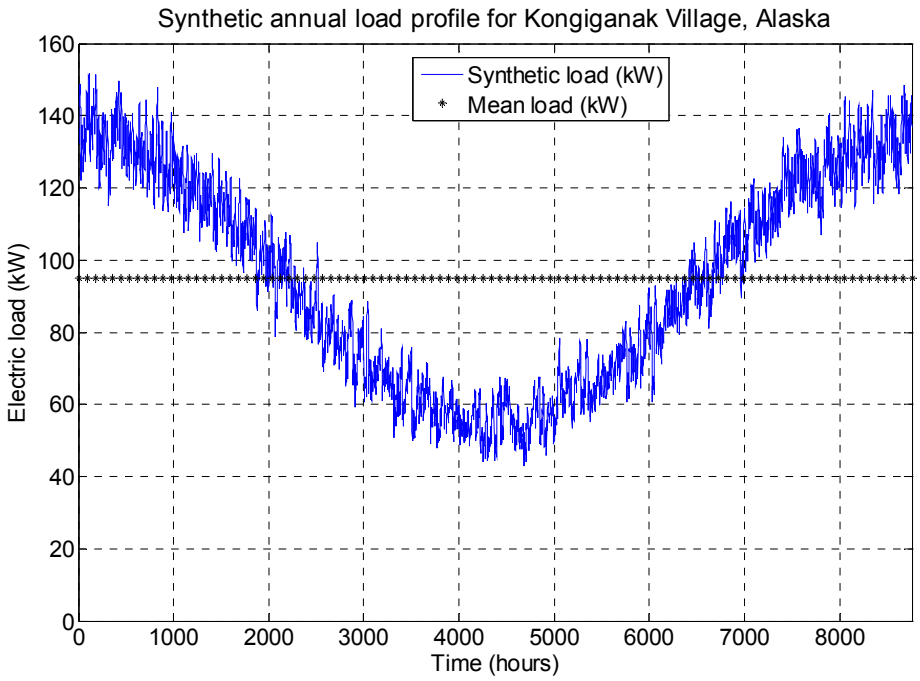

Figure 4.15: Synthetic annual load profile for Kongiganak Village, Alaska.

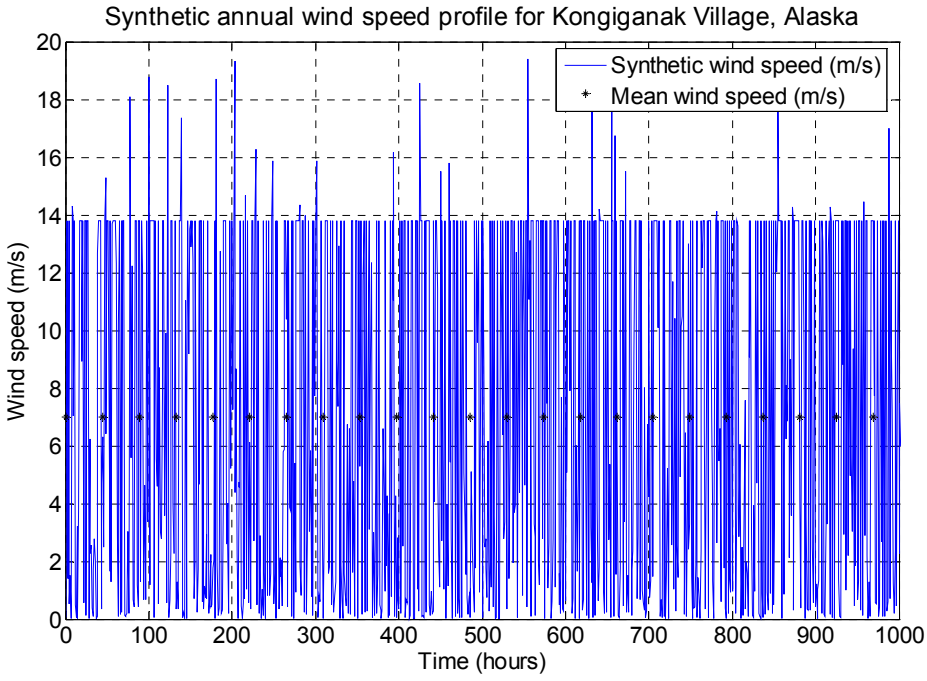

Figure 4.16: Synthetic annual wind speed profile for Kongiganak Village, Alaska.

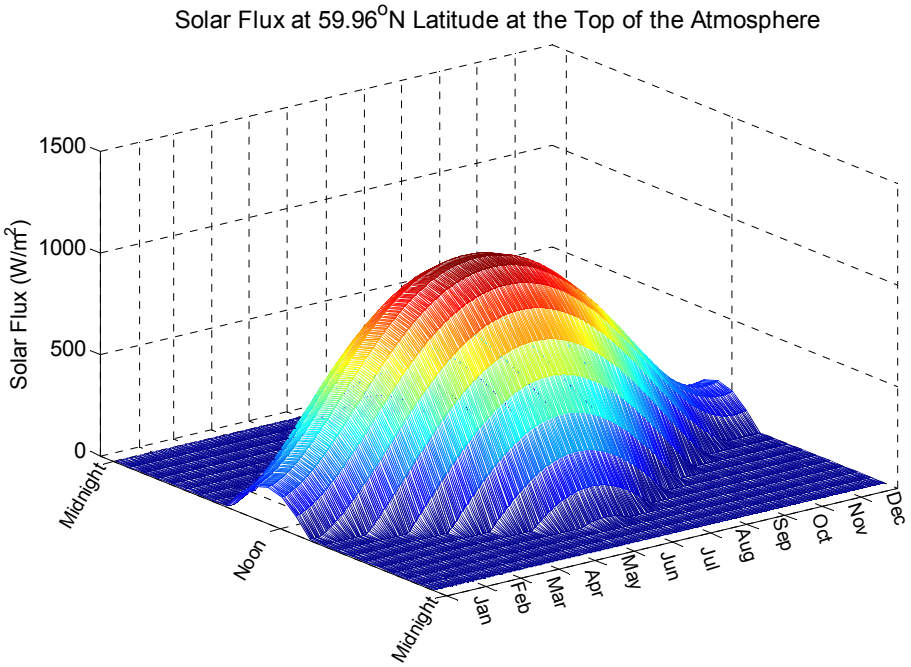

Figure 4.17: Annual solar flux for Kongiganak Village, Alaska.

Various hybrid power systems studied in this analysis include the diesel-battery system, the PV-diesel-battery system, the wind-diesel-battery system, and the PV-wind-diesel-battery system. Table 4.1 shows the installation cost (USD) for different components for the Kongiganak Village hybrid power system. The model was validated by comparing the results obtained from the Simulink® model, for supplying the annual load profile, with the available obtained from the HOMER software. The simulation results obtained from the HARPSim model were compared with those obtained from the HOMER software. Table 4.2 shows the comparison of results from the HARPSim model with HOMER for the Kongiganak Village hybrid power system. At the time of this analysis HOMER was not set up to calculate payback period or NO_x and PM_{10} emissions. The LCC and sensitivity analysis of NPV, COE, and payback for Kongiganak were examined as shown in Figures 4.18-4.21.

Results of the performance analysis showed the economic feasibility and fuel savings of installing WTGs and PV arrays. The life cycle costs LCC and sensitivity analysis of fuel cost and investment rate showed that as the price of bulk fuel rises, the payback period of the WTG and the PV array decreases. The cost of energy COE and the net present value NPV increases linearly while the payback period decreases with the increase in the fuel price. However, the current economic feasibility analysis of integrating PV alone into Alaska rural village systems results in paybacks that are near or longer than the life cycle of the project because of the cost of the PV panels and the lack of light in the winter months. As fuel costs increase and the cost of PV panels decreases in the future, PV panels will become more economical in Alaska rural village power systems.

Table 4.1: Installation cost for different components for Kongiganak Village.

Item	Cost per unit (USD)	No of units	Diesel-only system (USD)	Diesel-battery system (USD)	PV-diesel-battery system (USD)	Wind-diesel-battery system (USD)	PV-wind-diesel-battery system (USD)	2 wind-diesel-battery system (USD)
140 kW diesel generator	40,000	1	40,000	40,000	40,000	40,000	40,000	40,000
190 kW diesel generator	45,000	1	45,000	45,000	45,000	45,000	45,000	45,000
Switch gear to automate control of the system	16,000	1	16,000	18,000	20,000	20,000	22,000	30,000
Rectification/Inversion	18,000	1	0	18,000	18,000	18,000	18,000	28,000
New Absolyte IIP 6-90A13 battery bank	2,143	16	0	34,288	34,288	34,288	34,288	68,576
AOC 15/50 wind turbine generator	55,000	1	0	0	0	55,000	55,000	110,000
Siemens M55 solar panels	262	180	0	0	47,160	0	47,160	0
Engineering		1	3,000	3,500	4,000	4,000	4,500	6,000
Commissioning, Installation, freight, travel, miscellaneous		1	13,000	14,000	16,000	18,000	20,000	30,000
		TOTAL	**117,000**	**172,788**	**224,448**	**234,288**	**285,948**	**357,576**

Table 4.2: Comparison of energy and economic analysis results for Kongiganak.

Item	Diesel-battery system		PV-diesel-battery system		Wind-diesel-battery system		PV-wind-diesel-battery system	
	HARPSim	HOMER	HARPSim	HOMER	HARPSim	HOMER	HARPSim	HOMER
System cost (USD)	172,788	172,788	224,448	224,450	234,288	234,288	285,948	285,950
Engine efficiency (%)	29.3	28.63	29.3	28.51	29.3	27.03	29.3	26.88
kWh/liter (kWh/gallon) for the engine	3.11 (11.75)	3.04 (11.48)	3.11 (11.75)	3.02 (11.43)	3.11 (11.75)	2.87 (10.84)	3.11 (11.75)	2.85 (10.78)
Fuel consumed in liters (gallons)	267,662 (70,810)	273,910 (72,463)	264,834 (70,062)	272,568 (72,108)	193,249 (51,124)	216,027 (57,150)	190,837 (50,486)	214,776 (56,819)
Total cost of fuel (USD)	212,429	217,390	210,185	216,325	153,373	171,451	151,458	170,456
Energy supplied								
(a) Diesel engine (kWh)	832,152	832,205	823,368	823,422	597145	619,504	588,362	612,287
(b) WTG (kWh)	-	-	-	-	235,007	238,000	235,007	238,000
(c) PV array (kWh)	-	-	8,784	8,783	-	-	8,784	8,783
Energy supplied to load (kWh)	832,152	832,205	832,152	832,205	832,152	832,205	832,152	832,205
Operational life								
(a) Generator (years)	5	1.87	5	1.87	5	1.8	5	1.8
(b) Battery bank (years)	5	12	5.5	12	5.5	12	6	12
Net present value (USD) with i = 7% and n = 20 years	-	1,992,488	2,545,084	2,945,502	1,954,127	2,383,766	1,974,389	2,421,502
Cost of Electricity (USD/kWh)	0.301	22.6	0.304	0.334	0.237	0.27	0.24	0.275
Payback period for renewable (years)	-	-	Never	-	1.07	-	2.12	-
Emissions								
(a) CO_2 in metric tons (US tons)	660 (728)	703 (775)	653 (720)	700 (772)	477 (526)	555 (612)	471 (519)	552 (608)
(b) NOx in kg (lbs)	7,322 (16,143)	-	7,245 (15,972)	-	5,288 (11,657)	-	5,222 (11,512)	-
(c) PM_{10} in kg (lbs)	308 (679)	-	305 (672)	-	222 (490)	-	220 (484)	-

Since the wind-diesel-battery system was observed to be the most cost effective, further work was carried out to study the effect of installing another WTG into the wind-diesel-battery system. The addition of a second WTG required an increase in the capacity of the battery bank to accommodate more energy storage. Therefore, the battery bank capacity and the inverter rating were increased from 100 kW and 100 kVA to 200 kW and 200 kVA, respectively. Table 4.3 shows the comparison of results from the HARPSim model with HOMER for the two wind-diesel-battery hybrid power system for Kongiganak Village. It can be observed that the addition of the second WTG into the wind-diesel-battery hybrid power system resulted in the further reduction in the NPV and the COE, while the payback period with the two WTGs increased slightly. The WTG penetration level increases to 50% for this case. The payback period of the WTGs increased to 1.56 years due to the extra cost involved in the addition of the second WTG.

A new 3 WTG-2 DEG system for Kongiganak has been commissioned through a Denali Commission grant and is currently in the design and procurement phase. A feasibility analysis using our model for the proposed system estimates the village will displace about 37,800 liters (10,000 gallons) of diesel fuel per wind turbine per year with a payback of about 3.5 years, while the contractor estimates about 45,360 liters (12,000 gallons) of diesel fuel per wind turbine per year with a payback of about 2.5 years.

Table 4.3: Comparison of results for two wind-diesel-battery hybrid power system.

Item	**Two wind-diesel-battery system**	
	HARPSim	HOMER
System cost (USD)	357,576	357,576
Engine efficiency (%)	29.3	26.6
kWh/liter (kWh/gallon) for the engine	3.11 (11.75)	2.78 (10.53)
Fuel consumed in liters (gallons)	151,252 (39,961)	201,444 (53,222)
Total cost of fuel (USD)	119,883	159,876
Energy supplied		
(a) Diesel engine (kWh)	469,542	561,741
(b) WTG (kWh)	470,015	475,999
Energy supplied to load (kWh)	832,152	832,205
Operational life		
(a) Generator (years)	5	1.8
(b) Battery bank (years)	5.5	12
Net present value (USD) with i = 7% and n = 20 years	1,748,988	2,407,895
Cost of Electricity (USD/kWh)	0.22	0.273
Payback period for WTG (years)	1.56	-
Emissions		
(a) CO_2 in metric tons (US ton)	367 (405)	517 (570)
(b) NOx in kg (lbs)	4,068 (9,112)	-
(c) PM_{10} in kg (lbs)	171 (383)	-

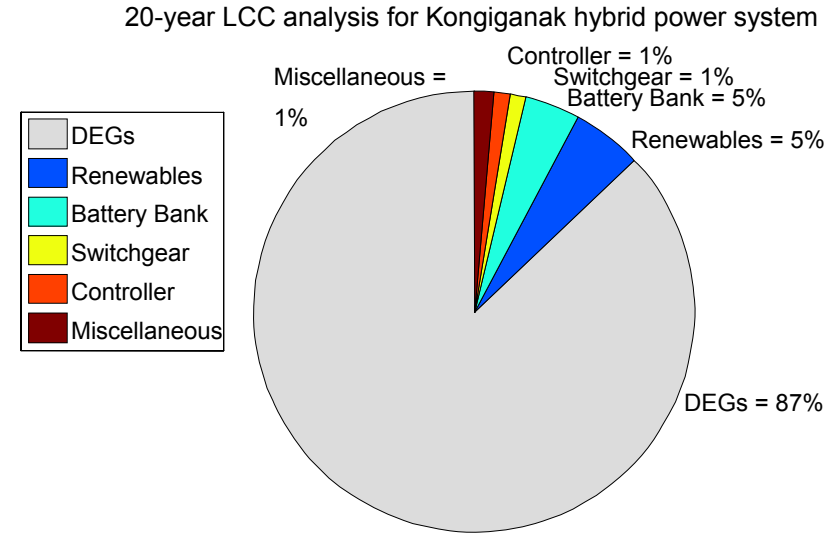

Figure 4.18: 20-year LCC analysis of the proposed Kongiganak hybrid power system.

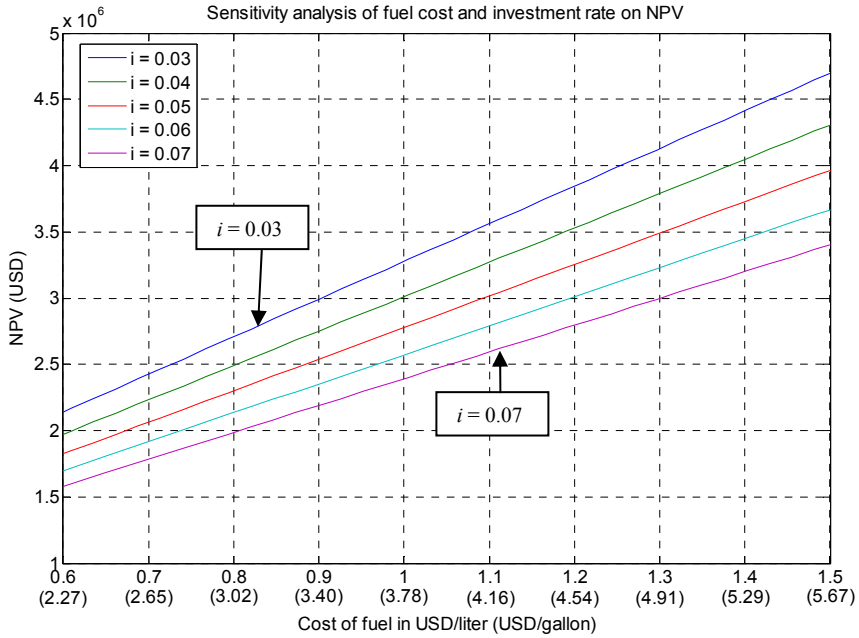

Figure 4.19: Sensitivity analysis of fuel cost and investment rate on the NPV for Kongiganak.

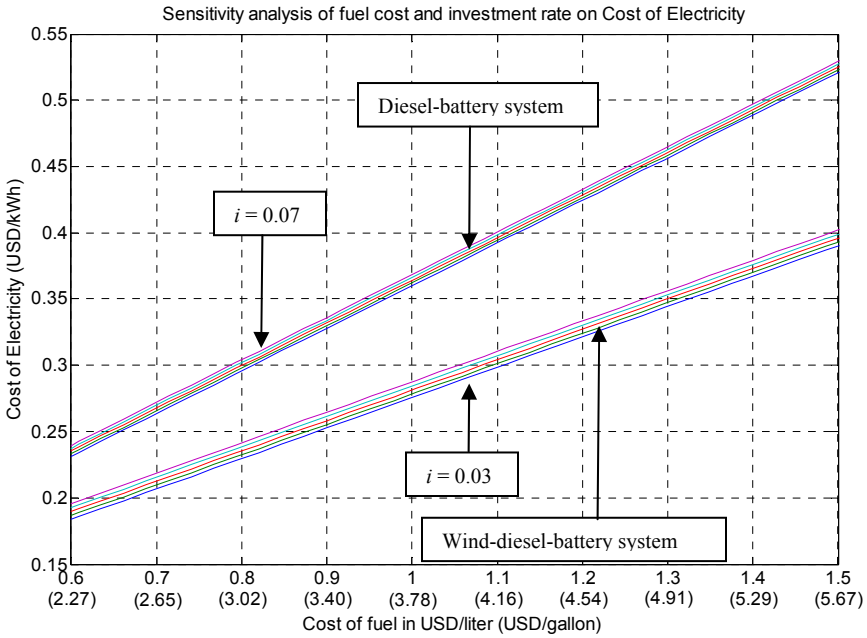

Figure 4.20: Sensitivity analysis of fuel cost and investment rate on the COE for Kongiganak.

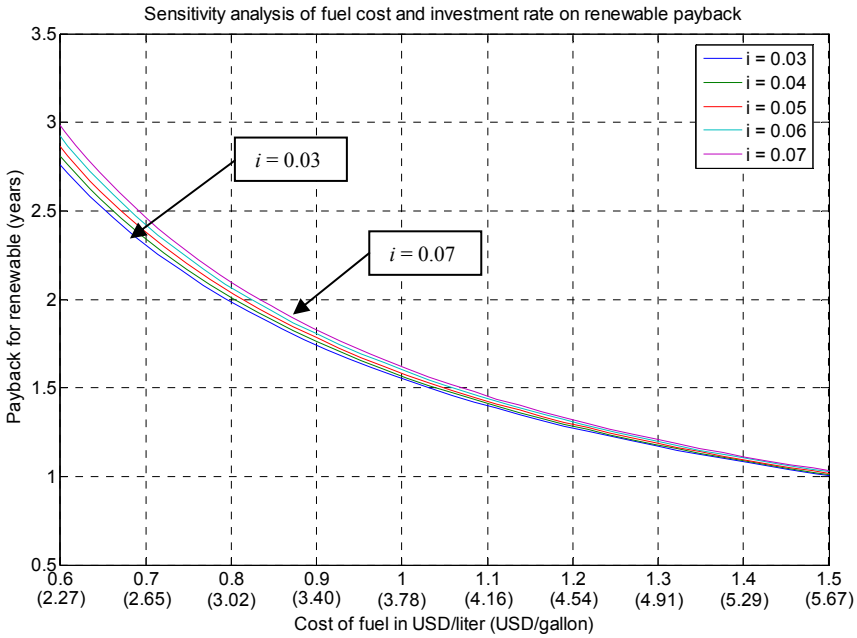

Figure 4.21: Sensitivity analysis of fuel cost and investment rate on the payback period for Kongiganak.

4.3.2 Performance Analysis for Wales Village, Alaska

The wind-diesel-battery hybrid power system of Wales Village has been in reliable operation since the summer of 2000. A Simulink® model for the hybrid power system was developed. The load and wind profiles shown in Figures 4.22 and 4.23 were input into the model. The annual

load data were recorded at Wales Village from August 1st, 1993 to July 31st, 1994 with the sampling period of 15 minutes. The average wind speed is about 8.4 m/s.

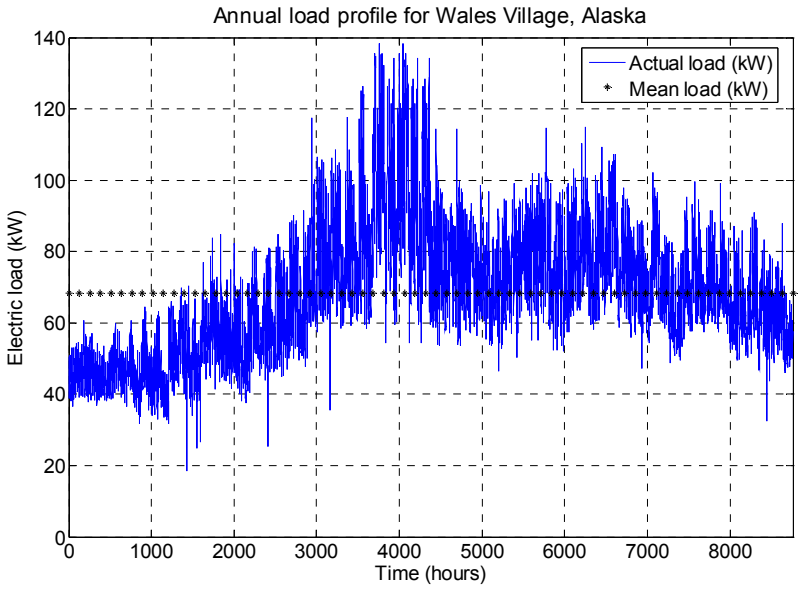

Figure 4.22: Annual load profile for Wales Village, Alaska.

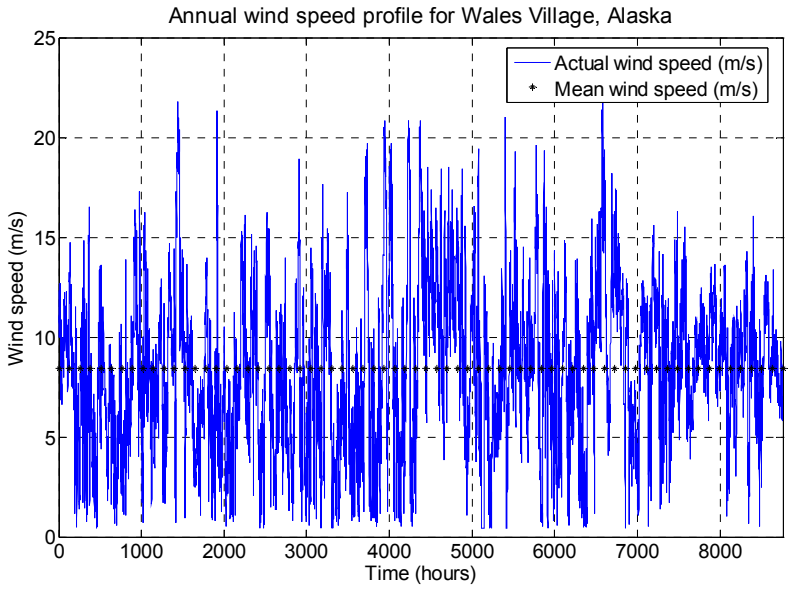

Figure 4.23: Annual wind speed profile for Wales Village, Alaska.

The model was validated by comparing the results obtained from the Simulink® model, for supplying an annual load profile, with those obtained from the HOMER software. Table 4.4 shows the overall comparison chart for the two models. It should be noted that the LCC analysis for 20 years with an investment rate of 7% is performed with the battery bank indoors. This is

Table 4.4: Comparison of results for Wales Village with HOMER.

Parameter	Simulink® Model			HOMER	
	Diesel-battery system	Wind-diesel-battery system		Diesel-battery system	Wind-diesel-battery system
	Battery Indoors (@ 20 °C)	Battery Indoors (@ 20 °C)	Battery Outdoors (Avg: -0.5 °C)	Battery Indoors (@ 20 °C)	Battery Indoors (@ 20 °C)
System cost (USD)	167,800	283,800	-	167,800	283,800
Engine efficiency (%)	29.55	29.55	29.55	29.4	29.55
kWh/liter (kWh/gallon) for the engine	3.13 (11.85)	3.13 (11.85)	3.13 (11.85)	3.09 (11.7)	3.13 (11.85)
Fuel consumed in liter (gallons)	199,890 (52,881)	155,762 (41,207)	185,020 (48,947)	196,621 (50,016)	156,653 (41,443)
Total cost of fuel (USD)	158,643	123,621	146,841	156,039	124,320
Energy generated					
(a) Diesel engine (kWh)	626,876	488,484	580,239	606,501	490,507
(b) WTG (kWh)	0	137,266	137,266	0	139,830
(c) Excess energy (kWh)	28,939	0	119,568	92.8	11,988
Energy supplied to load (kWh)	597,937	597,937	597,937	597,871	597,871
Operational life					
(a) Generator (years)	5.5	5.5	5.5	3.62	4.6
(b) Battery bank (years)	5.0	5.5	3.0	12	12
Net present value (USD) with i = 7% and n = 20 years	-	1,652,820	1,923,997	2,008,969	1,754,711
Cost of Electricity (USD/kWh)	0.32	0.28	0.32	0.32	0.28
Payback period for WTGs (years)	-	4.867	Never	-	-
Emissions					
(a) CO_2 in metric tons (US tons)	498.65 (549.67)	388.57 (428.33)	461.55 (508.77)	497.10 (547.96)	*402.41 (443.58)
(b) NOx in kg (Pounds)	5516.45 (12161.69)	4298.62 (9476.83)	5106.048 (11256.91)	-	-
(c) PM in kg (Pounds)	231.94 (511.34)	180.74 (398.49)	214.69 (473.3)	-	-

*Based on 88% carbon content in the diesel fuel

because in HOMER the battery bank is assumed to be kept at an optimal temperature. The results obtained with the battery bank kept outdoors are also presented in Table 4.4. The LCC and air emissions results of the Simulink® model were comparable with those obtained from the HOMER software. It was observed that the COE for the wind-diesel-battery hybrid power system is less than the COE for the diesel-battery system, thus making the wind-diesel-battery system more economical while emitting less pollution. The payback period of the WTG with a fuel cost of 0.793 USD per liter (3.00 USD per gallon) was less than 5 years and it decreases with the increase in the cost of fuel. The wind-diesel-battery hybrid power system will consume less fuel and emit less CO_2, NOx, and PM_{10}. If the external costs associated with these

emissions are taken into account (see Table 4.5), the PV system payback period will decrease further, thus making these systems more viable and affordable.

Table 4.5: Avoided cost for different pollutants for Wales Village, Alaska.

Emission	Avoided costs
CO_2	-194 USD/metric ton (176 USD/US ton)
PM_{10}	-478 USD/kg (-217 USD/lb)
NOx	-20 USD/kg (-9 USD/lb)

4.3.3 Performance Analysis for Lime Village, Alaska

The PV-diesel-battery hybrid power system of Lime Village has been in reliable operation since July 2001. A Simulink® model for the hybrid power system was developed. The load and wind profiles shown in Figures 4.24 and 4.25 were input into the model. Table 4.6 shows the costs of the different components installed at Lime Village. The costs of the different components were obtained from the various manufacturers. The engineering cost, commissioning, installation, freight and other miscellaneous costs were obtained from a report prepared by the Alaska Energy Authority (AEA) [40]. Due to the remoteness of the site, the cost for transporting and installing the various components is relatively high.

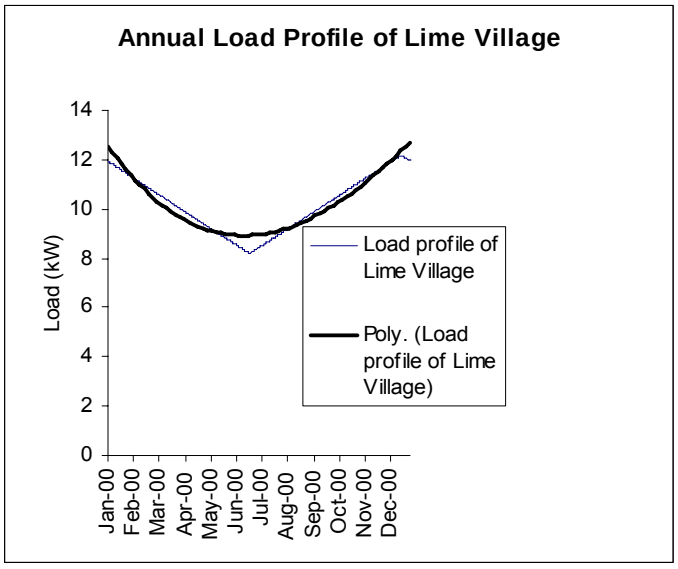

Figure 4.24: Annual load profile for Lime Village, Alaska.

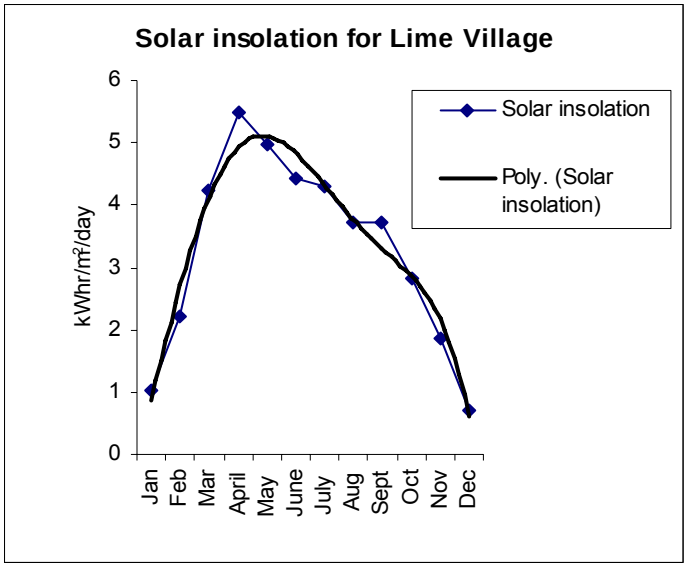

Figure 4.25: Annual solar insolation profile for Lime Village, Alaska.

The model was validated by comparing the results obtained from the Simulink® model, for supplying an annual load profile, with those obtained from the HOMER software. Table 4.7 shows the results obtained from the HARPSim model. In this model the roundtrip efficiency of the rectifier/inverter and the internal loss in the battery bank per cycle was considered as 90%. The collector efficiency for the PV array is assumed as 12%. As mentioned in HOMER, the heating value of fuel is assumed to be 48.5 MJ/kg (20,852 BTU/lb) and the density of fuel is assumed to be 840 kg/m^3 (52.44 lb/ft^3). The post-simulation analysis includes an economic and environmental component illustrating the simple payback and avoided cost of emissions using the PV array. The results obtained from HARPSim for the three systems shows that the addition of the battery bank and the PV array with the DEGs improves the system efficiency and reliability and decreases the fuel consumption and the environmental pollutants.

Table 4.8 shows the comparison of results from HARPSim with HOMER for the current Lime Village hybrid power system. The LCC and air emissions results of the Simulink® model were comparable to those obtained from the HOMER software. Although there is a significant capital investment to purchase a PV system for this application, the PV system may have acceptable 20-year life cycle costs for many remote locations. Furthermore, over its life cycle the PV-diesel-battery hybrid power system will consume less fuel and emit less CO_2, NOx, and PM_{10} than the diesel-battery system. If the external costs associated with these emissions are taken into account (see Table 4.9), the PV system payback period will decrease further, thus making these systems more viable and affordable. A simple payback period for the PV array of Lime Village with a fuel cost of 1.057 USD per liter (4.00 USD per gallon) was about 18 years and it decreases with the increase in the cost of fuel. The long payback period here is a direct result of the cost of the PV array and the lack of sunlight in the winter months.

Table 4.6: Component and installation costs for Lime Village.

Item	Cost per unit (USD)	No of units	Diesel-only system (USD)	Diesel-battery system (USD)	PV-diesel-battery system (USD)
35 kW diesel generator	28,000	1	28,000	28,000	28,000
21 kW diesel generator	18,500	1	18,500	18,500	18,500
Switch gear to automate control of both diesels	16,000	1	16,000	16,000	16,000
Rectification/Inversion	18,000	1	0	18,000	18,000
New Absolyte IIP 6-90A13 battery bank	2,143	16	0	34,288	34,288
BP275 Solar	329	105	0	0	34,545
Siemens M55 Solar	262	75	0	0	19,650
Engineering		1	3,000	3,500	4,000
Commissioning, Installation, freight, travel, miscellaneous		1	13,000	14,000	16,000
		TOTAL	**78,500**	**132,288**	**188,983**

Table 4.7: Simulation results of Lime Village using HARPSim.

Parameter	Diesel-only system	Diesel-battery system	PV-diesel-battery system
System cost (USD)	78,500	132,288	188,983
System efficiency (%)*	26.22%	29.94%	29.96%
kWh/liter (kWh/gallon)	2.81 (10.61)	3.20 (12.1)	3.20 (12.1)
Fuel consumed in liters (gallons)	31,789.80 (8410)	27,847.26 (7367)	24,883.74 (6583)
Total cost of fuel (USD)**	33,640	29,470	26,340
CO_2 emitted in metric tons (US tons)	81.05 (89.34)	70.93 (78.19)	63.64 (70.15)
PM_{10} emitted in kg (lbs)	33.01 (72.77)	32.84 (72.4)	27.18 (59.92)
NOx emitted in kg (lbs)	785.17 (1731)	784.71 (1730)	646.37 (1425)
System load (kWh)	89220	89220	89220
Energy supplied			
(a) DEG (kWh)	101900	100100	89500
(b) PV (kWh)	0	0	9445
Electrical efficiency of DEG (%)	87.56	89.13	90.17

*In this project System efficiency is the ratio of the total electrical energy supplied by the diesel generator to the total energy available from the fuel.
**Based on a diesel fuel price of 1.057 USD per liter (4.00 USD per gallon) for Lime Village, Alaska.

Table 4.8: Comparison of results for Lime Village with HOMER.

Parameter	HOMER	HARPSim
System cost (USD)	188,983	188,983
System efficiency (%)	29.9	29.96
kWh/liter (kWh/gallon)	3.13 (11.84)	3.20 (12.1)
Fuel consumed in liters (gallons)	25,768.26 (6,817)	24,883.74 (6,583)
Total cost of fuel (USD)	27,058	26,340
Energy generated		
(a) Diesel engine (kWh)	87,064	82,497
(b) PV (kWh)	9,444	9,445
Energy supplied to load (kWh)	89,224	89,220
Operational life		
(a) Generator (years)	4.62	5.4
(b) Battery bank(years)	6.07	5.4
Net present value (NPV) (USD)	581,350	557,154
Payback (Years)	-	18.11
Emissions		
(a) CO_2 in metric tons (US tons)	*68.58 (75.60)	63.64 (70.15)
(b) NOx in kg (lbs)	-	646.37 (1425)
(c) PM_{10} in kg (lbs)	-	27.18 (59.92)

*Based on 88% carbon content in the diesel fuel.

Table 4.9: Avoided cost of emissions for Lime Village.

Emission	Avoided costs
CO_2	28.94 USD/metric ton (26.31 USD/US ton)
PM_{10}	37.28 USD/kg (16.91 USD/pound)
NOx	1.52 USD/kg (0.69 USD/pound)

4.4 Economic Dispatch Feasibility of Multi-DEG Systems

A software program was also developed for economic load dispatch for multi-DEG systems taking into account the fuel efficiency curves, the output power factor, and the thermodynamic model of each DEG.

4.4.1 Economic Dispatch Feasibility for Buckland, Alaska

For communities such as Buckland, Alaska, which operates a 175 kWe and a 455 kWe Caterpillar® (CAT®) diesel electric generator (see Figure 4.26), simply examining the manufacturer's fuel efficiency curves (see Figure 4.27) for the electric load range shows that they need to turn off the less efficient 175 kWe DEG and just operate the 455 kWe DEG, so there is no real need for an automated economic dispatch system at this time. In this case the 455 kWe DEG has a new CAT® fuel injection controller which provides for a flatter efficiency curve over a wider range of electric load (see Figure 4.27). Each of the DEGs specifications were obtained from the CAT® website.

Figure 4.26: CAT® Diesel Electric Generators at Buckland, AK (455 kWe on left and 175 kWe on right).

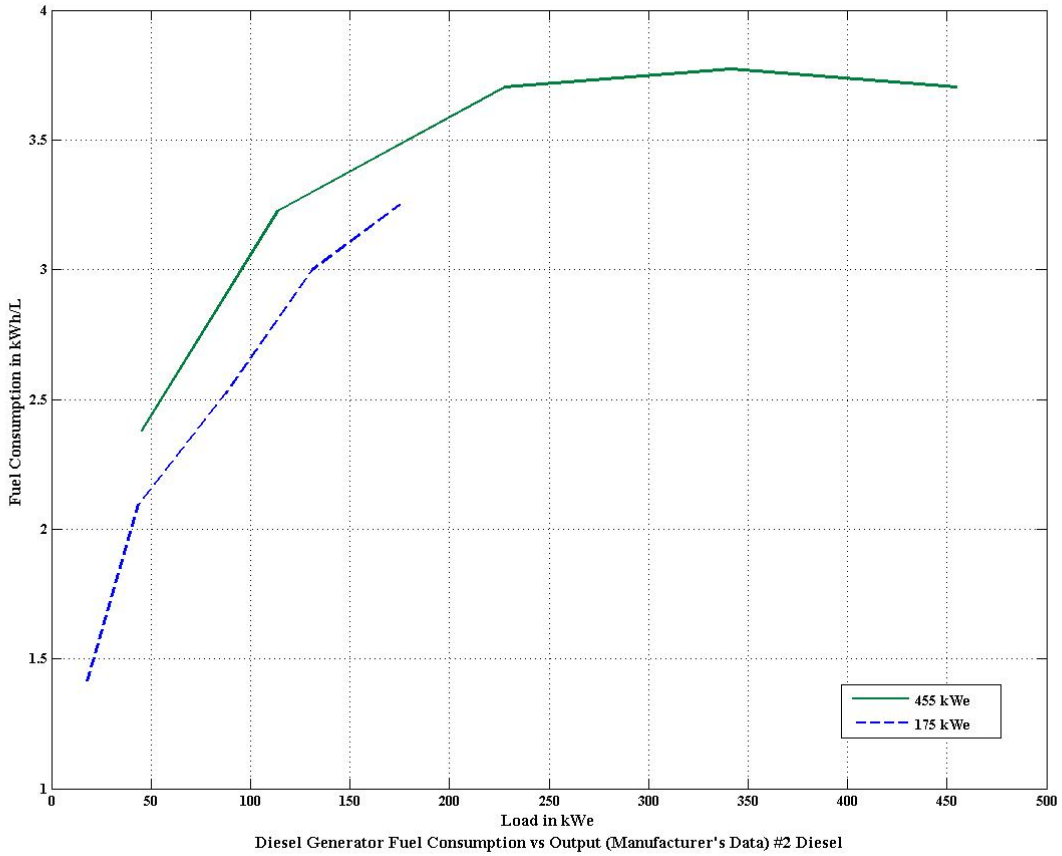

Figure 4.27: Manufacturer's fuel curves for CAT® 175 kWe and 455 kWe diesel electric generators.

4.4.2 Economic Dispatch Feasibility for Kongiganak, Alaska

Villages such as Kongiganak, Alaska would benefit from implementing an economic dispatch system. Power demand for the village of Kongiganak is supplied by Puvurnag Power Company which operates four diesel generator units: one 235 kWe John Deere® 6125AF, two 190 kWe John Deere® 6081AF, and one 140 kWe John Deere® 6081TF. With this information each of the DEGs specifications were obtained from the John Deere® website. The fuel efficiency curves for the three DEGs were constructed as shown in Figures 3.49 and 3.50 in Section 3.5.2.3 and three different load dispatch schemes were implemented: 1) even load distribution (ELD) 2) pre-configured control (PCC) and 3) economic dispatch.

Comparing economic dispatch ED where the load demand and the efficiency of each DEG is considered with PCC using #1 diesel fuel (see Table 4.10) shows a reduction in fuel consumption of about 9.5% by employing an economic dispatch system using the load and temperature profiles shown in Figure 4.28.

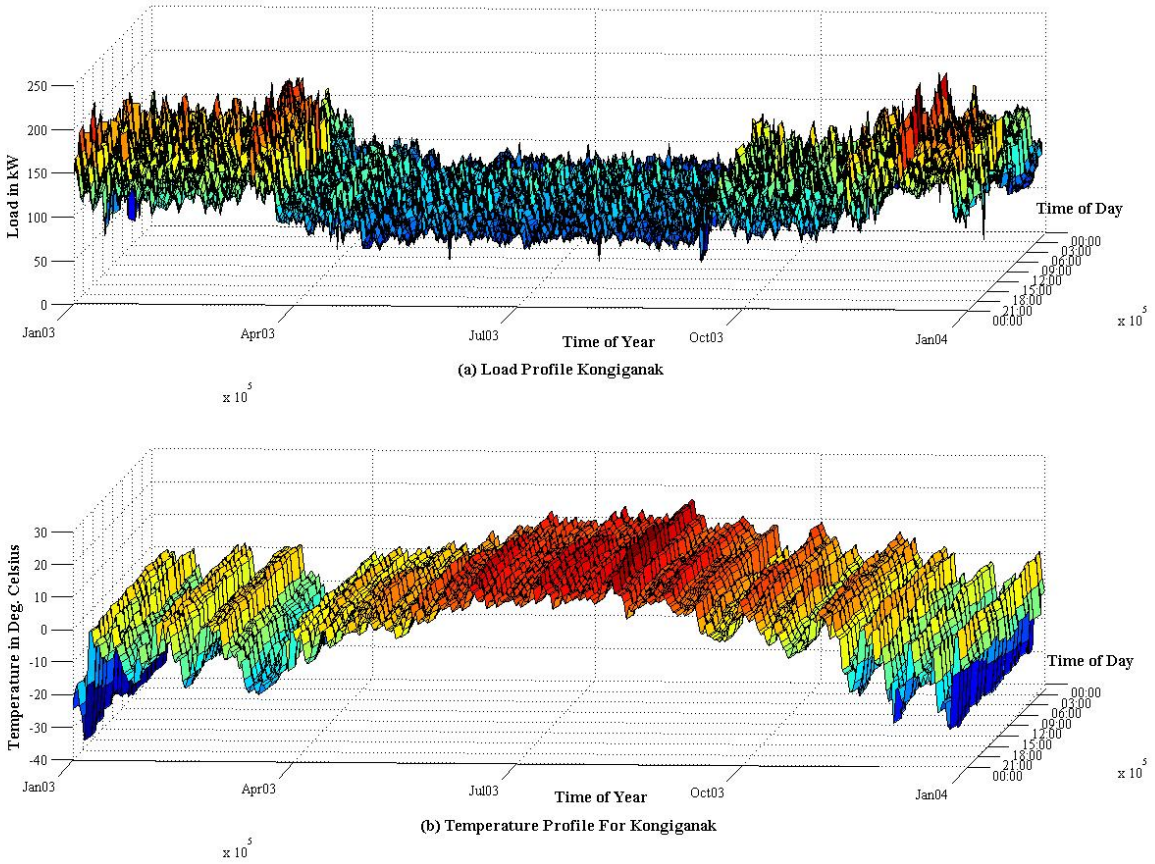

Figure 4.28: Kongiganak Load and Temperature Profiles for January 1, 2003 through January 1, 2004: (a) Load Profile (kW) (b) Ambient Temperature Profile (°C).

Given their current cost of bulk fuel at $0.93/liter ($3.50/gallon) for #1 diesel in Kongiganak and the installed cost of a basic economic dispatch system at $114.2k (see Table 4.11b) offers a

payback of less than one year (see Table 4.12 below). Similar results are obtained for #2 diesel fuel. The two options in Table 4.11 are: 1) a basic system without security and 2) a more detailed system with security. Puvarnaq Power also received a Denali Commission grant for a new system with two DEGs and three WTGs so some of the cost for the economic dispatch system can be incorporated into this grant.

Table 4.10: PCC and ED results for Kongiganak system using #1 diesel fuel.

Parameter (for #1 Diesel)	Simulation / Scenario Data							
	PCC Control		Temperature Change Comparison	ED Control		Temperature Change Comparison	Control Scheme Comparison	
Ambient Temp Change in [°C]	0	3	-	0	3	-	0	3
Load energy- kWh	919433.5378	919433.5378	-	919433.5378	919433.5378	-	-	-
Fuel consumed- L (gal)	489808.0 (129,393.6)	490559.0 (129,591.9)	751.0 (198.4)	442987.0 (117,024.8)	443891.6 (117,263.7)	904.6 (239.0)	-46821.0 (-12,368.8)	-46667.3 (-12,328.2)
Efficiency of engine- kWh/L (kWh/gal)	1.8771 (7.0956)	1.8743 (7.0847)	-0.0029 (-0.0109)	2.0755 (7.8455)	2.0713 (7.8295)	-0.0042 (-0.0160)	0.198 (0.750)	0.197 (0.745)
Total annual cost of fuel	0	0						
at $1.082/L ($3.50/gal)	$529,972.2	$530,784.8	$812.6	$479,311.9	$480,290.7	$978.8	-$50,660.3	-$50,494.1
at $1.3209/L ($5.00/gal)	$646,987.4	$647,979.3	$992.0	$585,141.5	$586,336.4	$1,194.9	-$61,845.9	-$61,642.9
NO_X emitted- ton_m (lbs)	12260.7 (27,030.2)	12279.5 (27,071.7)	18.80 (41.44)	11088.7 (24,446.4)	11111.4 (24,496.3)	22.64 (49.92)	-1172.01 (-2,583.8)	-1168.16 (-2,575.4)
PM_{10} emitted- kg (lbs)	92.2 (203.3)	92.4 (203.6)	0.14 (0.31)	83.4 (183.9)	83.6 (184.2)	0.17 (0.37)	-8.82 (-19.4)	-8.79 (-19.4)
CO_2 emitted- kg (lbs)	1105963.9 (2,438,230.2)	1107659.6 (2,441,968.6)	1695.69 (3,738.34)	1000244.2 (2,205,158.5)	1002286.9 (2,209,661.7)	2042.65 (4,503.27)	-105719.70 (-233,071.8)	-105372.74 (-232,306.9)
Annual fuel savings			-0.153%			-0.204%	9.559%	9.513%

Table 4.11: Installation costs for two economic dispatch control schemes.

(a)Generator Control Automation Upgrade for a Three-Machine Plant (Buckland)

Item	Installed Cost ($)	
	Option 1	Option 2
PLC/ Communications Hardware	26,625	33,571
PLC/ Communications Software	16,206	23,153
Plant Wiring	4,630	9,261
Transducer Installation	3,473	5,788
Setup and Commissioning	6,946	9,261
Total without RTED Software	**$57,880**	**$81,034**
RTED Software	27,783	27,783
Total with RTED Software	**$85,663**	**$108,817**

(b)Generator Control Automation Upgrade for a Four-Machine Plant (Kong)

Item	Installed Cost ($)	
	Option 1	Option 2
PLC/ Communications Hardware	35,501	44,762
PLC/ Communications Software	21,609	30,870
Plant Wiring	6,174	12,348
Transducer Installation	4,630	7,718
Setup and Commissioning	9,261	12,348
Total without RTED Software	**$77,175**	**$108,046**
RTED Software	37,044	37,044
Total with RTED Software	**$114,219**	**$145,090**

Table 4.12: Payback periods for the PCC and ED control schemes at Kongiganak using #1 diesel.

Variable	Payback Period at Different Average Fuel Costs Utilizing Control Schemes (yrs)			
	$1.082/L ($3.50/gal)		$1.3029/L ($5.00/gal)	
	PCC	ED	PCC	ED
Option 1				
Annual Fuel Savings ($/yr)	150,301	50,660	183,487	61,846
Installation Cost ($)	77,175	37,044	77,175	37,044
Payback Period (yrs)	0.51	0.73	0.42	0.60
Option 2				
Annual Fuel Savings ($/yr)	150,301	50,660	183,487	61,846
Installation Cost ($)	108,046	37,044	108,046	37,044
Payback Period (yrs)	0.72	0.73	0.59	0.60

4.4.4 DEG Efficiency versus Ambient Air Temperature

This same economic dispatch program was also used to incorporate ambient temperature variations and was tested for Kongiganak, Alaska as shown in Figure 4.28. The curves shown in Figure 4.29 below give the efficiency and fuel consumption of the 190 kWe John Deere® DEG at Kongiganak as a function of ambient air temperature between -40 °C and 80 °C. The intake air temperature will be higher than the ambient air temperature due to heating of the incoming air by the building. An expected intake air temperature would likely be in the range from 4 °C to 20 °C. Given a 3 °C rise in ambient air temperature over the next 50 years as predicted by scientist at the UAF Geophysical Institute's Alaska Climate Research Center, there is approximately a 0.2% change in DEG efficiency which is negligible (see Table 4.11).

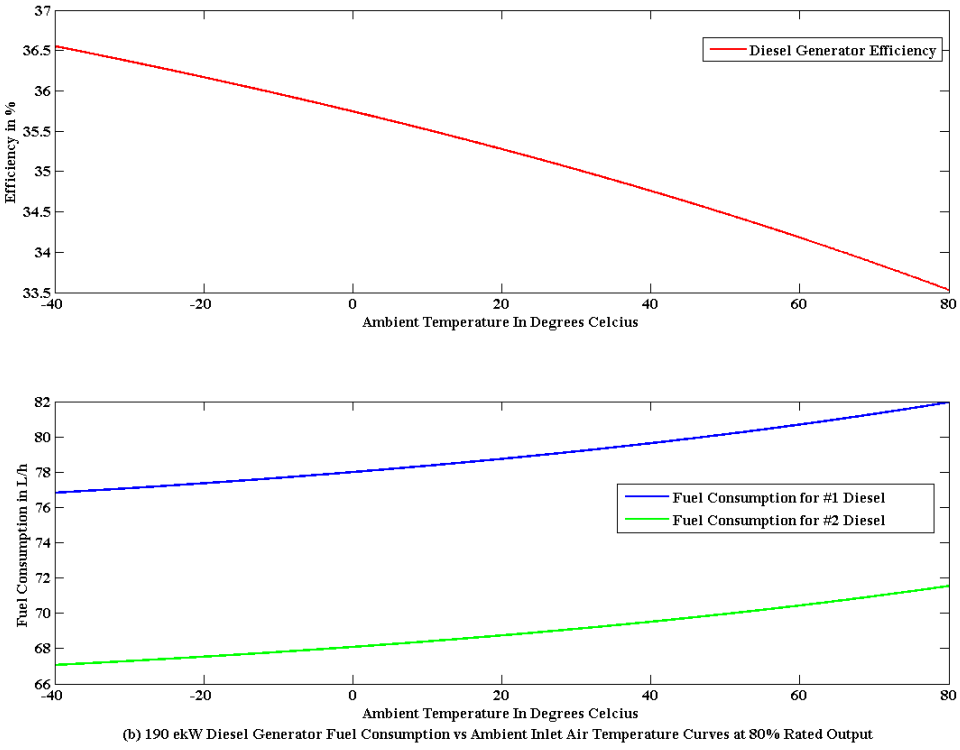

Figure 4.29: Ambient air temp vs. efficiency for 190 kWe John Deere® DEG at 80% rated output.

5. Conclusion

Diesel electric power systems in Alaska rural villages are quite costly to operate given the price of bulk fuel to power the plants. The rising price of bulk fuel is motivating many rural utilities to investigate and implement renewable technologies for power generation in the villages and find ways of making the current DEG systems more efficient. The process used in this project included surveying the current state of Alaska village power systems, creating a consortium of rural utilities and state energy organizations with a vested interest in village energy, collecting available data, modeling village power systems for long term performance and feasibility analysis, and installing new remote monitoring systems in a select number of villages.

There has been a need to design remote monitoring systems for these villages in order to obtain reliable data for analysis to make recommendations for efficiency improvements in these plants. A survey of 25 villages in AEAs service territory revealed a number of issues with regards to power system data. There is simply either a lack of data or unreliable data in many cases either because a remote monitoring system was not in place or was not completely reliable due to equipment faults. Furthermore, the accuracy of the fuel and coolant flow meters and the intake, coolant and exhaust temperature sensors is critical in achieving reliable data as was demonstrated on the UAF Energy Center diesel. However, also of importance is the format in which the data is collected and stored with a number of villages to remotely monitor which is best served by using a central computer and server.

The analysis process used MATLAB® Simulink® to build a computer model of the DEG(s) to study the economic feasibility of integrating renewables such as WTGs and PV arrays into these stand-alone systems and economic dispatch control systems to improve system efficiency.
The results demonstrate that the integration of renewables such as WTGs and PV arrays into stand-alone hybrid power systems and the implementation of economic dispatch systems in Alaska rural villages improves system efficiency and reduces the operating costs and particulate matter emitted to the atmosphere. The results also demonstrate that while the integration of PV arrays into these systems has relatively long payback periods that exceed the life cycle of the project, the integration of WTGs results in much shorter payback periods in villages with a reliable wind resource. The implementation of economic dispatch control systems in villages with two or more DEGs results in even shorter payback periods making this an attractive first step for village utilities who are looking to cut the costs of electric power and do not have another reliable source of energy. The sensitivity analysis of fuel cost and investment rate showed that as the price of bulk fuel rises, the payback period of implementing the WTG, the PV array, and the economic dispatch system decreases. The cost of energy COE and the net present value NPV increases linearly with the increase in the fuel price.

In conclusion, this project served as a means of identifying the current state of power and energy in Alaska rural villages and suggests methods that are economically feasible for implementing more efficient standalone power systems which use DEGs as their main source of power and must operate in extreme climates like those found in Alaska. The assessment tools developed here which have been used to demonstrate the economic feasibility of integrating renewable energy sources and economic dispatch control systems into standalone village power systems using DEGs in Alaska are applicable to similar systems in other standalone applications such as remote oil platforms, remote sections of oil and gas pipelines, and remote mining.

References

[1] Institute of Social and Economic Research, *Alaska electric power statistics (with Alaska energy balance)*, Report Prepared for Alaska Energy Authority, Regulatory Commission of Alaska, and Denali Commission, November 2003.

[2] Alaska Energy Task Force, "NonRailbelt report findings and recommendations," Anchorage, Alaska, [Online]. Accessed February 18th, 2008. Available: http://www.akenergyauthority.org/EnergyPolicyTaskForce/FinalNonRailbeltReport.pdf

[3] Northern Economics, *Screening report for Alaska rural energy plan*, Report Prepared for the Alaska Industrial Development and Export Authority, April 2006.

[4] www.ni.com/pdf/manuals/322759c.pdf, National Instruments Fieldpoint 2015 Manual, accessed August 18th, 2008.

[5] http://www.powerlogic.com/products.cfm?id=64, Powerlogic ION 7350 product information page, accessed August 18th, 2008.

[6] http://www.pcorp.com.au/index.php?option=com_content&task=view&id=119&Itemid=171, Powercorp Commander information page, accessed August 18th, 2008.

[7] http://www.electroind.com/nexus1252.htm, Electroindustries Nexus 1252 information, accessed August 18th, 2008.

[8] National Instruments Application Note 043, pp. 1-35.

[9] http://omega.com/manuals/manualpdf/M1966.pdf, Omega FTB 720 turbine flow meter manual, accessed August 18th, 2008.

[10] http://www.lesman.com/unleashd/catalog/transmit/sitransfm_mag50006000blind_manED1.pdf, Magflo 7000 magnetic flow meter manual, accessed August 18th, 2008.

[11] http://www.efunda.com/designstandards/sensors/flowmeters/flowmeter_mag.cfm, Magnetic Flow Meter Tutorial, accessed August 5th, 2004.

[12] http://www.eesiflo.com/products/eesiflo_5000_series.pdf, Eesiflo 5000 ultrasonic flow meter product manual, accessed August 18th, 2008.

[13] http://www.eesiflo.com/products/ultrasonic_flowmeter_portalok7s_01.html, Eesiflo S-Series ultrasonic flow meter product manual, accessed August 18th, 2008.

[14] Sonntag, R. E., Borgnakke, C., and Wylen, G. J. V., "Fundamentals of Thermodynamics", *John Wiley & Sons, Inc.*, Fifth Edition, 1998.

[15] http://www.engineeringtoolbox.com, Ethylene Glycol Heat – Transfer Fluid and Properties of Air, accessed Nov. 15th, 2004.

[16] http://www.marathonelectric.com/MGPS/standard.jsp, Marathon Electric Generator main page, accessed August 18th, 2008.

[17] http://www.deere.com/en_US/rg/productsequipment/productcatalog/gst/index.html?promo=jdps_home&bug=gendrive&tm=jdps, John Deere diesel engines for generators, accessed August 18th, 2008.

[18] Malosh, J. A. and Johnson, R. A., "Part-Load Economy of Diesel-Electric Generators", *a report prepared for Department of Transportation and Public Facilities*, report # AK-RD-86-01, Jun 1985.

[19] http://www.aocwind.net/1550brochure.pdf, Official Webpage for the Atlantic Orient Corporation, accessed Nov 2002.

[20] M. Patel, “Wind and Solar Power Systems”, *Florida: CRC Press LLC*, 1St Edition, 1999.

[21] http://www.nrel.gov/gis/solar.html, Official Webpage of the National Renewable Energy, accessed Mar 22nd, 2006.

[22] W. D. Winsor and K. A. Butt, “Selection of Battery Power Supplies for Cold Temperature Application”, *Technical report, C-CORE Publication* No. 78-13, Sep 1978.

[23] Sandia National Laboratories, “Stand-Alone Photovoltaic Systems - A Handbook of Recommended Design Practices”, *a report prepared by Sandia National Laboratories*, report # SAND87-7023, Mar 1995.

[24] Y. A. Cengel and M. A. Boles, “Engineering Thermodynamics”, *McGraw Hill Publications*, 4th ed., 2002.

[25] R. G. Narula, H. Wen, K. Himes, B. Power, “Incremental Cost of CO_2 Reduction in Power Plants”, *ASME Turbo Expo*, 2002.

[26] CATERPILLAR®, “Diesel Generator Set 175 ekW,” Document Num.: LEHE6275-03, April, 2007. [Online]. Accessed April, 2007. Available: www.CAT-ElectricPower.com

[27] WikiPedia, “P-v diagram for the ideal diesel cycle,” [Online]. Accessed February 18, 2008. Available: http://en.wikipedia.org/wiki/Diesel_cycle

[28] CATERPILLAR®, “Diesel Generator Set 455 ekW,” Document Num.: LEHE1826-01, April, 2002. [Online]. Accessed April, 2007. Available: www.CAT-ElectricPower.com

[29] A. N. Agrawal, *Modeling and optimization of hybrid electric power systems for remote locations in extreme northern climates*, M.S. Thesis, University of Alaska Fairbanks, August 2003. Fairbanks, Alaska.

[30] T. Purtill and R. Robinson, “125 kWe Detroit Diesel AC Generator Curves,” National Oilwell Varco, private communication, July 2007. Available: www.nov.com

[31] K. Sastry, *Properties and performance evaluation of syntroleum synthetic diesel fuels*, M.S. Thesis, University of Alaska Fairbanks, December 2005. Fairbanks, Alaska.

[32] Chevron Products Company, *Diesel fuels technical review (FTR-2)*, Chevron U.S.A. Inc, 1998.

[33] A. Burcat and B. Ruscic, *Third millennium ideal gas and condensed phase thermochemical database for combustion with updates from active thermochemical tables*, Argonne National Laboratory, Chicago, Sept. 2005.

[34] ThermoBuild, “Thermochemical Database,” *Glenn Research Center,* NASA. [Online], accessed May 23rd, 2007. Available: http://cea.grc.nasa.gov/

[35] M. J. Zehe, S. Gordon, and B. J. McBride, “CAP: A computer code for generating tabular thermodynamic functions from NASA Lewis coefficients,” *Glenn Research Center,* NASA, Doc. NASA/TP—2001-210959, rev. 1, February 2002.

[36] A. R. Bergen and V. Vittal, *Power systems analysis*, 2nd Ed., New Jersey: Prentice-Hall, 2000.

[37] A. J. Wood and B. F. Wollenberg, *Power generation, operation, and control*, 2nd Ed., New York: John Wiley & Sons, Inc., 1996.

[38] Syntroleum Corporation Technical Staff, *Syntroleum® S-2 Synthetic Diesel, Driving Clean-Fuel Innovation*, Syntroleum Corporation Publication, 2002.

[39] http://rredc.nrel.gov/solar, Official Webpage of National Renewable Energy Laboratory, accessed Oct 2003.

[40] D. Meiners, “Lime Village Power System Alternatives”, *Alaska Energy Authority*, 2001.

Project Publications

As a result of research efforts on this project one book, three peer-review journal papers, fourteen conference proceedings, one Ph. D. dissertation and three M. S. theses have been published. Also, a portion of a book chapter which is currently in press contains some information with regards to village energy and environmental issues which is a direct result of efforts on this project.

Book:

1) A. N. Agrawal, R. W. Wies, and R. A. Johnson, *Hybrid Electric Power Systems: Modeling, Optimization, and Control*, VDM Verlag, 2007.

Journal Publications:

1) R. W. Wies, R. A. Johnson, and A. N. Agrawal, "Life Cycle Cost Analysis and Environmental Impacts of Integrating Wind-Turbine Generators (WTGs) into Standalone Hybrid Power Systems," *WSEAS Transactions on Systems*, iss. 9, vol. 4, pp. 1383-1393, 2005.
2) R. W. Wies, A. N. Agrawal, and T. J. Chubb, "Optimization of a PV with Diesel-Battery System for Remote Villages," *International Energy Journal*, vol. 6, no.1, part 3, pp. 107-118, 2005.
3) R. W. Wies, R. A. Johnson, A. N. Agrawal, and T. J. Chubb, "Simulink Model for Economic Analysis and Environmental Impacts of a PV with Diesel-Battery System for Remote Villages," *IEEE Transactions on Power Systems*, vol. 20, no. 2, pp. 692-700, 2005.

Conference Publications:

1) R. W. Wies, R. A. Johnson, and L. G. Brouhard, "Efficiency Improvements for Diesel Electric Generation Systems in Alaska Rural Villages through Economic Dispatch," *2008 Alaska Rural Energy Conference*, Girdwood (AK), 2008.
2) R. W. Wies, L. G. Brouhard, R. A. Johnson, and C. S. Lin, "Effects of Rising Electric Load and Ambient Air Temperature on Diesel Electric Generators in Alaska Rural Villages," *Proceedings of the 2007 Arctic Energy Summit*, Anchorage, AK, 2007.
3) R. W. Wies, R. A. Johnson, and A. N. Agrawal, "Life Cycle Cost, Efficiency and Environmental Impact Analysis for Integrating Renewable Energy Sources into Standalone Village Power Systems in Remote Arctic Climates," *Proceedings of the 2007 Arctic Energy Summit*, Anchorage, AK, 2007.
4) A. N. Agrawal, V. S. Sonwalkar, and R. W. Wies, "A Feasibility Analysis of Deploying Photovoltaic Array in a Remote Arctic Community," *Proceedings of the 2007 Arctic Energy Summit*, Anchorage, AK, 2007.
5) R. W. Wies and R. A. Johnson, "Village Metering and Power Study," *2007 Alaska Rural Energy Conference*, Session T5-C, Fairbanks (AK), 2007.
6) R. W. Wies, A. N. Agrawal, R. A. Johnson, and T. J. Chubb, "Implementation of a Remote Terminal Unit on a Diesel Electric Generator for Performance Analysis of Remote Power Systems in Rural Alaska," *2005 Alaska Rural Energy Conference*, Valdez (AK), 2005.
7) R. W. Wies, R. A. Johnson, and A. N. Agrawal, "Integration of Wind-Turbine Generators (WTGs) into Hybrid Distributed Generation Systems in Extreme Northern Climates," *2005 Alaska Rural Energy Conference*, Valdez (AK), 2005.
8) R. W. Wies, R. A. Johnson, and A. N. Agrawal, "Integration of Wind-Turbine Generators (WTGs) into Standalone Hybrid Power Systems in Extreme Northern Climates," *5th WSEAS International Conference on Power Systems and Electromagnetic Compatibility*, Corfu Island, Greece, 2005.
9) R. W. Wies, R. A. Johnson, A. N. Agrawal and T. J. Chubb, "Using HOMER and Simulink for Long-Term Performance Analysis of a Hybrid Electric Power System in a Remote Alaskan Village," *NREL World Renewable Energy Congress VIII*, Denver, CO, 2004.

10) R. W. Wies, R. A. Johnson, A. N. Agrawal, and T. J. Chubb, “Economic Analysis and Environmental Impacts of a PV with Diesel-Battery System for Remote Villages,” *Proceedings of the 2004 IEEE Power Engineering Society General Meeting*, Denver, CO, 2004.

11) R. W. Wies, A. N. Agrawal, T. J. Chubb and R. A. Johnson, “Simulink Model for Economic Analysis & Environmental Impacts of a Photovoltaic with Diesel-Battery System for Remote Villages,” *2004 Alaska Rural Energy Conference*, Talkeetna (AK), 2004.

12) R. W. Wies, A. N. Agrawal, and T. J. Chubb, “Electric Power Quality of Distributed Generation Systems in Rural Alaskan Villages,” *2004 Alaska Rural Energy Conference*, Talkeetna (AK), 2004.

13) R. W. Wies, A. N. Agrawal, and T. J. Chubb, “Optimization of a PV with Diesel-Battery System for Remote Villages,” *International Conference on Electric Supply Industry in Transition*, Asian Institute of Technology, Bangkok, Thailand, 2004.

14) R. W. Wies and A. N. Agrawal, “Integration of Wind-Turbine Generators (WTGs) into Hybrid Distributed Generation Systems in Extreme Northern Climates,” *Proceedings of the 2003 International Yukon Wind Energy Conference: Cold Climate Opportunities*, 2003.

15) R. W. Wies and A. N. Agrawal, “Modeling and Optimization of Hybrid Electric Power Systems for Remote Locations in Extreme Climates,” *Proceedings of the 2003 IASTED International Conference on Power and Energy Systems*, paper 379-190, pp. 241-246, 2003.

Ph. D. Dissertation:

1) A. N. Agrawal, *Hybrid Electric Power Systems In Remote Arctic Villages: Economic And Environmental Analysis For Monitoring, Optimization, and Control*, Ph. D. Dissertation, University of Alaska Fairbanks, August 2006. Fairbanks, Alaska.

M. S. Thesis:

1) L. G. Brouhard, *Economic Dispatch and Control for Efficiency Improvements on Diesel Electric Power Systems in Alaska Rural Villages*, M.S. Thesis, University of Alaska Fairbanks, August 2008. Fairbanks, Alaska.

2) T. Chubb, *Performance Analysis for Remote Power Systems in Rural Alaska*, M.S. Thesis, University of Alaska Fairbanks, May 2004. Fairbanks, Alaska.

3) A. N. Agrawal, *Modeling and optimization of hybrid electric power systems for remote locations in extreme northern climates*, M.S. Thesis, University of Alaska Fairbanks, August 2003. Fairbanks, Alaska.

List of Acronyms and Abbreviations

AEA – Alaska Energy Authority
AVEC – Alaska Village Electric Cooperative
CAT – Caterpillar®
COE – cost of energy
DEG – diesel electric generator
HARPSIM – Hybrid Arctic Remote Power Simulator
HOMER – Hybrid Optimization Model for Energy Efficient Renewables
kWe – kilowatt electric
kWh – kilowatt-hour
LCC – life cycle costs
MWh – megawatt-hour
NPV – net present value
NREL – National Renewable Energy Laboratory
PCE – power cost equalization
PF – power factor
PI – principal investigator
PV – photovoltaics
RTU – remote terminal unit
UAF – University of Alaska Fairbanks
WTG – wind turbine generator

National Energy Technology Laboratory

626 Cochrans Mill Road
P.O. Box 10940
Pittsburgh, PA 15236-0940

3610 Collins Ferry Road
P.O. Box 880
Morgantown, WV 26507-0880

One West Third Street, Suite 1400
Tulsa, OK 74103-3519

1450 Queen Avenue SW
Albany, OR 97321-2198

525 Duckering Bldg./UAF Campus
P.O. Box 755910
Fairbanks, AK 99775-5910

Visit the NETL website at:
www.netl.doe.gov

Customer Service:
1-800-553-7681